ACCESSIBILITY
OPEN

OSLO METROPOLITAN UNIVERSITY
STORBYUNIVERSITETET

Master's Degree in
Structural Engineering and Building Technology
Department of Civil Engineering and Energy Technology

MASTER THESIS

THESIS TITLE	DATE
Comparison of Concrete Shear Wall and Mega-Braced Steel Frame Regarding Seismic Performance	14.06.2020
	NUMBER OF PAGES 113 / 7
AUTHORS Caroline Tveit Hansen Katrine Myhre	SUPERVISORS Emrah Erduran Mahdi Kioumarsi Mehdi Ebadi Jamkhaneh

IN COLLABORATION WITH	CONTACT PERSON
Multiconsult AS	Rune Strand

SUMMARY
The seismic behavior of two different lateral force resisting systems are compared regarding base shear, roof displacement and drift ratio through nonlinear static and dynamic analyses in the software SAP2000. The case study building is a 16-story commercial building located in Western Norway with shear wall core structure as the lateral force resisting system. During this report, the seismic behavior of this system is compared to the behavior of a mega-braced steel frame to evaluate whether this can be a beneficial solution for high-rise buildings in Norway. Further, the effect of adding friction dampers is investigated.

It was found that the shear wall and MBF structure behaved differently during the seismic events. While the shear wall structure exerted largest base shear forces, the MBF clearly experienced larger roof deformations and story drifts. During the largest earthquake, the MBF also experienced failure in hinges of some braces, eventually resulting in initiation of collapse.

The results of the nonlinear static analysis generally deviated from the direct integration and modal time-history analyses, which showed satisfying agreement in the obtained results.

3 KEYWORDS
High-Rise Building
Lateral Force Resisting System
Nonlinear Analysis

List of Contents

LIST OF FIGURES

LIST OF TABLES

ABSTRACT

The seismic behavior of two different lateral force resisting systems are compared regarding base shear, roof displacement and drift ratio through nonlinear static and dynamic analyses in the software SAP2000. The case study building is a 16-story commercial building located in Western Norway with shear wall core structure as the lateral force resisting system. During this report, the seismic behavior of this system is compared to the behavior of a mega-braced steel frame to evaluate whether this can be a beneficial solution for high-rise buildings in Norway. Further, the effect of adding friction dampers is investigated.

It was found that the shear wall and MBF structure behaved differently during the seismic events. While the shear wall structure exerted largest base shear forces, the MBF clearly experienced larger roof deformations and story drifts. During the largest earthquake, the MBF also experienced failure in hinges of some braces, eventually resulting in initiation of collapse.

The results of the nonlinear static analysis generally deviated from the direct integration and modal time-history analyses, which showed satisfying agreement in the obtained results.

ACKNOWLEDGEMENTS

The research presented in this thesis was conducted at Oslo Metropolitan University (OsloMet), Department of Civil Engineering and Building Technology and in cooperation with Multiconsult AS[1].

Through our first three semesters of the master's program we have been introduced to many interesting topics within structural engineering. Structural dynamics caught our interest early and after participating in a seminar about high-rise buildings we both knew that we wanted to include high-rise buildings and their seismic behavior in our thesis.

We would like to express our sincere gratitude to our supervisors from OsloMet, Associate Professors Mahdi Kioumarsi and Emrah Erduran for inspiration to our research question, your time and patience and for motivating us when we have faced challenges in our work. Your support throughout the unusual situation during these months of conducting the study is greatly appreciated.

We also want to thank our external supervisor, Assistant Professor at Damghan University Mehdi Ebadi Jamkhaneh, for sharing your expertise and offering great guidance and support, which have been highly essential for us to complete this thesis. We truly value your time investment and patience and for responding to our many questions at all hours.

Finally, we would like to express our gratefulness to the employees of Multiconsult for offering details and information on a case study building, not to mention your hospitality by welcoming us to your offices and providing work space and support. Your interest in us and our thesis is appreciated.

Last but not least, we want to thank each other for supporting and motivating one another.

[1] *https://www.multiconsult.no/*

1 INTRODUCTION

The word urbanization describes the process of people moving to urban areas from outside the cities. As more and more people move to the city centers, the need for residences and workplaces increase. It is beneficial to place large structures with many users close to the city center or public transport hubs. Having easy access to the workplace will also contribute to reduce the use of car transport and increase the use of "greener" transport methods such as public transport, walking or cycling. Still, it can be challenging to find available areas for new structures in these locations in dense cities. A solution is to design and build taller structures to utilize the area above ground, increasing the capacity of the same ground area compared to lower buildings.

When the height of structures increases, the horizontal loads like wind and seismic loads increase, as well as the consequences of severe damage or collapse. Several incidents of major earthquakes that have led to severe damage, both regarding human lives and economic expenses, can be mentioned. An earthquake that hit Kobe in Japan in 1995 resulted in more than 5000 lost human lives, more than 30.000 seriously injured people and more than 300.000 lost their home. Two other severe events were the earthquakes in Loma Prieta in 1989 and Northridge in 1994, due to which damage costs of more than US$ 50 billion occurred [1]. Therefore, it is necessary to design suitable lateral force resisting systems that can carry these loads and ensure a safe structure for the users and the surroundings. A widely used system in Norway is concrete shear walls, often seen as elevator shafts and stairwells. In this thesis, a mega-braced steel system, which is more frequently used other places in the world, will be compared to the traditional concrete shear wall system regarding seismic behavior.

Although Norway is considered a low seismicity region, structural engineers are required to perform seismic design according to Eurocode 8 [2], further referred to as EC8. There are different methods to perform a seismic analysis with various accuracy and complexity. The time-history analysis is a nonlinear dynamic analysis and is the most time consuming and complex type of seismic analysis. Both modal and direct integration can be performed. The modal analysis uses modal superposition while the direct integration analysis solves the full equations of motion without modal superposition. Both of these methods are introduced in Chapter 3.2.

Even though the time-history analysis provides the "exact" solution, it is not widely used in everyday engineering routine due to the complexity and time commitment [3]. Another simpler

method is the pushover method, which is a nonlinear static analysis. In this analysis, a calculated target deformation, which represents the expected deformation during a design earthquake, is monotonically applied until the value is reached. Further introduction of the pushover analysis is included in Chapter 3.1. This method is recommended in several codes, including EC8 [2]. Even though the results are not as accurate as those obtained from a time-history analysis, it provides more results compared to the simpler linear analyses. In addition, it is a lot less time consuming compared to the time-history analysis.

In this thesis, the seismic performance of the two lateral force resisting systems will be evaluated using both pushover and time-history analyses. In addition, a relatively new method of using friction dampers as a lateral force resisting system analyzed through fast nonlinear analysis will be studied. Further, the results of the three nonlinear analyses will be compared, regarding variation in results, complexity and time investment.

1.1 Objectives

The aim of this report is to compare the seismic behavior of two different core systems – concrete shear walls and mega-braced steel frames – in high rise buildings. Through nonlinear static and dynamic analyses, the seismic behavior of these lateral force resisting systems will be studied and compared.

The main objective of the study is:

“Comparison of two different lateral force resisting systems in high-rise buildings with regard to seismic performance”

The secondary objectives of this study are:

- Conduct a literature review on different lateral force resisting systems and nonlinear static and dynamic analysis
- Design an alternative lateral force resisting system using mega-braced steel frames
- Perform nonlinear static and dynamic analyses on the shear wall and MBF structure
- Compare seismic behavior of the shear wall and MBF structure by studying factors such as base shear, roof displacement, drift ratio and hinge formation
- Compare the results of nonlinear static and dynamic analyses regarding variation in results, complexity and time investment

1.2 Outline of the Thesis

This thesis consists of seven chapters and two appendices. A short description of each chapter is given as follows:

Chapter 1 – Introduction

In this chapter an introduction to high-rise structures and lateral force resisting systems is given. Further, the objectives of the thesis are presented.

Chapter 2 – Seismic Design

This chapter introduces some of the seismic design codes in Europe and USA and describes the lateral force resisting systems that will be analyzed in the study.

Chapter 3 – Seismic Analysis Methods

The principles of the seismic analysis methods, pushover analysis and time-history analysis, are described and the methods are reviewed through previous studies.

Chapter 4 – Modelling

In this chapter, the case study building is introduced and the method of establishing the model and executing the analyses are described.

Chapter 5 – Results

The results of the nonlinear static and dynamic analyses are presented. Further, the two LFRS and the nonlinear analysis methods are compared.

Chapter 6 – Discussion

In the first subchapter the results of the analyses of the two substructures are assessed and discussed. Further, the second subchapter contains a discussion of the pushover and the time-history analyses.

Chapter 7 – Concluding Remarks

This chapter presents the concluding remarks of the study.

Recommendations for Further Work

Based on the findings of this study, scope of further work is proposed.

Appendices

Appendix A contains calculations of the applied loads for design of the steel MBF. In appendix B, the target displacements used in the pushover analyses are calculated.

2 SEISMIC DESIGN

2.1 Earthquake Effects on Structures

A significant factor affecting the structure that experiences seismic loading is the combination of acceleration and duration of the earthquake. If subjected to repeatedly moderate acceleration cycles, this can be harder to withstand than a single acceleration cycle of notable larger magnitude, as a constant shaking over time tears down the structure of the building. The ground type below the structure is also of great significance as, although the velocity of the ground is slow, the acceleration can be amplified depending on the ground shaking intensity, the ground type and depth. Earthquakes tend to cause more damage for buildings located on soft ground [4].

The natural period of an object is the period at which this object will continue to vibrate if it is given a push. When a structure is subjected to a seismic wave, it will continue to vibrate at its natural period. Building height is an important factor affecting the natural period. For low buildings of four stories a period of 0,5 s is common, while for structures of 10-20 stories 1-2 s is common. If an earthquake ground motion imparts a push to a structure which is at its natural period, resonance may occur, and the vibration will increase up to four or five times compared to the initial vibration. This means that the greatest damage of a structure during seismic events occurs when the period is close to the structure's natural period [4]. A well-known example of this phenomena and the severe damages that can occur is the collapse of the Tacoma Narrows Bridge from 1940, which was caused by the severe damage due to resonance [5].

2.2 Seismic Design Codes

The purpose of standards and design codes is to provide guidelines for safe design of structures to protect human lives. In addition to permanent and frequent loads such as dead load, live load and forces from snow and wind, structures must also be designed to withstand forces from an earthquake. There is a general agreement in most codes that structures should not undergo collapse during or after a seismic event, and it should be possible for the structure to remain operational after an earthquake. There are rules, recommendations and assumptions that must be considered when performing seismic analysis for structures. Such information is given in standards and design codes.

EC8 [2] is the standard for design of structures with consideration to earthquakes in Europe and it consists of six parts. Part 1 includes basic performance requirements, general rules, seismic action, assumptions and rules for buildings with different materials. The remaining parts include

assessment and retrofitting of existing buildings, bridges, tanks, foundations and towers among other things. The purpose of EC8 [2] is to provide guidelines for design of structures in a way that human lives are protected, severe damage is limited and to ensure that important buildings remain operational after the earthquake. There are two fundamental requirements when designing a structure that withstands seismic action according to EC8 [2]. The first requirement is no-collapse, the structure shall be designed and constructed in a way that prevents any global or local collapse during a seismic event. Furthermore, the structural load bearing capacity should be retained after a seismic event. The second requirement is damage limitation, the structure should manage to withstand a seismic action with a bigger probability of occurrence than the design seismic action [2].

Table 2.1 Different US Design Codes and their content

US Design Code	**Content**
ASCE 7-16: Minimum Design Loads and Associated Criteria for Buildings and Other Structure [6]	Design load for earthquake and seismic maps
FEMA 356 – Prestandard and Commentary for the Seismic Rehabilitation of Buildings (FEMA356) [7]	Seismic rehabilitation for existing structures and the standard also consists of damage assessment on seismic performance
ASCE 41-13: Seismic Evaluation and Retrofit of Existing Buildings [8]	Procedures for seismic evaluation and for seismic retrofit of existing buildings
ATC 40 Seismic Evaluation and Retrofit of Concrete Buildings [9]	Seismic design criteria for concrete structures
ANSI/AISC 341-16: Seismic Provisions for Structural Steel Buildings (ASCE341) [10]	Seismic design of steel structures

2.3 Assessment for Seismic Evaluation

Most seismic design codes today provide different methods for assessments of seismic evaluation. It is common to use either linear or nonlinear analyses to find design force and design displacement acting on a structure. EC8 [2] describes two linear analyses and two nonlinear analyses. The linear analyses are the lateral force method of analysis and the modal response spectrum analysis, and the nonlinear analyses are the nonlinear static (pushover)

analysis and the nonlinear dynamic (time-history) analysis. The nonlinear methods require state-of-the-art software, such as SAP2000, which can analyze advanced models to get applicable results [11].

2.4 Seismic Action

The definition of seismic action is unclear due to the large difference in seismic hazard characteristics in various countries. The definition is therefore modified in the National Annexes of the design codes and it is a general term in EC8 [2]. The seismic action can be represented in three different ways in EC8 [2], by response spectra, by power spectral density function and duration of strong motion and by a set of time histories of acceleration. The three representations should in theory effect the structure in the same way. Which representation is most beneficial depends on the type of structure and the type of analyses to perform [12].

The seismic hazard mainly depends on the location of the structure and the ground type beneath the structure, which has a significant impact on the applied force during an earthquake as the ground type highly affects the motion and acceleration of the ground. The ground acceleration during an earthquake can be represented by an elastic response spectrum, of which the magnitude also depends on the ground type and the location. The National Annex in EC8 [2] shows a map over different seismic zones in Norway with different reference peak ground acceleration, a_{g40Hz}, which corresponds to the reference return period, $T_{NCR,}$ of the seismic action the no-collapse requirement. Further, EC8 [2] states that in nonlinear methods, depending on the structure's geometry, the seismic action should be applied in both positive and negative directions [11].

2.5 Modeling

In seismic analyses, the structure should be modeled with a representation of mass and stiffness, so the natural frequencies can be easily computed. This way, a representation of the structure's mode shapes can be obtained. In addition, the mass and stiffness are important parameters affecting the structural behavior during a seismic event, not to mention that the stiffness reduces large deformations and drift, that may lead to severe damage. Further, EC8 [2] states that the distribution of capacity should be represented through a non-linear analysis. During the analysis, the joints between frame elements should be taken into consideration, essentially at the end of beams and columns, as it can contribute to the deformation of the structure [2].

A significant difference between linear static and linear dynamic is the level of forces and their distribution along the height of the structure. In linear dynamic analysis, a structure can be

defined through three key factors: stiffness, mass and damping. As nonlinear analyses require the estimation of yield load and post-yield behavior, nonlinear static and dynamic analyses may be considered beneficial compared to linear analyses. This is due to the possibility of analyzing inelastic behavior, which is more close to the actual performance [13].

As a structure moves, it dissipates energy through damping. If a structure is completely undamped, it would, when set in motion, vibrate indefinitely. There are various types of dampers with their respective methods of dissipating energy, e.g. the friction damper dissipates energy through friction. The friction damper is introduced in Chapter 2.6.3 and studied as an additional lateral force resisting system to the concrete shear walls and MBF. The damping ratio, ξ, can be assumed based on previous experience of similar structures. In structural engineering values of ξ ranging from 0,01-0,1 are common, and especially a ratio of 0,05 is frequently assumed [14].

2.6 Lateral Force Resisting Systems

When designing any structure, it is crucial to ensure that the structural members have adequate capacity to carry the occurring loads. The vertical loads, like dead-, live- and snow load are carried to the ground by the structural system consisting of walls, columns and beams. To carry the horizontal loads, like wind- and seismic loads, shear walls or frames of concrete or steel are common solutions. Another common solution in large structures is the use of various dampers to dissipate energy and reduce the impact from horizontal loads.

Whether or not tall buildings are more vulnerable to earthquakes than lower buildings depends on the stiffness of the structure as well as the magnitude and location of the earthquake. Tall buildings are more flexible and are associated with longer fundamental periods than lower buildings. Earthquakes generally release less energy at longer periods than they do at shorter periods, indicating that tall buildings may perform better during such events. On the other hand, earthquakes of greater magnitude release more energy at longer periods than smaller earthquakes. If such large earthquakes occur close to tall structures, the impact could be magnified due to effects from the proximity to the center of the earthquake [15].

As wind increases with height, and the surface the wind acts on gets larger with increased height, taller buildings will be subjected to larger horizontal loads than lower buildings. Although high-rise buildings are not necessarily more vulnerable to earthquake impacts, they will have greater consequences in the event of a collapse. A tall building requires a large amount of human and material resources and may be a home or a workplace for hundreds of people.

Thus, it is important to design a suitable lateral force resisting system (LFRS) to carry the horizontal loads and prevent great damage, or in worst case collapse, as a consequence of load impacts [15].

The aim of building codes in the United States that consider seismic loads are different at various magnitudes of earthquakes. For small earthquakes, the structure should be designed to suffer little or no structural damage. After moderate earthquakes, repairable structural damage is acceptable and for major earthquakes severe structural damage can occur, but loss of lives or limbs are not acceptable [15]. According to EC8 [2], a structure must be designed in a way such that during the event of an earthquake, human lives must be protected, structural damage is limited and that buildings that are important for the civil population remain operative.

Often a LFRS of concrete or steel, or a combination of both, is used. Some typical solutions are shear walls or various frames. In this thesis, concrete shear walls and mega-braced steel frames with and without dampers will be evaluated and compared as a LFRS of a high-rise building in Norway.

2.6.1 Concrete Shear Walls

A widely used solution in Norway is concrete shear walls. The shear walls are often used to form elevator shafts and stair wells in a building. The number of elevator shafts and stair wells can vary, depending on the size of the building. In such cases, the LFRS is a core system. Alternatively, the shear walls can be exterior, or both exterior and core shear walls can be used. This depends on the desired stiffness and behavior of the building, and it is also often affected by the architectural planning.

One of the properties of concrete is the high stiffness and thus the concrete shear walls have the ability to withstand lateral forces. Due to the high stiffness, combined with low tensile strength, the walls usually experience a non-linear behavior with reduced stiffness due to cracking of the material, even under the impact of service loads [16]. Therefore, the post-cracking properties of concrete is important when determining the behavior and deflection of concrete shear walls.

A study comparing different LFRS, both concrete and steel, of a 20-story building considered the seismic behavior of the various systems, as well as initial and repair costs. The results show that all systems investigated in this study exhibit acceptable seismic behavior, including the concrete shear walls. Further, the study indicates that for this building the damage and repair costs of the concrete shear walls are higher compared to steel frames, due to more expected damage during earthquakes, and that the initial costs are quite low compared to the alternatives

[17]. Still, the level of damage of the different systems will vary with magnitude and location of the earthquake, and thus the findings are only valid for this building with the conditions assumed for this particular dynamic analysis.

The lateral forces acting on a structure increase with increasing height, which will lead to increased forces acting on the shear walls. The American Society of Civil Engineers (ASCE) 7-10 [18] Standard prohibits the use of concrete shear walls as the only type of bracing in structures taller than 50-75 m that are located in high-seismicity areas [15]. Even though Norway is considered a low seismicity region, due to this prohibition, it is reasonable to investigate the possibility and potential advantages of using other types of LFRS. Additionally, stiffer structures generally attract higher ground accelerations, meaning that the structural members are subjected to greater forces, which also speaks in favor of choosing different solutions [1].

2.6.2 Mega-Braced Steel Frames

Another common LFRS in buildings is the steel moment resisting frame (MRF). In an MRF, the seismic forces are resisted by shear and flexure in the members and joints of the frame [19]. Under major earthquakes the MRF has proven to give large deformations, and thus recently more attention has been paid to braces to limit story drifts. This way, problems that ascend from geometric nonlinearities and fracture of beam-to-column connections can be avoided, also reducing the risk of severe damage on non-structural elements [20].

The steel braced frames act as vertical trusses with the columns acting as chords and the beams and braces correspond to the web members [19]. Several types of steel braced frames are used in structures today, with variations in geometry and amount of steel braces. Commonly, the different types are divided into concentrically braced frames (CBF) and eccentrically braced frames (EBF). In both the American Institute of Steel Construction (AISC) 341 [10] and EC8 [2] several geometries of CBF are defined – single diagonal, cross-bracing, V-bracing, inverted V-bracing and K-bracing. EC8 [2] also mentions y-bracing, which includes special cases where the braces are discontinuous. K-braced systems are prohibited for seismic design according to both provisions due to risk of plastic hinge formation in the middle of the column [21]. The members of a CBF are primarily exposed to axial forces [19]. Another system is the mega-braced frame, which stands out from the other mentioned LFRS by having diagonal braces that reach across more than one story. Figure 2-1 illustrates the difference between MRF, CBF and MBF, which are commonly used LFRS.

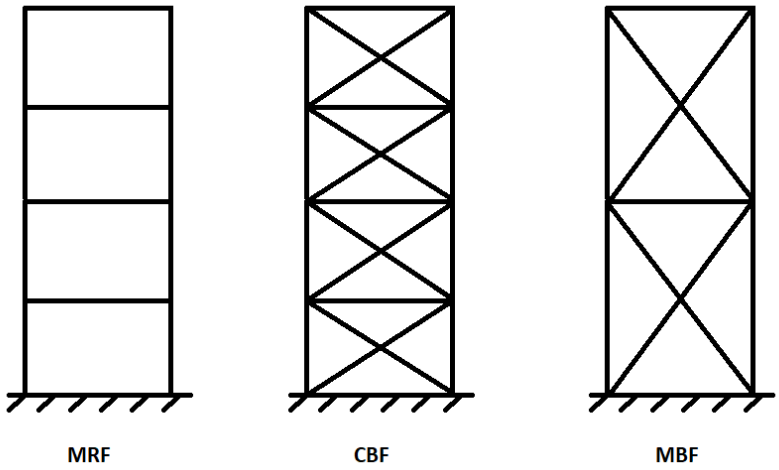

Figure 2-1 Illustration of MRF, CBF and MBF

According to AISC341 [10], FEMA273 [19] and EC8 [2], CBFs are defined as systems in which the horizontal forces are primarily carried by members subjected to axial forces [21]. According to FEMA273 [19], CBF are "braced systems whose worklines intersect at points". However, the provision allows minor eccentricities as long as these are accounted for in the design [19]. When the CBF is subjected to lateral loads, some braces are in compression and some are in tension. Ideally, if buckling occurs in the compression braces and the load carrying capacity and stiffness is reduced, the forces are redistributed to the braces in tension. The post-buckling capacity and behavior should be considered in a realistic model. However, AISC341 [10] usually considers the pre-buckled stage of the braces while EC8 [2] considers both the pre- and post-buckled stage, depending on the current case. For cases in which both the pre- and post-buckled stage is considered for design, the model includes the braces in both compression and tension. If the post-buckled stage is to be considered, only the braces under tension are included, termed tension-only bracing. As the tension-only bracing method is conservative, it leads to lower lateral stiffness and increased periods of vibration compared to a case in which also the compression braces are included. AISC341[10] prohibits the tension-only bracing, while EC8 [2] allows it for some types of braces [21].

Today CBFs are commonly used as LFRS for steel structures, carrying horizontal forces ascending from wind and earthquakes. Studies have shown that using steel braced frames as LFRS can be economical and effective during wind and moderate earthquakes [22].

Both MRF and CBF have been popular solutions as LFRS in structures, and they both have their advantages and disadvantages. While MRF provide more architectural freedom due to fewer members, CBF provide more stiffness and stability to the structure. CBF has also in

several cases been preferred due to the economic benefits, as MRF is more costly. After fracture incidents such as during 1995 Kobe and 1994 Northridge earthquakes, modifications done to improve the MRF increased the costs and CBF became even more economical and popular. Fracture of several EBF during an earthquake in New Zealand in 2011 further increased the popularity of CBF. Today the CBF is one of the most widely used LFRS in steel structures, being economically friendly, easy to design and considered efficient for controlling lateral displacement of buildings during wind and earthquakes [21].

Several studies show that braced frames lead to improved seismic behavior compared to MRF [23]. Patil and Sangle [24] showed through their study that CBF leads to reduced story drift and lateral displacement compared to MRF. A study performed by Alshamrani et al. [25] showed that by using CBF instead of MRF as LFRS in a 40-story building, the lateral drift was reduced by 24 %. The same study indicated that core system is more efficient than exterior frames. Still, it should be noted that these results are valid for high-rise buildings subjected to strong wind forces and seismic behavior has not been investigated in this study [25].

Kioumarsi et al. [26] conducted a study comparing different LFRS. The LFRS included in the research were special moment resisting frames (SMRF), dual MRF-CBF and dual MRF and MBF, which is considered a special CBF (SCBF). The results revealed that CBF provided the maximum stiffness, which can be disadvantageous in case of seismic events. Oppositely, SMRF provided the minimum stiffness. The main scope of the study was to investigate the effect of span lengths on the LFRS mentioned above. The different frames were analyzed for the different span lengths in twelve 15-story buildings, and according to the results CBF is more affected by variations in aspect ratio compared to the other LFRS investigated. Further, the MBF system lead to the lowest story drift and lateral displacement, which was also found in the study by L. Di Sarno and A. S. Elnashai [27].

2.6.3 Friction Dampers

Although steel braced frames are considered effective in controlling lateral deformations, their performance during severe earthquakes are not necessarily adequate as their ability to dissipate seismic energy is limited [1]. Thus, another method to reduce the seismic demands on structures has been proposed by researchers. The method involves adding passive energy dissipating devices, i.e. dampers, to the structural system of new or existing buildings. The purpose of a damper is to reduce the impact from horizontal loads on the structure in such a way that the

other structural elements remain in the elastic phase, i.e. avoid inelastic deformations. This way, the damper functions as a “sacrificial” element [28].

By installing damping devices in a structure, supplemental damping of 20-50 % can be achieved, compared to the inherent damping with no damping device of 1-5 %. Such devices reduce the forces acting on the structure, the deformations and the amplitude of vibrations significantly. Further, this can lead to reduced drifts with a factor of 2-3, and according to FEMA356 [7] even larger factors if the device provides stiffness [22].

Dampers can be divided into two categories – hysteretic and viscoelastic. The hysteretic dampers are affected by the displacement of the elements that are located within the device and dissipate energy by either metallic yielding or friction between two surfaces. Viscoelastic dampers are affected by velocity [28]. Friction dampers bear several advantages compared to the aforementioned dampers. Compared to viscoelastic dampers, the maximum earthquake force is well defined, as for viscoelastic dampers it is affected by velocity. Furthermore, as the friction damper is velocity independent, the force exerted by the damper is constant for all earthquakes, making the design of connections and members more economical. A friction damper also adds stiffness to the structure, unlike viscous dampers, which will help avoid overturning of the structure. Another advantage is that 70 friction dampers will provide the same damping as 100 viscous dampers, i.e. the friction damper exerts only 70 % of the forces compared to viscous dampers. This is also economically beneficial [22].

The friction damper also has several advantages compared to other hysteretic devices. The hysteretic devices that dissipate energy by metallic yielding require repair or replacement after an earthquake, unlike friction dampers, which remain functional. In addition, metallic yielding devices may be damaged due to fatigue after being frequently subjected to wind loads which introduces a need for regular inspections [1]. Consequently, due to repairs, replacement and inspections, the metallic yielding devices can potentially cause more economical expenses.

The friction damping devices was developed in the late 1970s. There exist friction dampers suitable for various structural systems, among these are concrete shear walls, steel braced frames, concrete frames and low-rise buildings [1]. A widely used friction damper is the Pall friction damper, further referred to as friction damper in this chapter, which was developed in the late 1970s. This new damping device was based on the concept of the friction brake, which is an effective, reliable and economical tool to dissipate energy and have been used in airplanes, cars etc. for centuries. The device consists of steel plates that are treated to develop reliable

friction. The steel plates are clamped together and allowed to slip at a specified slip load. These dampers can be bolted or welded when installed [22].

Studies have shown that the friction dampers are inexpensive and simple in construction. Proof tests with shake tables were performed of the Pall friction dampers in 1986-1987. The results showed that even at large accelerations the friction-damped braced frame suffered no damage, compared to the conventional braced frames which suffered significant damage at lower accelerations [22], [29].

In friction dampers, the energy from e.g. seismic loads is dissipated through the friction that occurs when two surfaces are sliding relative to each other. When designing a structural system with friction dampers, the damper is designed with a slip load. The slip load can be set to a value which can lead to optimum behavior of the structure during impact of lateral loads [1], [30]. Studies have shown that the optimum slip load value is a structural property rather than an earthquake motion-dependent parameter. Further, results have shown that a variation of $\pm 20\%$ of the slip load does not significantly affect the seismic response. If the slip load is very low or very high, the response is high. It is also stated that the natural period of structures supplied with friction dampers varies with the magnitude of the earthquake, which eliminates the risk of resonance during ground motions from earthquakes [1], [22].

Friction dampers are designed not to slip under the impact of wind loads or moderate earthquakes, and during major earthquakes the damper should slip, i.e. reach slip load, prior to the initiation of yielding of the remaining structural members [1], [30]. Optimally, this means that the design slip load of the friction damper is reached simultaneously as the internal forces in the structural system reaches the highest acceptable value during impact of the seismic loads. Further, the peak interstory drift should be obtained at the same time as the maximum slip distance provided by the friction damper is reached [28].

During major earthquakes, the slipping of friction dampers is similar to the elasto-plastic behavior of steel. This means that the hysteretic loop of the friction damper is like the shape of the loop of an elastic-perfectly plastic material, with the slip load corresponding to the yield force of such a material [1].

Studies have shown that Pall friction dampers are a practical and economical supplement to structures undergoing seismic action. An experiment conducted by Chandra et al. [29] showed a reduction in the seismic forces acting on a structure equipped with friction dampers, which leads to reduced material use. Further, the conclusion of their study states that a friction-damped

structure should perform satisfyingly during a major earthquake, which in turn leads to lower need of repairs [29]. The reduced material usage and repair need can potentially reduce both the initial and total costs of the structure.

Building codes providing design criteria regarding seismic behavior does not explicitly apply to friction-damped structures. Still, some building codes allow the use of friction dampers for seismic control of structures. The requirement is that it must, through nonlinear analysis, be documented that the behavior of the structure is equal or better than a non-friction-damped structure [29]. As described in Chapter 2.2, the criterion in conventional building codes is that a structure should be designed in a way that it does not suffer severe damage and does not collapse during a major earthquake.

Friction dampers can be installed in line with the braces in single-diagonal or chevron braced frames, at the intersection of X-braces or in parallel with the beam located at the top of chevron braced frames [28]. After an earthquake, frictions dampers are not in need of repairs, maintenance of repairs, which can be economically beneficial. Building codes in Canada, United States and several other countries accept the use of friction dampers in structures [1].

The first building in North America built with seismic dampers was equipped with friction dampers. Later, friction dampers have been used for seismic protection of more than 80 buildings (number from 2004), both new and existing, in several countries. The applications are, among others, hospitals, telecommunication buildings, educational institutions, police headquarters, office buildings and residential buildings. To highlight economical savings, The City and County of San Francisco saved US$ 2.25 million after using friction dampers for seismic control of Moscone West Convention Center compared to viscous dampers. The concept has also saved Boeing US$ 30 million, who has used the friction dampers in one of their airplane factories in Washington, which is the largest building in the world, measured in volume [22].

3 SEISMIC ANALYSIS METHODS

3.1 Pushover Analysis

Pushover analysis is a nonlinear static analysis and a frequently used tool for evaluation of seismic performance and behavior of new and existing structures [31]. The pushover method is recommended in several performance-based design codes, such as ATC-40 [9] and EC8 [2]. Using this method, the structural behavior during an earthquake can be predicted [32].

The pushover analysis is based on a target displacement or force approach for predicting the behavior of the structure under seismic loading. The method involves applying a calculated displacement or force on the top of the structure to compute a pushover curve. The structure is exposed to a monotonically applied incremental lateral load and will slowly be "pushed". During this application of a horizontal displacement, a reaction base shear force occurs at the base of the structure relative to the displacement at the roof. This will represent the relative inertia forces generated at the mass-center in each floor [33].

Plastic behavior like hinge formation, cracks and yielding will take place, finally resulting in failure of structural elements. Further, the information obtained from the pushover curve can be used to calculate the target displacement according to EC8 [2], or the desired design code. After the target displacement is calculated, it is used to find the seismic capacity and seismic demands of the structure. The seismic capacity shows the structure's ability to resist earthquake effects and the seismic demands provide a description of the earthquake effect [33].

During an earthquake, structures are subjected to large forces and will potentially cause yielding or damage of structural elements. As elements yield or fail, the forces will be redistributed to be carried by other components. When performing a pushover analysis using the traditional method, loads representing the intertial forces from the ground acceleration are gradually applied in an invariant load pattern until the weaker parts of the structure are identified, i.e. the elements that become the first to yield or fail. The process is repeated until a complete yield pattern during the earthquake is identified [3].

The analysis provides an approximate solution, unlike nonlinear time-history analysis which is an "exact" method. The method described in FEMA356 [7] and ATC-40 [9] are widely used and they are similar to the pushover analysis in EC8 [2] with the target displacement approach. The coefficient method (CM) is defined in FEMA356 [7] and the capacity spectrum method (CSM) is defined in ATC40 [9]. The CM is a displacement modification procedure in which

the target displacement is calculated by modifying displacement of a linear-elastic system by several empirically derived factors to modify the response. The CSM is a type of equivalent linearization where the target displacement is found by multiplying the fundamental mode participation by the elastic displacement of a single-degree-of-freedom (SDOF) system. To estimate the displacement of an equivalent linear SDOF system, the CSM uses empirical relationships for the effective period and damping as a function of ductility [34], [35]. Thus, the behavior of the structure is expressed by a single mode, the fundamental mode, which keeps a constant shape during the earthquake, including after the structure yields. Although this is an approximate assumption after the structured has experienced yielding, studies have shown that the traditional pushover method provides satisfying precision of the response, presumed that the actual response is dominated by a single mode, specifically the fundamental mode [1].

3.1.1 Previous Studies

In some cases, the conventional pushover analysis is limited, as it only considers the fundamental mode and does not provide accurate results for systems dominated by higher modes. Consequently, the accuracy of the procedure is questionable, and some cases report of 75 % error compared to nonlinear time-history analysis [4].

Compared to elastic static or dynamic analysis, the nonlinear static pushover analysis can provide more results, some of which are: force demands on elements, consequences of weaker individual elements on the behavior of the whole structure, identification of critical components and estimation of interstory drift due to the discontinuity of strength and stiffness after deterioration of individual elements [31].

The purpose of the pushover analysis is to evaluate the expected performance of a structural system during an earthquake. Demands regarding strength and deformation from the analysis results are compared against demands for the required performance level of the structure. Parameters evaluated are, among others, global drift, interstory drift, inelastic element deformations, element- and connection forces and identification of weak points in the structure [31].

In general, the pushover analysis is not applicable for irregular buildings, tall buildings or buildings with long period. Still, the procedure has become popular in engineering routine especially for regular structures, as more and more software provide it. To obtain “exact” results, a non-linear time-history analysis should be performed. This is not widely used in

engineering practice, due to it being highly complex and time consuming compared to the static pushover analysis [3].

Currently, there are several versions of the pushover analysis that are used, with varying complexity and accuracy. The most widely known are the traditional, the modal and the adaptive procedure. The traditional pushover analysis only considers the fundamental mode, which may cause inaccurate results if the response of the structure is dominated by higher modes. Some cases have reported an error of 75 % compared to those of nonlinear time-history analysis [3].

The development of the modal pushover analysis (MPA) was performed by Chopra and Goel [36]. The procedure is equivalent to the traditional and assumes that the response is controlled by the fundamental mode. A significant difference is that MPA considers more mode shapes, often two or three. The peak response values from all the modes are then combined using the square root of the sum of squares (SRSS) method. Performing this analysis, the horizontal forces are statically applied such that the desired mode shape is obtained. The mode shape is, as in the traditional analysis, kept constant throughout the analysis even though elements yield or fail. Both the assumption that the response is dominated by the fundamental mode as well as the constant mode shape makes this procedure approximate [36].

Studies show that the MPA can provide satisfyingly accurate results regarding roof displacement and story drifts and locations of most plastic hinges. On the other hand, the plastic hinge rotations obtained from an MPA have shown a significant error compared to nonlinear time-history analysis. As the MPA considers higher mode shapes than the traditional approach, and the procedure has proven successful to estimate the contributions from higher modes on the behavior of the structure. Still, the method should not be used for buildings that deform far into the inelastic range [3]. When a structure deforms into the inelastic range, it experiences gradual degradation and softening, which results in longer period and changes in the mode shape [37].

Several studies have been conducted to investigate the accuracy of the MPA procedure. Boonyapinyo et al. [38] did research on the accuracy of pushover analysis and MPA for reinforced concrete buildings. They concluded that MPA is satisfyingly accurate for seismic performance evaluation compared to nonlinear dynamic analysis procedures for story drift of higher floors and a slight overestimation of the lower floors [38].

Oğuz [39] did research with another approach, investigating the accuracy of MPA for different frame heights and different load patterns. The results showed that the pushover analysis generally provided accurate results for low to mid-rise frames. For high-rise frames, which in this study was 12 stories, the accuracy of the story drift ratio decreased due to the contribution of higher modes. In addition, the accuracy was reduced when the frame deformed in the inelastic range, supporting the statement that pushover analysis is not applicable for such structures. Generally, the uniform load pattern lead to unacceptable demands compared to that of the triangular load pattern, but both patterns deviated from the "exact" solution. Furthermore, the predictions from the MPA were similar to, or more accurate, than the triangular load pattern according to this study [39]. These results were in agreement with those of Taghinezhad's study [40], which showed negligible error of 7,5 % for a 3-story frame, 19,1 % for a 6-story frame and 22,6 % for a 9-story frame under the influence of a uniform load pattern. For multimode load patterns the results were more accurate regarding story drifts, resulting in the lowest error values in this study [40].

In their study, Hassan and Reyes [3] performed MPA for mid-rise concrete buildings. The results showed that the procedure lead to an overestimation of peak floor displacement over the height. Maximum error of 30.2 % was found in the 5^{th} floor, and minimum error of 6,5 % was detected in the 1^{st} floor. Further, the interstory drift ratio varied from an underestimation of 11,6 % to an overestimation of 27,3 %, compared to nonlinear time-history analysis. Regarding the peak floor displacement, one mode alone was adequate to obtain satisfyingly accurate results, while two or three modes were required to get accurate results of the interstory drift ratio [3].

In general, MPA is considered a strong competitor to NL-RHA, especially due to the significant savings in computational efforts and time spent. It has been shown that the procedure provides satisfyingly accurate results for estimation of seismic response, especially for structures like frame structures [41].

Although the MPA is an improvement compared to the traditional pushover analysis procedure, it has some limitations. For instance, the total response is calculated using modal combination rules like SRSS, which is considered a rough estimate when the response is non-linear. In addition, the total deformed shape is determined by using superposition of the deformed shape of each mode, which is valid only in the elastic range [41].

Due to these limitations, among others, Chopra and Goel [36] developed a modified MPA procedure. This new method includes the PΔ-effects from the gravity loads for all modes. Further, the plastic rotations are determined from the value of total story drifts. In the "unmodified" procedure, the value of plastic rotations was determined from gravity load and MPA. This method takes into consideration an assumed value of peak roof displacement and uses this as a basis for an idealization of the pushover curve, which to some extent depends on the ground motion.

After the development of the modified procedure, Chopra and Goel [36] evaluated the method regarding estimation of story drift demands on six buildings with 9 and 20 stories. The study showed that by including more modes, the story drift distribution and plastic rotations of beams were similar to the results conducted by NL-RHA. The results also indicated that the PΔ-effects increased the bias in the MPA for buildings that deform in the inelastic range. For buildings with large story drift that causes a sudden decrease in lateral capacity, the bias can be larger. In conclusion, Chopra and Goel [36] found that the MPA results regarding story-drift and plastic rotations of beams is satisfyingly accurate, compared to NL-RHA. However, they expect that the bias is at an unacceptable level for buildings that deform far into the inelastic range, and that in such cases non-linear time-history analysis should be performed to estimate seismic demands.

In general, there are some approximations related to the MPA procedure. When performing MPA, the total response is estimated using SRSS combination. According to Chopra and Goel [36], using the SRSS method to calculate the total response has 15-28 % error, while neglecting modal coupling in steel buildings has a small error of less than 5 %, provided that the building is not highly elastic. Additionally, a significant approximation to the MPA and the traditional pushover analysis, is that the model is not modified after yielding or damage, and thus a new procedure is developed, called adaptive pushover analysis.

3.2 Time-History Analysis

Time-history analysis is a nonlinear dynamic analysis method mentioned in EC8 [2], among other codes. It is based on using real recorded ground motions from previous earthquakes or generated artificial ground motions, which is usually defined by ground acceleration or velocity over time. As earthquakes are random in nature, they are also difficult to predict. For the nonlinear time-history analysis, EC8 [2] requires that at least three records of ground motion are to be used which are representable for the location of the building. EC8 [2] further states

that the response which is most unfavorable among the time-history analysis should be used as the design value of the action effect for the structure. If seven records are used, an average response from all the analysis should be used for the seismic evaluation.

Nonlinear time-history analysis is a step-by-step dynamic analysis that is used to determine the dynamic response of a structure subjected to arbitrary loading that may vary with time. The method is based on the direct numerical integration of the differential equations of motion by considering the elasto-plastic deformation of the structural element [13]. The dynamic equilibrium equations that are to be solved are given by Eq. 1 [42]:

$$Ku(t) + C\dot{u}(t) + M\ddot{u}(t) = r(t) \tag{1}$$

where *K* is the stiffness matrix, *C* is the damping matrix, *M* is the diagonal mass matrix and u, $\dot{u}$, and $\ddot{u}$ are the displacements, velocities and accelerations of the structure and *r* is the applied load [42].

The applied load, *r(t),* in a load case can be a function of space and time and can be written as a sum of spatial load vectors multiplied by time functions. The spatial load vectors are represented by load patterns or acceleration loads in a load case. If acceleration loads are used, the displacements, velocities and accelerations are measured relative to the ground [42].

Time-history is considered the "exact" solution of a structure's behavior, but is not commonly used in everyday engineering as it is significantly more time consuming and computationally demanding compared to e.g. response spectrum analysis and pushover analysis, which are often proved to provide satisfactory accurate results and therefore more commonly used methods [31].

3.2.1 Modal Time-History Analysis

Modal superposition provides a highly efficient procedure for performing time-history analysis. Performing this analysis, numerical instability problems never occur. The time increment can be defined as any value as long as it is fine enough to capture maximum response values. It is usually recommended to define the time increment as 1/10 of the time period of the highest mode, but if the contribution of higher modes is small, the value can be even larger without necessarily reducing the accuracy. The modes are computed from a modal analysis and for the modal time-history analysis Ritz-vector modes are used instead of eigenvectors. Ritz-vector algorithms are faster than those of eigenvectors as only the modes in the relevant frequency range are calculated, and these are usually recommended for time-history analyses [42], [43].

Another important factor is that the nonlinearities of a structure is broken down to a lump of elements with nonlinearity in only a few degrees of freedom. The method can be sensitive to physical parameters and loading conditions, especially for irregular structures and structures with advanced nonlinearity [44].

The modal damping in the structure is modeled using uncoupled modal damping. Each mode has a damping ratio which can be defined for each time-history load case. The modal damping ratios can either be constant for all modes, linearly interpolated depending on period or frequency or proportional to mass and stiffness [42].

3.2.2 Direct Integration Time-History Analysis

The direct integration method performs direct integration of the full equations of motion without modal superposition. Ideally, both the modal and the direct integration method should yield the same results, but the direct integration method is in some cases considered less accurate and less efficient than modal analysis. Another limitation is that the method is sensitive to size of the time-steps, unlike modal analysis. Still, this can be solved by running the analysis with gradually decreasing the time-step size until the steps are small enough to not affect the reliability of the results. Although this method has some disadvantages, there are also several benefits. By using this method, full damping that couples the modes can be considered, and for problems which excite several modes this can be a more efficient approach. In addition, this method considers more types of nonlinearity than modal analysis [42].

3.2.3 Previous Studies

As mentioned, time-history analysis is not commonly used in everyday engineering, due to increased complexity and thus computational effort and time investment. The challenges of this method are to reduce the complexity and increase the knowledge related to inspection of the results to make good design choices. Additionally, the software developer bears a responsibility to define efficient ways of displaying the results. Another challenge is that the analysis requires a set of ground motions that are representative for the building’s location [45].

Although there are some challenges related to the time-history analysis, there are several advantages to this method, especially considering accuracy of results. The time-history analysis is often considered to provide the results which are closest to the accurate solution. Especially for structures where other modes, than the fundamental mode, are important. The pushover analysis, which is a commonly used alternative to observe nonlinear behavior, occasionally falls

short, and time-history analysis can be a more suitable method. Thus, time-history analysis is by many considered the most appropriate method for safety check of structures [13].

Mohan and Prabha [46] performed a study comparing linear and nonlinear static and dynamic analysis of a 7- and 11-story RC core building with varying shear wall shapes in SAP2000. For the 7-story building with L-shaped shear frame, a variation of 42,55 % in story drift between the results of response spectrum and time-history analysis occurred. This was the highest detected deviation for the various shear frame shapes, but the variation in results of the two types of analyses were generally significant. For the 11-story building, the detected deviations between the results of the two methods were even higher, with the highest deviation being 61,39 % for a U-shaped shear frame. Thus, the results of this study indicate that for taller buildings the nonlinear dynamic method is preferable as the linear dynamic method is inaccurate. Mohan and Prahba [46] also concluded that the square shaped shear frame is most effective, and the L-shaped shear frame is least effective.

On October 23rd 2011, the Van earthquake in Turkey resulted in collapse of a RC building that was designed according to the 1975 Turkish Earthquake Code [47] (TEC-1975). In retrospect, a study has been conducted to evaluate the seismic performance of this building according to TEC-2007 [48]. To assess the performance, pushover and time-history analyses have been performed. Both analyses resulted in collapse performance level under earthquake loading. The authors suggest that this poor seismic behavior is caused by several factors – insufficient amount of transverse reinforcement, poor workmanship and concrete quality and insufficient steel detailing, which have been observed from the remaining elements of the building's ruins. Lack of shear walls and structural irregularities are also factors affecting the structural behavior [49].

According to both the pushover and time-history analysis, the building did not satisfy life safety (LS) performance level, due to significant damage in several structural elements, although this performance level was expected according to TEC-2007 [48]. Comparison of the results from the two methods showed that the pushover analysis underestimated damage level of structural elements compared to the time-history analysis. Still, considering the reduction in computational effort and complexity, the authors still recommend the pushover analysis and deemed it satisfyingly accurate [49].

In a study from 2011, Krawinkler et al. [45] compared the pushover analysis and time-history analysis' ability to predict nonlinear behavior of structures. Through several analyses, it was

observed that the accuracy of the single-mode pushover analysis was highly dependent on factors like system type, first mode mass participation, amount of inelastic deformations, variation of story strength and stiffness over structure height and the mechanisms governing the inelastic behavior. For the regular 2-story structures used in this study, the results from the pushover analysis were in good agreement with those of the time-history analysis. It was observed that the deviation between the two methods increased with increasing structure height.

The accuracy of time-history analysis was validated through comparison with a shaking table experiment conducted by Goggins and Salawdeh [50]. The results of the numerical analysis were in good agreement with the response obtained from the shaking table test considering the properties maximum displacement, base shear, dissipated energy and viscous damping. The temporary displacements and forces of the CBFs tested in this study were adequately predicted from the time-history analysis as well. The mean value of displacement and base shear from the analysis results were 0,87 and 1,11, respectively, of those measured from the shaking table. Although these values were well predicted by the analyses, total energy dissipated by most of the test frames was underestimated. This inaccuracy probably occurred as the connections between beams and columns in the model were perfectly pinned, which will not dissipate energy and may not be the realistic case. In addition to this, other probable energy dissipation phenomena may have caused an underestimation of total dissipated energy. In conclusion, the authors state that the nonlinear time-history analysis is suitable for predicting the seismic response of CBF when including material and geometric nonlinearities. Further, they suggest that also in the future, when developing seismic design methodologies, these should be validated through experimental testing [50].

4 MODELLING

In this chapter, the methods used for modeling the structures, designing structural members and performing the nonlinear analyses are described.

4.1 Case Study Building

The building used for the analyses in this thesis is an imaginary 16-story commercial building based on drawings of a commercial building in Oslo. All drawings and details of the building have been provided by Multiconsult AS[2]. It is chosen to locate the building in Bremanger in Western Norway, which, according to Figure NA.3(901) in EC8 [2], is one of the most high-seismicity regions in Norway.

4.1.1 Geometry

The geometry is simplified compared to the original building, which is shown in a three-dimensional (3D) view in Figure 4-1.

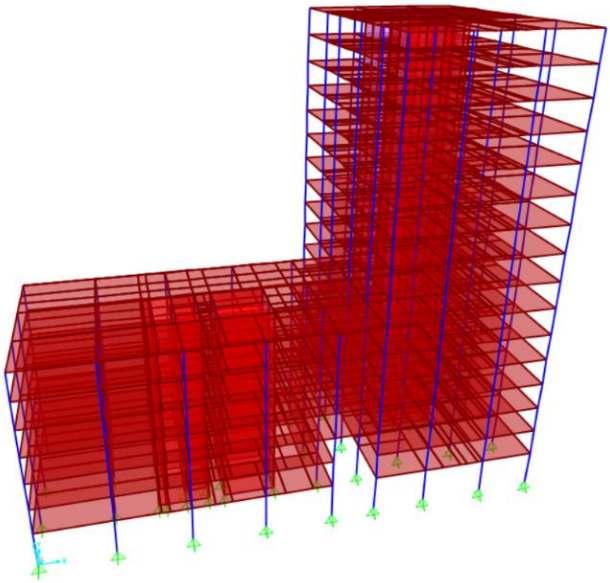

Figure 4-1 Three-dimensional (3D) view of the structure

As can be seen from Figure 4-1, there are some changes in the plan view along the height of the structure. In the first three stories of the building, the building consists of two separate parts, as shown in Figure 4-2. Hereafter, the two parts are called the lower part of the building (left) and the taller part of the building (right).

[2] *https://www.multiconsult.no/*

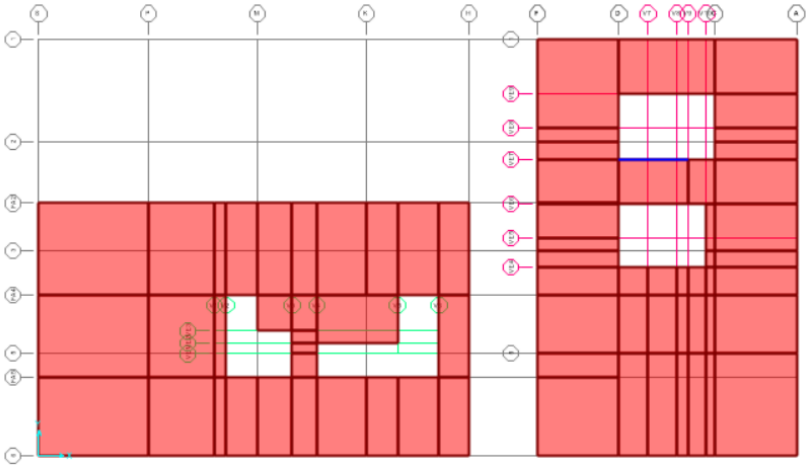

Figure 4-2 Story 1-3, consisting of two separate parts.

From story 4-7, the two parts are connected as shown in Figure 4-3.

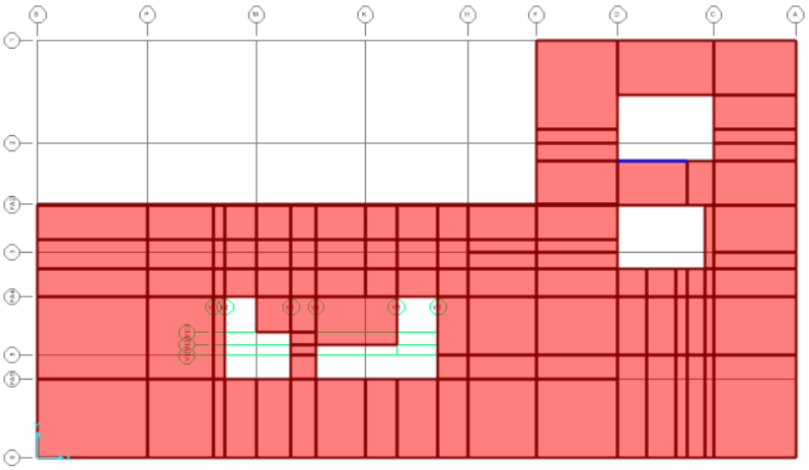

Figure 4-3 Story 4-7, the two parts are connected

Above story 7, only the taller part of the building continues, as shown in Figure 4-4.

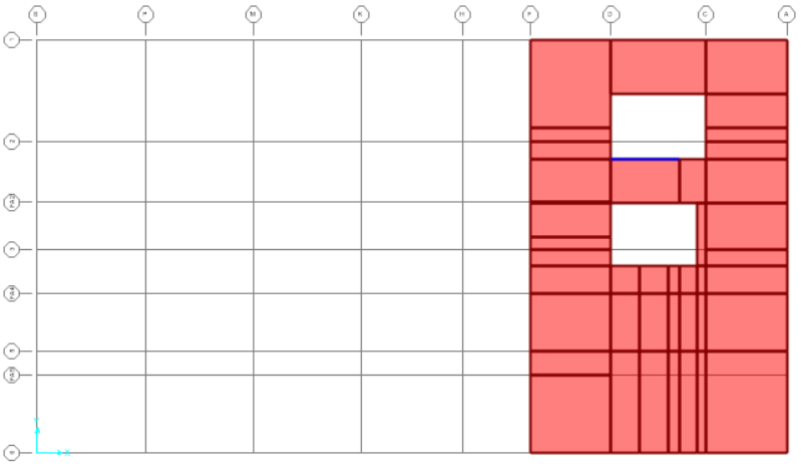

Figure 4-4 Story 7-15, only the taller part of the building

The figures also show that there are four shafts in total in the core of the building, consisting of concrete shear walls, representing the LFRS of the building.

4.2 Model

The model is based on models and drawings received from the designers of the structural system, and for the shear wall building the dimensions are kept the same as for the real structure, with some simplifications. For the MBF building, all elements are kept the same besides the concrete shear walls that are replaced by steel frame elements.

4.2.1 Grids

The first step of modelling the structure is defining grids according to the drawings. As mentioned, some adjustments have been made to simplify the geometry of the structure, and thus the grid is slightly modified.

In Figure 4-5 the main grid encloses the whole building and is drawn with grey color, while the shear wall grids for the lower and taller part of the building are drawn in green and pink, respectively.

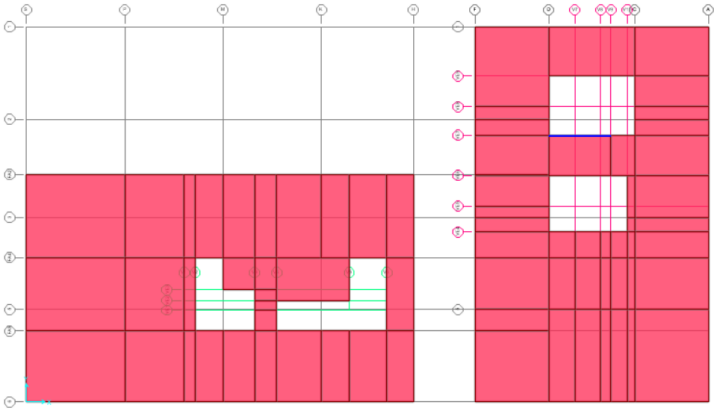

Figure 4-5 Separate grids

4.2.2 Loads

The applied loads are calculated according to EC8 [2] and are used for designing the steel members in the MBF.

4.2.2.1 Applied Dead Load

Additional dead load represents the non-structural elements of the structure. The value of this load is applied according to the received drawings. The applied additional dead load is 2,5 kN/m^2 and 1,5 kN/m^2 for the lower and taller part of the building, respectively.

4.2.2.2 Live Load

The two parts have different magnitudes of live load, due to different usage. On the lower part, an area live load with magnitude of $5{,}0\ kN/m^2$ is applied, while on the taller part the live load is $3{,}0\ kN/m^2$. The live loads are gathered from the received drawings of the commercial building.

4.2.2.3 Snow Load

The snow load is applied to the roof of both the lower and taller part, and is calculated according to EC1-3 [51]. From the National Annex of Norway, characteristic snow load on ground, $S_{k,0}$, is set to $2{,}5\ kN/m^2$. The design snow load on the taller part of the building is calculated according to Equation (5.1) in EC1-3 [51], shown in Eq. 2:

$$S = \mu_i \cdot C_e \cdot C_t \cdot S_k \tag{2}$$

where μ_i depends on the roof angle, which is flat for both the lower and taller part of the building. C_e is the terrain factor, C_t is the thermal coefficient and S_k is characteristic snow load on ground, which is equal to $S_{k,0}$.

For the lower part, snow falling from the taller part is considered. Still, this is a small contribution as the roof is flat and thus only snow falling due to the wind is considered. The applied snow load is $2{,}17\ kN/m^2$ and $2{,}0\ kN/m^2$ on the roof of the lower and taller part, respectively. Full calculations are shown in Appendix A.

4.2.2.4 Wind Load

The wind loads are automatically defined in SAP2000 according to EC1-4 [52] on the MBF model to design the steel members in the frame. Two load patterns in each direction are defined, i.e. X^+, X^-, Y^+ and Y^-. To apply the wind forces, "none" walls, which is areas with no section or material properties, are drawn as the building's façade, meaning that there are no structural properties defined for these elements. This way, the wind loads can be applied from all directions on the building, acting on the façades.

To simplify the calculations, the effects in the region in the first three floors where the two buildings are not connected, are neglected in the calculations, see Figure 4-6. Further, when dividing the façades across the wind direction into the different zones, the size of each zone has been approximated to fit the division of none walls. This is done to avoid dividing them into several elements. For each wind load case with its unique wind direction, it has been chosen to

consider the stories of the taller part of the building above story 7 as a separate building. This is also illustrated in Figure 4-6.

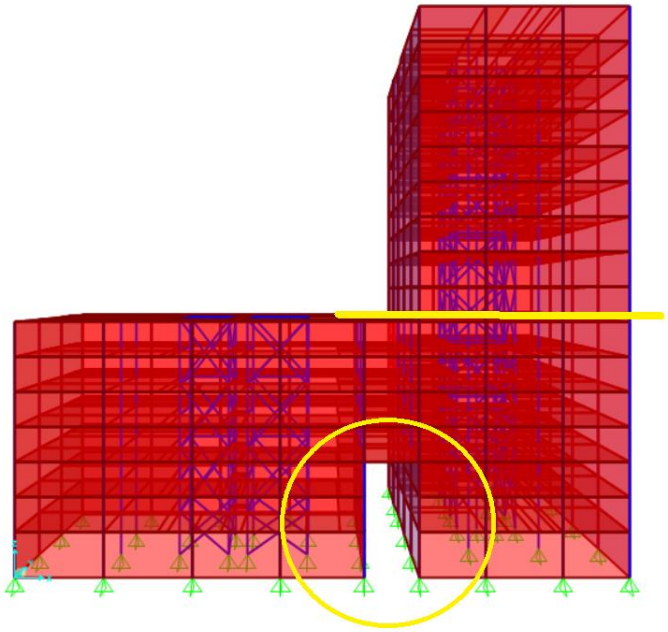

Figure 4-6 Neglected part of the structure during wind load analysis

The wind coefficients are defined according to EC1-4 [52]. As the building is imaginary and has no exact location, the terrain category is assumed to be II, which refers to an area with low vegetation and a distance from obstacles of minimum 20 times their height. The reference wind speed, $v_{b,0}$, for Bremanger in Western Norway is 29 m/s according to the National annex of EC1-4 [52].

The wind speed used in the analysis takes into consideration directional and seasonal factors, which are both recommended to be defined as 1,0 according to EC1-4 [52]. According to the calculation of Equation (4.1) in EC1-4 [52], given in Eq. 3, the wind speed is 29 m/s.

$$v_b = c_{dir} \cdot c_{season} \cdot v_{b,0} = 29\ m/s \tag{3}$$

Four wind load cases have been defined, as the building is unsymmetrical. Wind shape factors have been calculated for all façades in all four load cases. Full calculations of wind load can be found in Appendix A.

Figure 4-7 shows the wind pressure coefficients on the structure for the wind load case in positive x-direction visualized through a color scale. The colors illustrate the division of the structure in two different parts and the division in different shape factors. The dark blue color

represents the pressure coefficient of shape factor A. The part of the structure that ranges from story 1-7 is divided in shape factors A, B and C while the upper story part is divided in A and B. The roofs are divided into shape factor F, G, H and I. The division of shape factors are done according to Figure 7.1 and Figure 7.2 in EC1-4 [52].

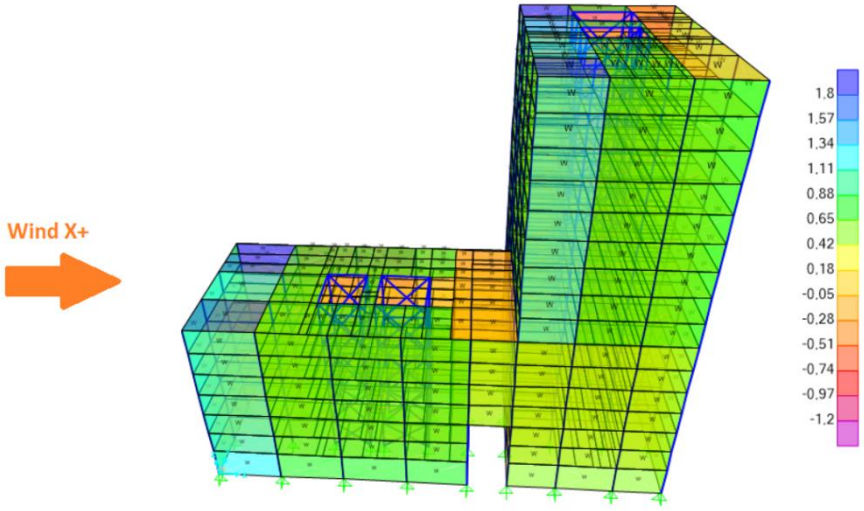

Figure 4-7 Wind pressure coefficient contours of wind load in positive x-direction

4.2.3 Materials

Materials are chosen from the Eurocode databases integrated in the software, to ensure correct values for the different material properties. Nonlinear material properties are also included in this database and are automatically defined. The materials used are C35 for concrete, S355 for steel and "Rebar" for the reinforcement.

4.2.3.1 Concrete

C35 with takeda hardening is defined for the concrete material used in the model. As Figure 4-8 illustrates, the tensile strength of concrete is very low compared to the compressive strength. Generally, the tensile strength is neglected as the reinforcement carries the tensile forces. The minimum and expected compressive strength is 35 MPa and the tensile strength at strain -0,0021 %. Ultimate strain capacity is according to the stress-strain plot -0,005 % at complete failure.

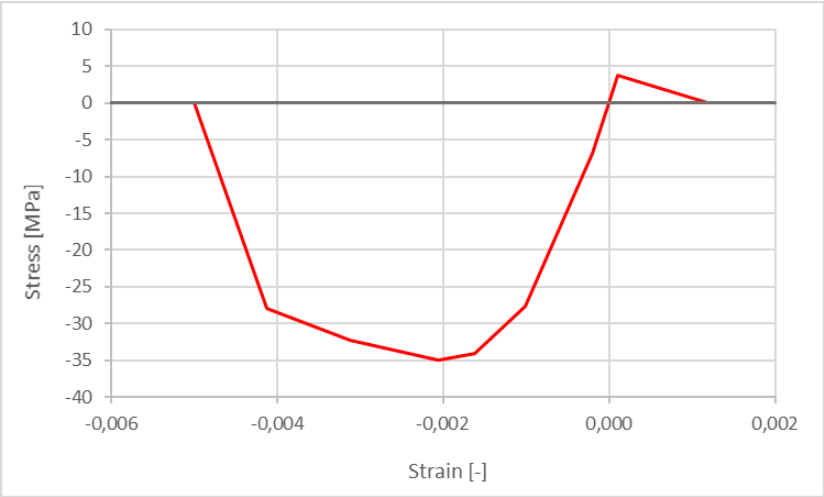

Figure 4-8 Stress-strain plot of C35 with takeda hardening

4.2.3.2 Steel

The selected steel quality is S355 with kinematic hardening. The stress-strain curve is shown in Figure 4-9. The minimum yield stress and ultimate stress are 355 MPa and 510 MPa, respectively, while the expected values are 390,5 MPa and 561 MPa. According to the plot, yield occurs at 0,015 % strain and the minimum ultimate stress occurs at 0,11 %. At 0,17 % the plot reaches point E and failure initiates until complete failure at 0,19 % strain.

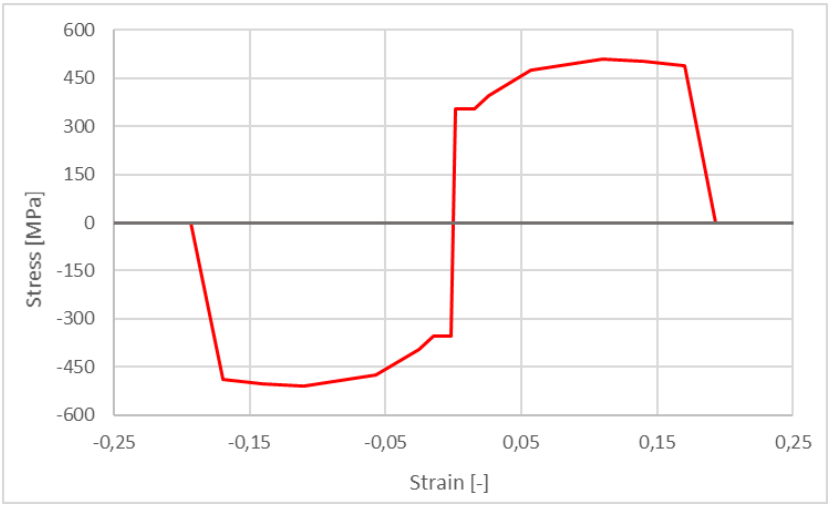

Figure 4-9 Stress-strain plot of S355 with kinematic hardening

4.2.3.3 Rebar

While S355 is commonly used for structural steel, other steel qualities with higher yield strength may be used for reinforcement. An option termed “Rebar” is available in the Eurocode database of SAP2000 to be defined for reinforcement, which is done for the reinforcement in this study.

The minimum and expected yield stress is 414 MPa and 455 MPa, respectively, and the minimum and expected ultimate strength is 621 MPa and 683 MPa.

The stress-strain relationship for the rebar material is plotted in Figure 4-10. The plot implies that yielding initiates at 0,01% strain, which is significantly lower than for S355.

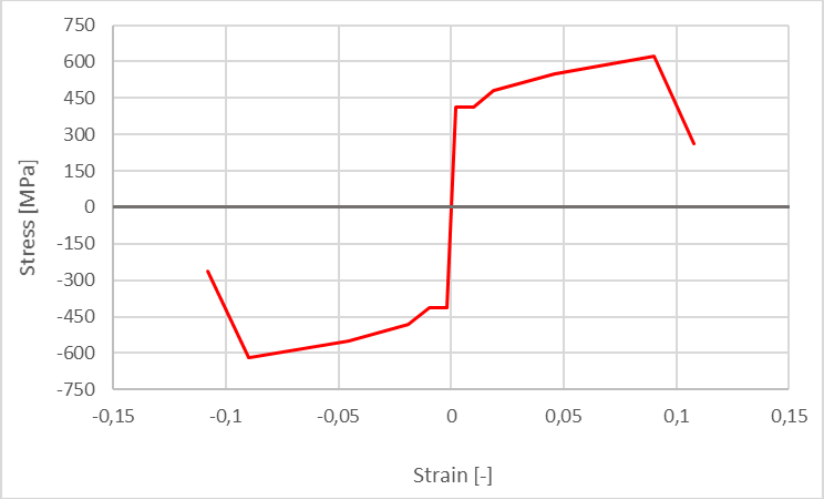

Figure 4-10 Stress-strain plot of rebar material with kinematic hardening

4.2.4 Sections

The various elements are modelled differently depending on the section type. The beams, columns and braces are modeled as frames while the slabs and shear walls are modeled as shells, all according to the information gathered from the received model and drawings. All structural elements in the first floor are pinned.

4.2.4.1 Frames

In the shear wall model, there are circular concrete columns with dimensions of 450 mm, 550 mm and 600 mm, steel UPE200 beams and concrete shear walls with thickness of 200 mm and 300 mm. The thickness of the concrete slab is 280 mm and 340 mm for the lower and taller part of the building, respectively, in both cases. The reinforcement in the columns are listed in Table 4.1:

Table 4.1 Reinforcement in concrete columns

Column dimension	**Longitudinal rebars**
Ø600	8Ø32
Ø550	9Ø32
Ø450	8Ø32

For the MBF structure, the concrete shear walls have been replaced by mega-braced steel frames consisting of steel beams, columns and braces, all modeled as frames. Thus, all the structural elements in this model besides the slab are steel sections. As this is an alternative solution of which the dimensions of the members are not already given, the sections of the frame in MBF have been designed according to EC3 [53] with the SAP2000 steel design tool.

To utilize this tool, a linear static analysis with the defined loads are completed so it is possible to run a steel design of the members. SAP2000 allows the user to choose between different codes to perform the design, and in this case the EC3 [53] with National Annex of Norway is chosen. As the building is located in one of the most high-seismicity regions in Norway, ductility class medium (DCM) is defined. All the other values are kept as defined by default.

The result of the steel design shows a color scale representing the utilization of the different members with their respective temporary sections. As the majority of the members are in red color, which can be seen in Figure 4-11, new sections should be assigned the different members so that the capacity is not exceeded during the linear static analysis.

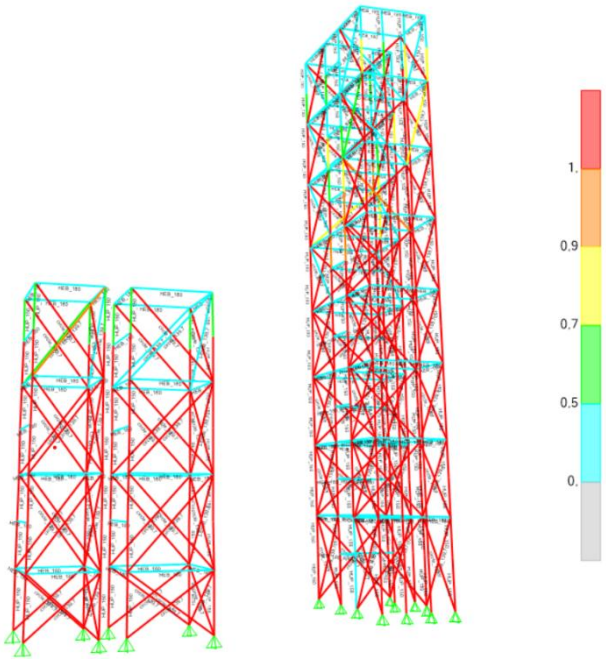

Figure 4-11 Results of steel design of the MBF steel members

Reasonable steel sections have been defined by the trial-and-error method. The steel design tool has been used to check whether the assumed sections have adequate capacity until appropriate values of utilization have been obtained. Based on the design results, new cross sections are defined for the steel members. The defined sections for the MBF members in the taller and lower part of the building are listed in Table 4.2 and

Table 4.3, respectively:

Table 4.2 Section of each element type of the MBF in the taller part after steel design in SAP2000

MBF element type	**Story**	**Section**
Column	1-4	HEB 900
Column	5-8	HEB 500
Column	9-12	HEB 320
Column	13-16	HEB 220
Brace	1-2	CFCHS 355.6 x 12.5
Brace	2-6	CFCHS 323.9 x 6
Brace	6-12	CFCHS 273 x 16
Brace	12-16	CFCHS 244.5 x 5
Beam	1-16	HEB 100

Table 4.3 Section of each element type of the MBF in the lower part after steel design in SAP2000

MBF element type	**Story**	**Section**
Column	1-3	HEB 400
Column	3-7	HEB 280
Brace	1-3	CFCHS 323.9 x 5
Brace	3-7	CFCHS 323.9 x 6
Beam	1-7	HEB 100

Figure 4-12 shows the utilization of the steel members as given in the tables above, which are to be used in the analyses.

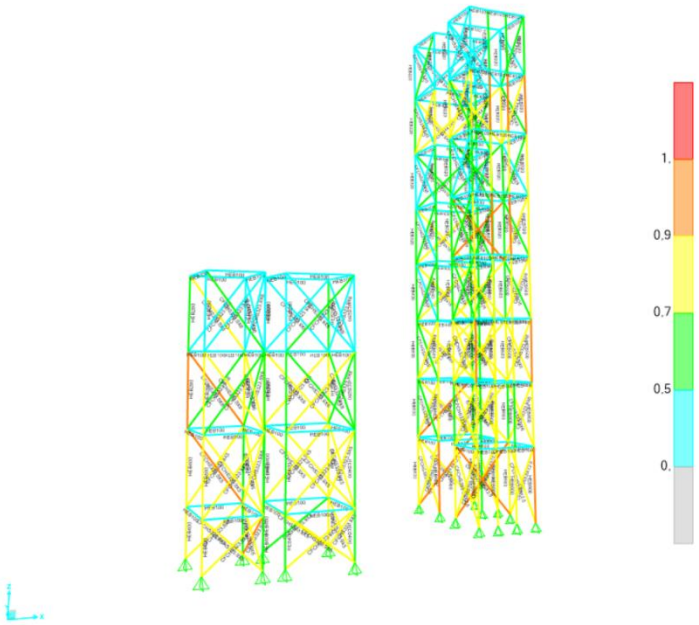

Figure 4-12 Results of steel design of the updated MBF steel members

As can be seen from the figure, some steel members are colored in red after the steel design with the adjusted dimensions as well. Although it looks like the capacity is exceeded, the maximum utilization ratio is 0,977 for the columns, which is less than 1 and thus acceptable.

To prevent moments in the MBF system, moment releases are assigned in the start and end of all the elements; beams, columns and braces. Also, torsion release is assigned at the start of the elements. The end releases are applied for the cause that the only lateral load carrying mechanism is the axial load action in the braces, as they are not supposed to carry moments.

4.2.4.1.1 Nonlinear Properties

As nonlinear analyses are to be performed, the structural elements that make up the lateral force resisting system should be assigned nonlinear properties. Depending on the section type, the nonlinearity is defined differently for the different LFRS.

When defining hinges, a plastic deformation curve is defined that describes the behavior of the hinge under different deformation values. Each curve contains five points which represents the stages of the hinge condition. An example of such a curve is illustrated in Figure 4-13.

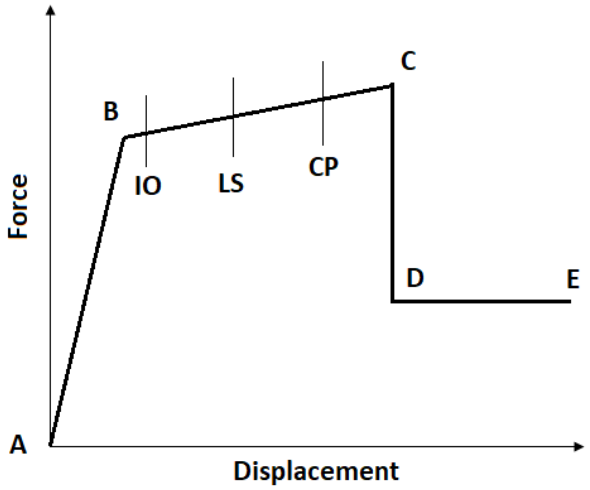

Figure 4-13 The five stages and performance levels of hinges. Based on Figure 40 in CSI Analysis Reference Manual [42]

Point A represents the original and unstressed stage of the hinge. At point B, the hinge has yielded, and the hinge experiences no deformation as it is still in the elastic range and all the elastic deformations occur in the frame element itself. Therefore, the elastic deformation at point B will be subtracted from the deformations at the following stages, namely C, D and E and only the plastic deformation will occur in the hinge. When the hinge reaches point C, the maximum capacity for the pushover analysis is reached. Point D represents the residual strength for the pushover analysis and point E refers to total failure of the hinge. If it is not desired that the hinge should fail this way, the deformation at point E should be defined as a large value. It is common to define additional points describing the performance level of the structure. These points are between stage B and C, meaning that the structure undergoes plastic deformations but does not reach the ultimate capacity. The performance levels are immediate occupancy (IO), life safety (LS) and collapse prevention (CP) [42].

For all hinges, load should be dropped after point E. Further, hinge overwrites are assigned to all hinges to discretize the members which in turn can provide better results [42].

The plastic hinges are assigned in the middle of each steel brace member in the MBF system to describe post-yield behavior. Default hinge properties from table 9-7 in ASCE41-13 [8] are used to give the braces plastic behavior under axial pressure, further the properties are modified to make the hinges elastic-perfectly plastic. This is done to reduce computational demand, as the software has trouble handling the sudden change in the hinge behavior. Thus, the plastic behavior is defined close to linear, also for failure.

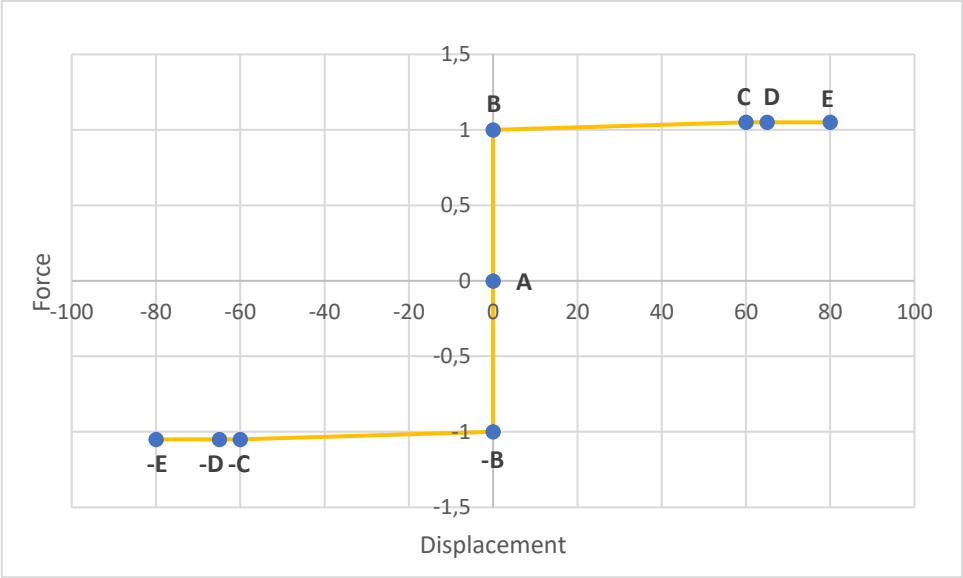

Figure 4-14 Force-Displacement curve of elastic-perfectly plastic hinges in braces

4.2.4.2 Shear Walls

The shear walls are defined as layered/nonlinear shell sections. This type of shell section allows to define several layers of the wall and define which layers and which directions are linear and nonlinear. A shell section in SAP2000 combines membrane and plate behavior, i.e. the layer strains are a result of all displacements and plate-bending rotations, and stresses contribute to all forces and plate-bending moments. The shell section should be used in most applications [42].

The layers are defined using the quick start tool. To automatically define the layers, some properties must be defined. In the shear walls, there are two layers of rebars with diameter 16 mm and center distance of 450 mm. The size and spacing are set equal for each rebar layer. The concrete and rebar materials are defined as C35 and Rebar, as described in Section 4.2.2. The behavior of the in-plane element component, the membrane layer, is defined with nonlinear behavior for stress component S22. The out-of-plane element component behavior is defined as linear, so only one concrete plate layer is defined. There are two shear wall sections, with thickness of 200 mm and 300 mm.

After these properties have been defined, the quick start tool proposes several layers of the shell element. All the horizontal layers are omitted, as well as the layers below the concrete plate layer which are defined with linear properties. In this case, four layers are defined: concrete membrane, two layers of vertical rebars and concrete plate. Figure 4-15 shows all four layers

with their respective thicknesses, material properties and material angles for the 200 mm shear wall section.

Layer Name	Distance	Thickness	Type	Num Int. Points	Material	Material Angle	Type	Material Component Behavior S11	S22	S12
ConcM	0,	200,	Membrane	1	C35/45	0,	Directional	Linear	Nonlinear	Linear
ConcM	0,	200,	Membrane	1	C35/45	0,	Directional	Linear	Nonlinear	Linear
TopBar2M	57,	0,446667	Membrane	1	Rebar	90,	Directional	Nonlinear	Inactive	Linear
BotBar2M	-57,	0,446667	Membrane	1	Rebar	90,	Directional	Nonlinear	Inactive	Linear
ConcP	0,	200,	Plate	2	C35/45	0,	Directional	Linear	Linear	Linear

Figure 4-15 200 mm shear wall layer definition in SAP2000

For each layer, the component is defined with linear or nonlinear material in each direction. Although the realistic case is to define all components as nonlinear, this is time consuming and can introduce several failing mechanisms and thus a simpler model should be used. The rebars are defined as nonlinear in S11. As the defined rebars are vertical, they align with the S22 direction which corresponds to the S22 shell stress behavior. If the rebar stress component S12 is set to nonlinear, rebars can carry shear forces when the concrete cracks. This can represent dowel action, although no dowels are present in the model. Whether this should be computed has to be evaluated in each case, but the most conservative approach is to define the rebar stress component S12 as inactive [42]. In this case, the S12 behavior is set to linear.

4.2.5 Controlling the Structure

After all the structural elements are modeled with their respective materials and the loads are applied, a linear static analysis is performed to investigate if the structure behaves as expected and that the elements are connected. To simplify this analysis and make it less time consuming, only the dead load is applied to the structure. If the behavior is reasonable, a modal analysis can be performed. The results of this analysis show the different mode shapes of the structure and the fundamental period, which can reveal if there are any errors in the modelling. The deformed shape of the different modes showing the rotational points of the structure can also reveal potential errors.

4.3 Pushover Analysis

After the structural elements and their nonlinearities have been correctly defined, a nonlinear static load case is defined. As initial conditions, the pushover analysis continues from the state at the end of the nonlinear dead load case. This means, that the dead load case should be defined as nonlinear static. The PΔ-effects should be considered in the analysis, which is a type of geometric nonlinearity. Figure 4-16 illustrates the PΔ-effect.

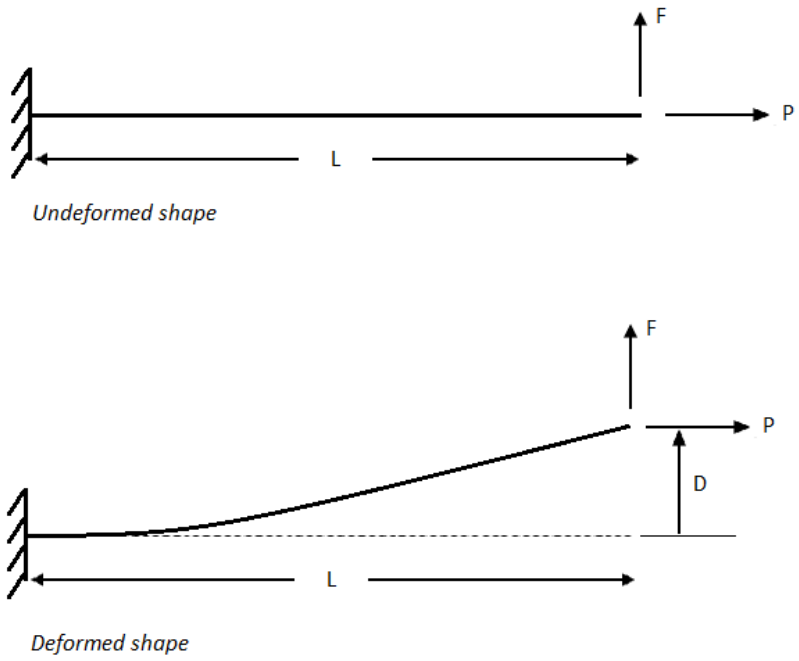

Figure 4-16 Illustration of the PΔ-effect. Based on Figure 84 in CSI Analysis Reference Manual [42]

Imagine a cantilever beam subjected to a vertical force F and a horizontal (axial) force P at length L. When calculating this as a linear case, the vertical force would apply a moment to the cantilever beam equal to $F \cdot L$. As the force P is axial, there is no moment. But when the vertical force F acts on the cantilever, the beam experiences a deformation Δ. Realistically, this deformation should be considered in the calculations as this will result in an extra moment equal to $\Delta \cdot P$. In linear calculations this is not considered, but in nonlinear cases this is a geometric nonlinearity that should be considered as this will increase the impact on structural elements and provide more accurate results [42].

4.3.1 Load Pattern

SAP2000 provides automatically defined load types for pushover analysis, termed acceleration and mode load type. When defining the load as acceleration load, the displacements, velocities and accelerations are measured relative to the ground. Utilizing this feature, the software automatically computes acceleration loads for all directions. This load is applied to each joint and element, and the total sum is calculated over the whole structure and is equal to the negative value of the element mass [42].

When defining the mode load type, the lateral loads are applied in a pattern such that the given mode shape is obtained. The value of mode shape for each direction is determined from the results of the modal analysis. The mode shape of which the majority of masses are acting in x-

direction, i.e. the participating mass ratio is highest in x-direction, is the current mode shape in x-direction [42].

In this study, the mode load type is used for the pushover analyses. For both the shear wall and MBF building mode shape 1 corresponds to the y-direction mode shape, and mode shape 2 corresponds to the x-direction mode shape. Thus, the load name of the modal x- and y-pushover analysis is 2 and 1, respectively.

4.3.2 Target Displacement

The intention of the target displacement is to represent the maximum displacement that the structure is likely to be subjected to during the design earthquakes [19]. Thus, it is affected by seismic parameters that are specific for the location as well as the dynamic behavior of the structure. The target displacement is calculated for both structures according to Equation (3-11) in FEMA273 [19], shown in Eq. 4.

$$\delta = C_0 C_1 C_2 C_3 S_a \frac{T_e^2}{4\pi^2} g \tag{4}$$

where:

C_0 is a factor to relate spectral displacement and probable roof displacement;

C_1 is a factor to relate expected maximum inelastic displacement to the displacement calculated for linear elastic response;

C_2 is a factor to represent the effect of the hysteresis shape on the maximum displacement response;

C_3 is a factor to represent increase in displacement due to PΔ-effects;

S_a is the response spectrum acceleration at the effective fundamental period and the damping ratio of the considered structure;

T_e is the effective fundamental period of the structure in each direction. For simplicity, this factor is set equal to the period of mode shape 1.

The response acceleration, S_a, is calculated according to EC8 [2] for both structures. The results of the calculated target displacement for all pushover load cases of each structure are listed in Table 4.4.

Table 4.4 Calculated target displacement of the two structures

Structure	**δ [mm]**
Shear wall	422
MBF	786

Full calculations of the target displacement can be found in Appendix B.

4.4 Time-History Analysis

To perform a nonlinear time-history analysis, earthquake records must be defined as time-history functions. For this case, three earthquake records have been selected. The earthquakes are from Dursun, Friuli and Gazli. The records are defined as time and function values from text files downloaded from the PEER Ground Motion Database [54]. As this database does not have any records of earthquake events in Norway, records from Europe, specifically Italy and Turkey, have been chosen and assumed adequately representative for possible seismic events in Norway. It has been assumed that these seismic events at these locations are representative for similar events in Norway.

Figure 4-17, Figure 4-18 and Figure 4-19 show earthquake motions from Dursun, Friuli and Gazli, respectively. As the figures show, the chosen records have various patterns, which is beneficial as the structure will be controlled for several different seismic magnitudes and ground motions and is more likely to obtain safe design.

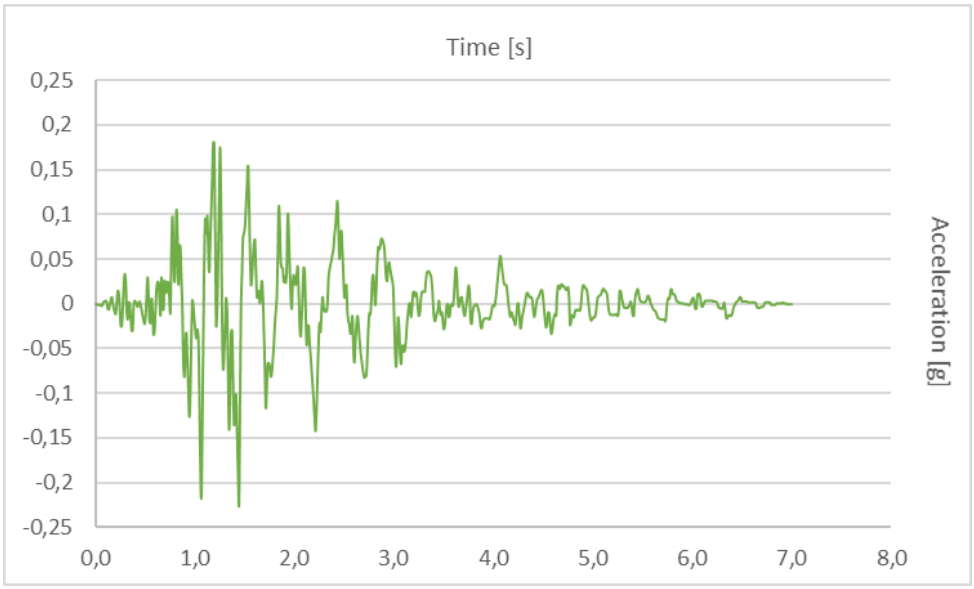

Figure 4-17 Earthquake record from Dursun

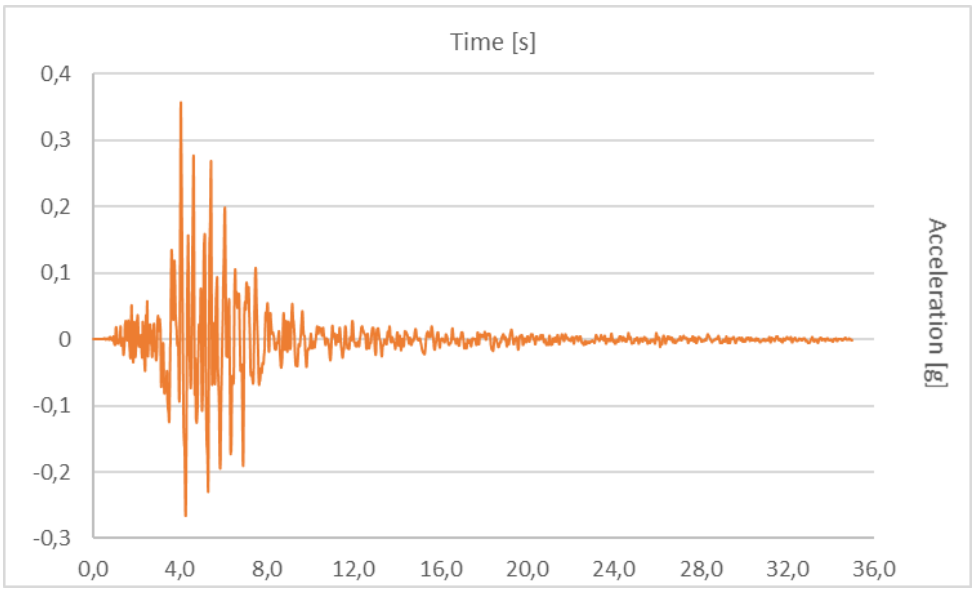

Figure 4-18 Earthquake record from Friuli

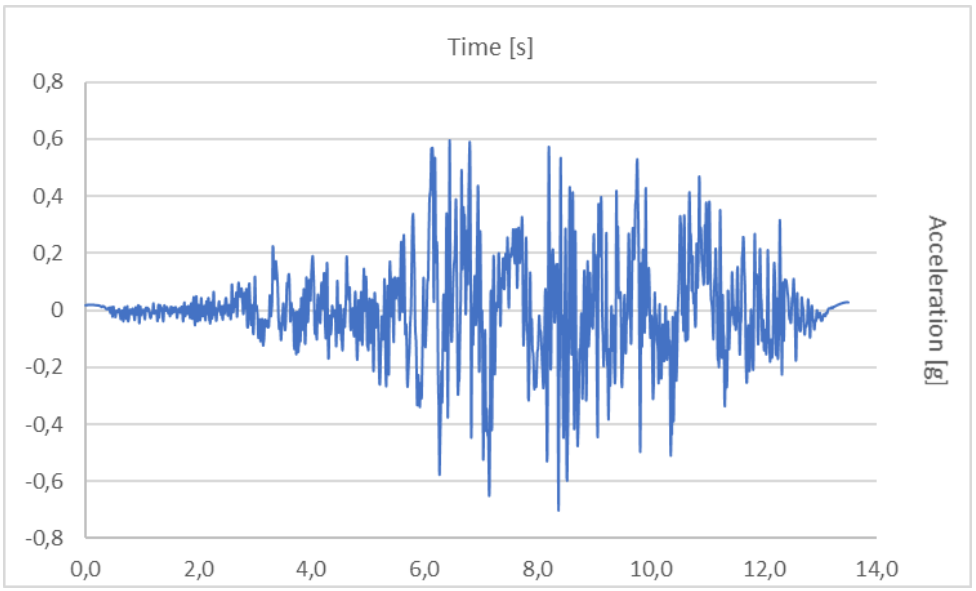

Figure 4-19 Earthquake record from Gazli

The peak acceleration values are 0,224 *g*, 0,354 *g* and 0,702 *g* for the Dursun, Friuli and Gazli earthquakes, respectively. This shows that the Gazli earthquake is significantly larger and experiences frequent large acceleration waves compared to the two other earthquakes. This indicates that the Gazli earthquake will lead to the most severe impact or potential damage on the structure, as it not only has the largest acceleration but also the most frequent large waves which may cause a continuous vibration, as described in Chapter 2.1.

The time-history load cases are performed with direct integration with consideration of *PΔ* nonlinearity as well as a modal time-history analysis, which is also termed fast nonlinear analysis (FNA). As gravity load always acts on the structure, it is defined that the time-history load case should be started from the dead load case. The load type is defined as acceleration in the U1 and U2 direction for the x- and y-directions, respectively, and the time-history functions are defined for each respective time-history case.

Number of output time steps and output time step size are defined according to the information in the earthquake text files. By defining less steps or larger step size than the record, the accuracy may be reduced and if defining more steps or smaller step size the analysis will require more disk space [55].

Damping is specified by periods from a modal analysis corresponding to mode 1 and mode 2. The damping for the RC is 5 % and 2 % for steel, i.e. in the shear wall structure the damping is 5 % and in the MBF structure the damping is 2 % [56].

Time-history analysis with the abovementioned parameters have been performed in both x- and y-direction for all three time-history functions.

4.4.1 Modal Time-History Analysis

As the pushover and direct integration time-history analyses are quite time consuming for a large 3D structure like the building in this study, an alternative method has been tested to make the analysis less computationally demanding. In this alternative method, two friction dampers are added in y-direction of each story. The purpose of the dampers is to keep the other structural elements in the elastic range, i.e. avoid inelastic deformation and behavior. This means that the slip load of the friction damper will be reached before yielding of other structural elements initiate. Thus, all structural elements apart from the dampers are defined with linear properties. This significantly reduces the computational effort required to perform the analysis and is therefore less time consuming.

The dampers are modeled as Pall friction dampers and are defined as a link/support with Wen plasticity property. Nonlinear directional properties are defined for the x-direction, while for y- and z-direction as well as rotations the properties are fixed, and nonlinearity is not defined.

The nonlinear force-deformation relationship of the Wen plasticity model is given by Eq. 5 [42]:

$$f = \boldsymbol{ratio} \cdot \boldsymbol{k} \cdot d + (1 - \boldsymbol{ratio}) \cdot \boldsymbol{yield} \cdot z \quad (5)$$

Where *k* is the elastic spring constant, *ratio* is the defined ratio of post-yield stiffness to elastic stiffness *k*, *yield* is the yield force, *z* is an internal hysteretic variable. The initial value of *z* is 0 but has a range of $-1 \leq z \leq 1$, i.e. the yield surface is represented by $|z| = 1$. For friction dampers, the *ratio* should be zero [42].

Initially, the slip load or yield strength of the damper is assumed. After defining a value, the hysteresis loop of each damper can be computed as the relationship between axial displacement and axial load of the damper element. Further, the yield strength can be redefined until a rectangular shape similar to an elastic-perfectly plastic material is obtained. Further, the slip load can be increased depending on the demand of the structure for the damper to absorb more energy. The stiffness is defined as 1000 times the yield force.

Two friction dampers are placed in frames in each story of both structures, see Figure 4-20 and Figure 4-21. The dampers are drawn as 2-joint links in an MRF.

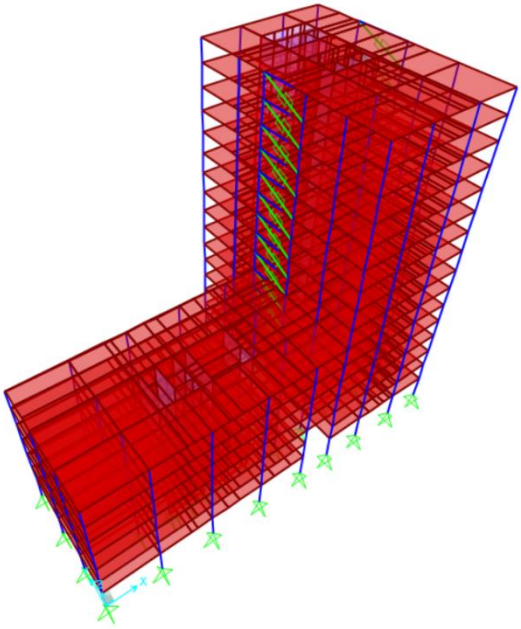

Figure 4-20 Shear wall model with friction dampers

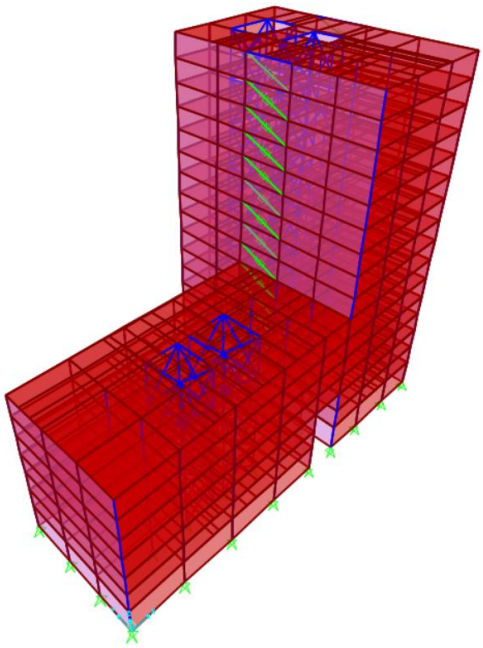

Figure 4-21 MBF model with friction dampers

The purpose of the dampers is to avoid or delay yielding in other structural elements, as the dampers will work as a sacrificial element. By including friction dampers, a fast nonlinear analysis can be performed in terms of a modal time-history analysis which was introduced in Chapter 3.2.1. This method is suitable for structures with dampers as the model should primarily be linear-elastic and only a limited number of elements should be defined with nonlinear properties. Instead of defining nonlinear elements, dampers are defined. Hence, in the following

analyses, only the shear walls and MBF are defined with nonlinear properties for the two structures, while all other structural elements are linearly defined.

As for the previous performed time-history analyses, time-history functions are defined equally. In addition, a time-history function for the application of the dead load is defined. A ramp function with an amplitude of 1 and time of 10 is defined for this purpose. The dead load case is then defined as a modal time-history load case so that the final state of this load case can be used as initial conditions for the modal time-history analysis. A modal damping of 99,9 % is defined to apply the dead load slowly to avoid that dynamic behavior occurs.

When defining the fast nonlinear load case, it is defined as a nonlinear modal time-history analysis using load dependent Ritz vectors, as these vectors are necessary for a fast nonlinear analysis. The loads applied for the modal analysis are acceleration in the x-direction, the dead load, as well as the built-in deformation load for the links, i.e. the dampers. The load type of the time-history load case is the acceleration load type with the earthquake records for the considered seismic events.

5 RESULTS

The results of the modal, pushover and time-history analyses of the shear walls and MBF structure are presented in the following chapter.

5.1 Modal Analysis

The results of the modal analysis for the shear wall and MBF model in both x- and y-direction are presented below.

5.1.1 Shear Walls

The deformed shapes of mode 1 and 2, which represents y- and x-direction, respectively, are shown in Figure 5-1 and Figure 5-2. As the deformations are low, the initial shape of the building is shown as a wire shadow to clearly see the direction of the deformation. This reveals that mode 1 acts in y-direction and mode 2 acts in x-direction. As can be seen, the deformed shapes are in the negative x- and y-directions.

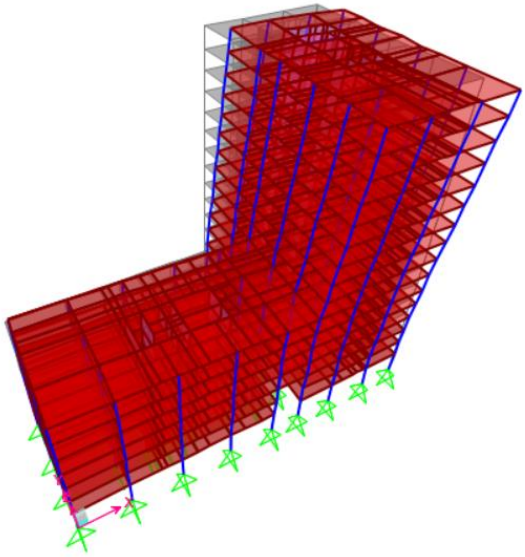

Figure 5-1 Mode shape 1 (y-direction) for the shear wall structure

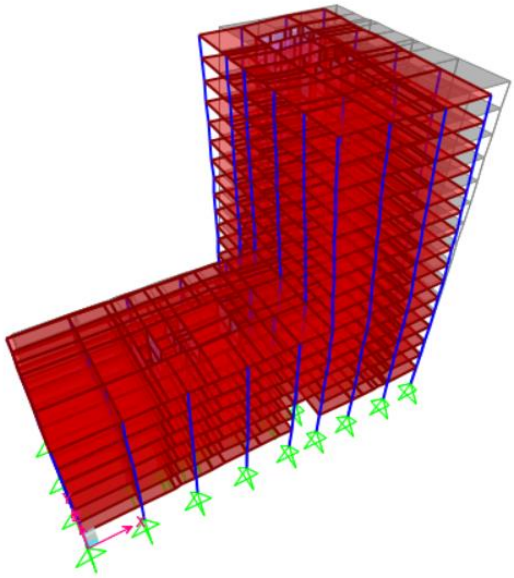

Figure 5-2 Mode shape 2 (x-direction) for the shear wall structure

The direction of each mode can also be found from the modal participating mass ratios. According to these ratios, that are conducted from the modal analysis results, 42 % of the total mass acts in y-direction during mode 1 and 43 % of the mass acts in x-direction during mode 2. This confirms the visualized results of the directions of the modes. The periods are 0,962 s and 0,855 s for mode 1 and 2, respectively.

5.1.2 MBF

The mode shape 1 for the MBF system moves in y-direction, while mode 2 moves in the x-direction. This is found by the deformation of the modes and by the participating mass ratio which is 42 % in y-direction in mode 1 and 57 % in x-direction in mode 2. From the modal analysis, the natural period for the structure is 1,8905 s for mode 1 and 1,78663 s for mode 2. Figure 5-3 and Figure 5-4 show the deformation of mode shape 1 and 2, respectively, where the wire shadow shows the original shape of the structure.

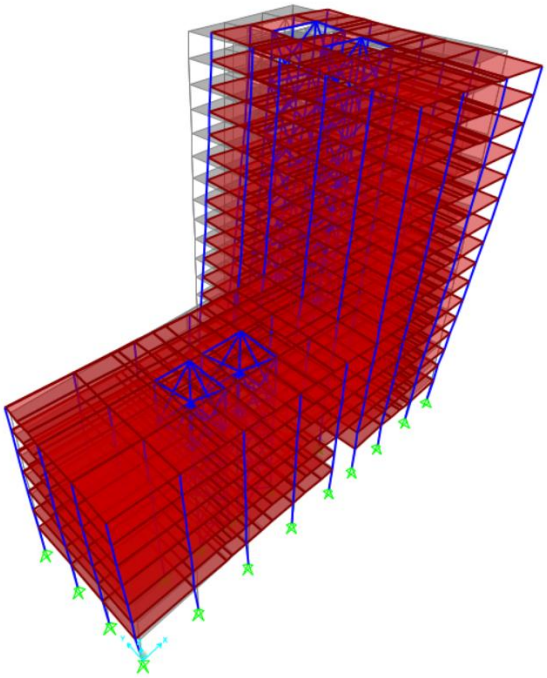

Figure 5-3 Mode shape 1 (y-direction) of the MBF structure

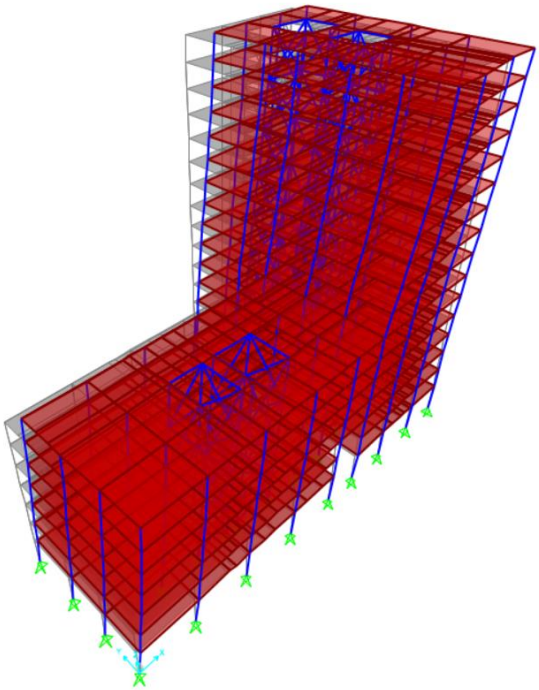

Figure 5-4 Mode shape 2 (x-direction) of the MBF structure

5.2 Pushover Analysis

For the pushover analysis, the pushover curves for the two structures are analyzed, and maximum values of drift ratio are computed. Further, the formation of plastic hinges in MBF is described.

5.2.1 Shear Walls

The results from the pushover analyses of the shear wall structure are presented in the following chapter.

5.2.1.1 Target Displacement

The target deformation in each pushover load case is applied at node 5660, which is shown in Figure 5-5. This node is chosen as the monitored joint as it is close to the mean value of center of mass in each story, placed in the top story.

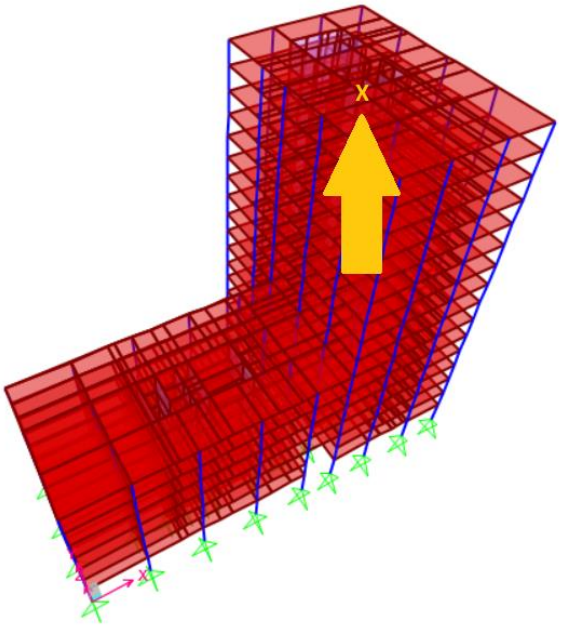

Figure 5-5 Position of monitored joint of the shear wall structure

For both directions the target deformation, δ, is defined according to the results of the calculations presented in Chapter 4.3.2. The applied deformation is 422 mm in both x- and y-direction.

5.2.1.2 Pushover Curve

Figure 5-6 and Figure 5-7 show the pushover curves for the pushover analysis in both x- and y-direction. The pushover curves display the variation in displacement of the node at which the deformation is applied, with base shear in the same direction. The total forces and moments about the global origin that are required of the supports to resist the response-spectrum loading are called base reactions. The base shear is a measure of the horizontal forces for seismic analyses [42].

The values of the curve are measured at the node at which the displacement is applied, which is node 5660.

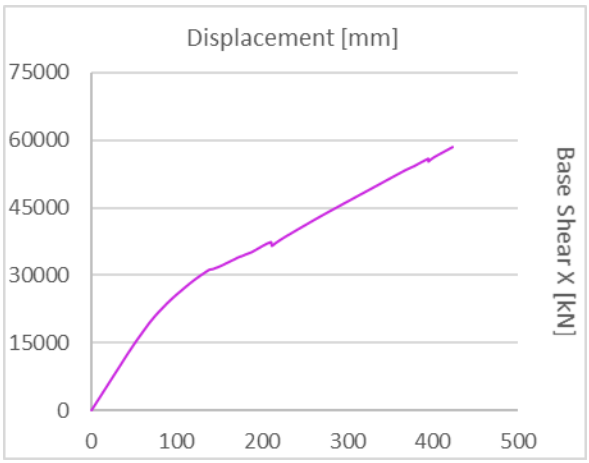

Figure 5-6 Pushover curve in x-direction of shear wall

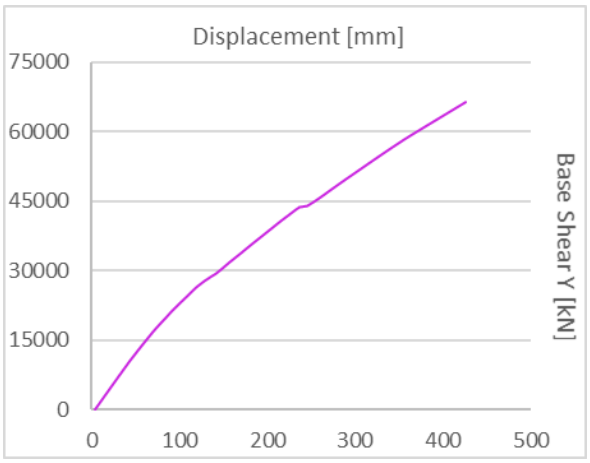

Figure 5-7 Pushover curve in y-direction of shear wall

The maximum reached base shear reactions during the pushover analysis in both directions are listed in Table 5.1. There is a difference between the base shear values in x- and y-direction, which may be due to irregularities in the geometry of the structure.

Table 5.1 Maximum base shear from pushover in both directions of shear wall

Pushover Load Case	**Maximum Base Shear X/Y [kN]**
X	58 530
Y	66 380

5.2.1.3 Drift Ratio

The roof drift is automatically calculated by defining generalized displacements in SAP2000. To obtain these results, the generalized displacement at node 5683 is plotted with scale factor 1/62000, which is the height of the structure, in x- and y-direction depending on the direction of the analysis. Using these results, the maximum roof drift for both directions can be automatically computed. The roof drifts of the x- and y-direction are plotted and visualized in Figure 5-8 and Figure 5-9, respectively.

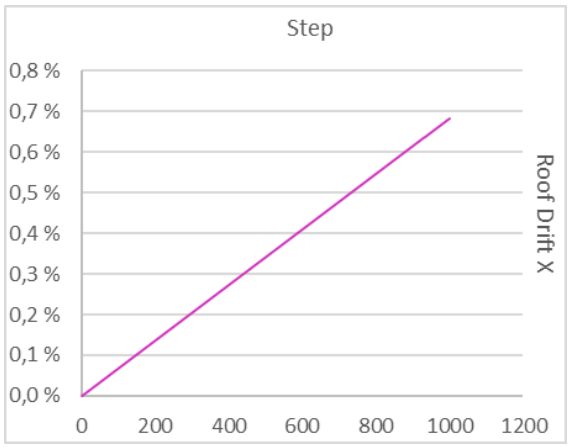

Figure 5-8 Roof drift from pushover in x-direction of shear wall

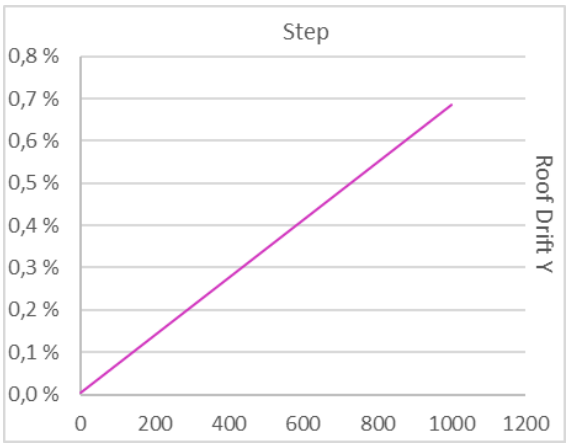

Figure 5-9 Roof drift from pushover in y-direction of shear wall

As can be seen from Figure 5-8 and Figure 5-9 the roof drift over the building height is linear, which is reasonable as the load is applied monotonically at one node.

The roof drifts for each direction of pushover analysis are listed in Table 5.2. As can be seen, the roof drift is the same in both directions, which is reasonable as the roof displacement is equal.

Table 5.2 Maximum roof drift from pushover in both directions of shear wall

Pushover Load Case	Maximum Roof Drift X/Y [%]
X	0,68
Y	0,68

5.2.2 MBF

In the following chapter, the results from the pushover analyses of the MBF structure are presented.

5.2.2.1 Target Displacement

The monitored joint used for the pushover analysis of the MBF structure is shown as an yellow “x” in Figure 5-10, which is based on the center of mass. As the geometry of the building is irregular, the joint closest to the average center of mass from each floor is used at the top story.

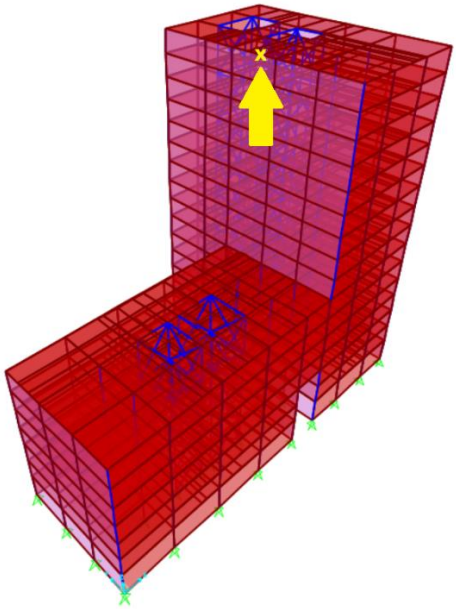

Figure 5-10 Position of monitored joint of the MBF structure

The target displacement, δ, for the MBF structure is calculated to 786 mm according to FEMA273 [19] in Chapter 4.3.2 and is the same for x- and y-direction. The calculated value is relatively large as the MBF structure is ductile, and it is highly affected by the period of the structure.

5.2.2.2 Pushover Curve

The pushover curves for x- and y-direction are shown in Figure 5-11 and Figure 5-12, respectively. The curves are computed from the displacement of the monitored joint and the base shear that occurs when the joint is «pushed». The pushover curve for the load case in y-direction has a change in the slope at a displacement of approximately 250 mm where the base shear does not increase as much. Oppositely, the pushover curve for the x-direction has a more linear slope.

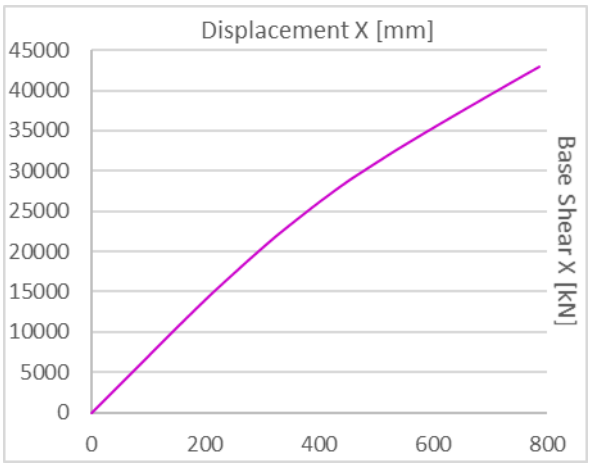

Figure 5-11 Pushover curve in x-direction of MBF structure

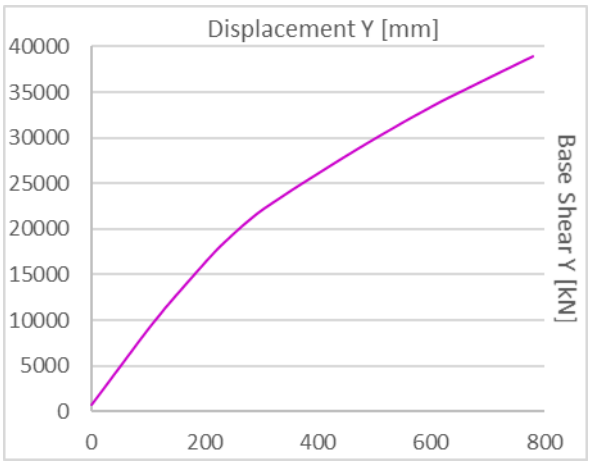

Figure 5-12 Pushover curve in y-direction of MBF structure

Table 5.3 presents the maximum base shear for the pushover analysis in x- and y-direction. From the results, the maximum base shear for the pushover analysis in x-direction is higher than in y-direction. The reason may be because of the irregularity of the mass distribution in the structure as the geometry of the structure is also irregular.

Table 5.3 Maximum base shear from pushover in both directions of MBF

Pushover Load Case	**Maximum Base Shear X/Y [kN]**
X	42 927
Y	38 962

5.2.2.3 Drift Ratio

The drift ratio from the pushover analysis in x- and y-direction are found in SAP2000 by defining a generalized displacement at the monitored joint. This is made for each direction and they are scaled by dividing 1 by the height of the structure. The results of the roof drift for the MBF structure are displayed as graphs shown in Figure 5-13 and Figure 5-14. From the figures, the curves are almost linear and equal for both directions. This is because the target displacement is equal for both directions and monitored joint is being “pushed” with a constant speed.

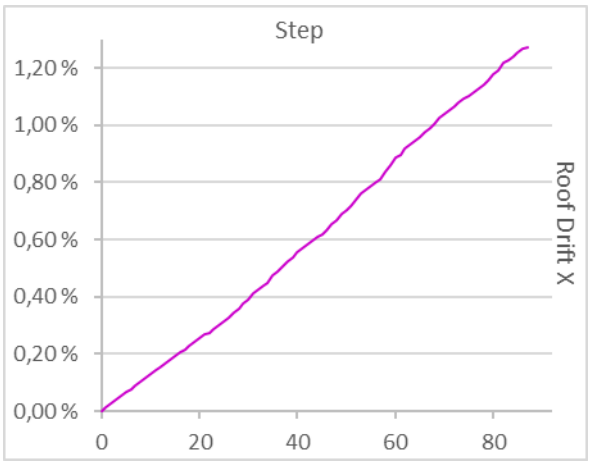

Figure 5-13 Roof drift from pushover in x-direction of MBF

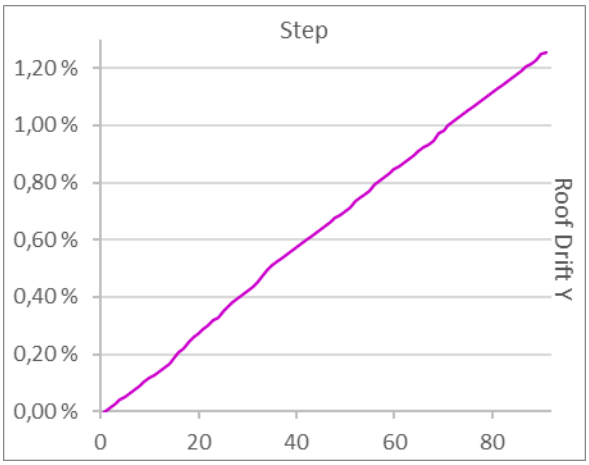

Figure 5-14 Roof drift from pushover in y-direction of MBF

The maximum roof drift for the pushover analysis of the monitored joint in each direction is presented in Table 5.4. The reason that the roof drift is equal for both directions is because the displacement is equal, and the displacement is applied with a constant speed. Also, the roof drifts are high as the target displacements are high.

Table 5.4 Maximum roof drift from pushover in both directions of MBF

Pushover Load Case	**Maximum Roof Drift X/Y**
X	1,27 %
Y	1,27 %

5.2.2.4 Hinge Formation

The pushover analysis in y-direction of the MBF structure resulted in more hinge deformation in the braces compared to the x-direction. Figure 5-15 and Figure 5-16 show the deformation of the lateral force resisting system in the MBF structure and the hinge formation in the braces from the last step of the pushover analysis for x- and y-direction, respectively. The grey wired "shadow" shows the original position of the structure and the color scale on the right side describes the performance levels of the hinges. The pink colored hinges imply that the hinges have yielded, and the blue hinges indicate that the hinges have reached life safety performance level.

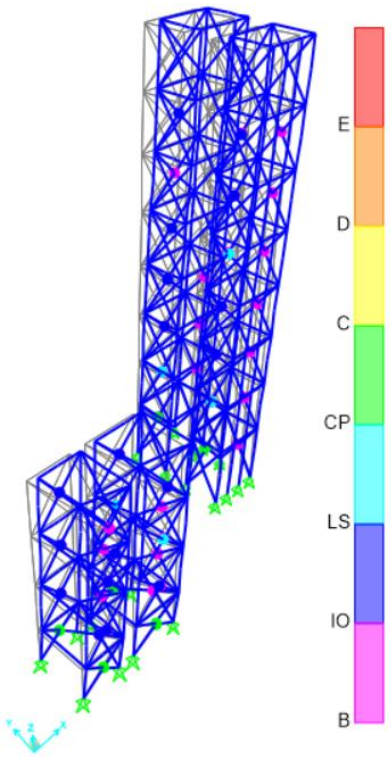

Figure 5-15 Hinge formation from pushover in x-direction of MBF

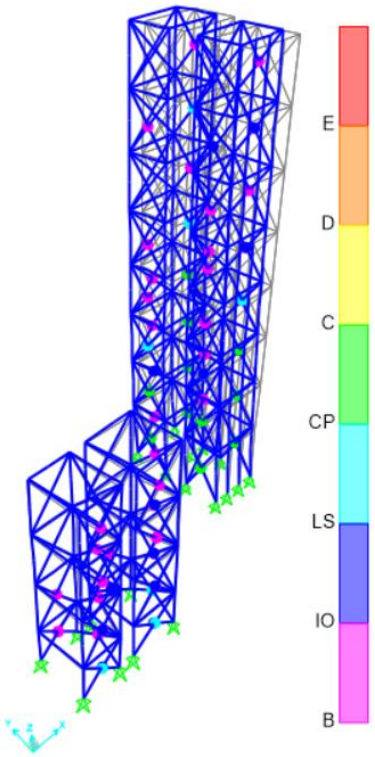

Figure 5-16 Hinge formation from pushover in y-direction of MBF

5.3 Direct Integration Time-History Analysis

The following chapter presents the results of the time-history analyses for both the shear wall and MBF structure.

5.3.1 Shear Walls

For the shear walls the resulting base shear reactions, roof displacements and drift ratio are considered for the three time-history functions in both x- and y-direction.

5.3.1.1 Base Shear Reaction

The variation of base shear reaction for each time-history load case in the respective direction is shown in Figure 5-17 to Figure 5-22. The vertical axis represents the current base shear reaction in kN and the horizontal axis represents the time.

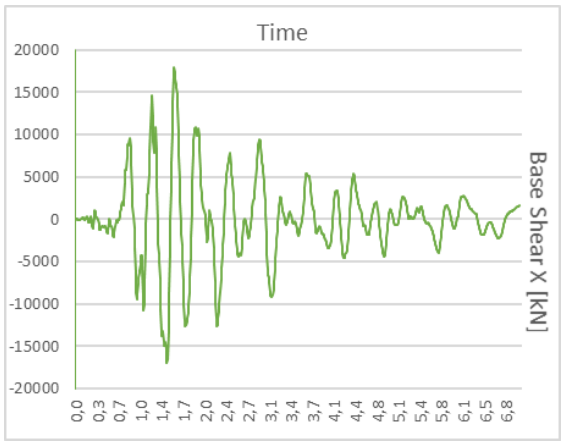

Figure 5-17 Base shear from direct integration T-H for Dursun X of shear wall

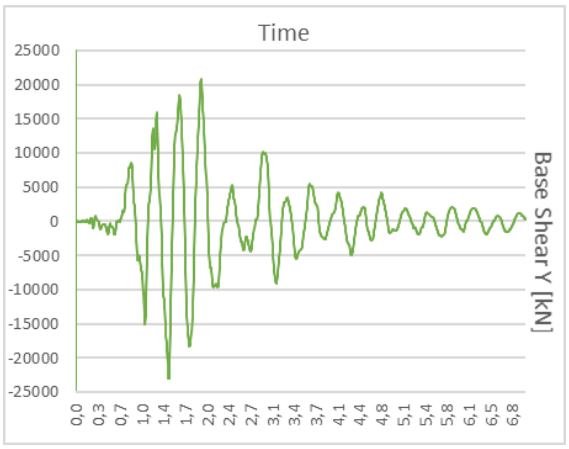

Figure 5-18 Base shear from direct integration T-H for Dursun Y of shear wall

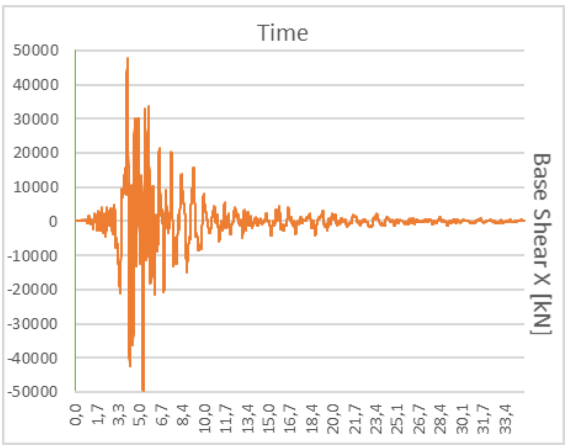

Figure 5-19 Base shear from direct integration T-H for Friuli X of shear wall

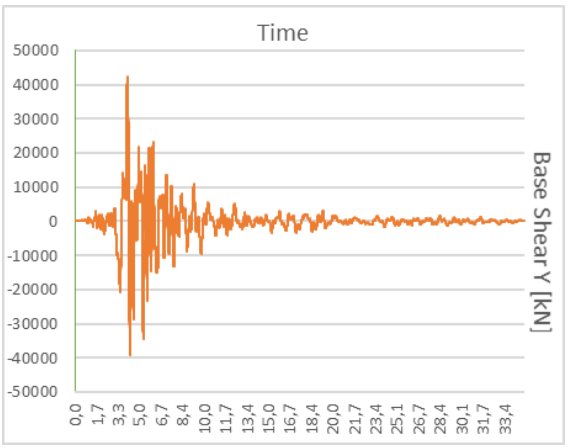

Figure 5-20 Base shear from direct integration T-H for Friuli Y of shear wall

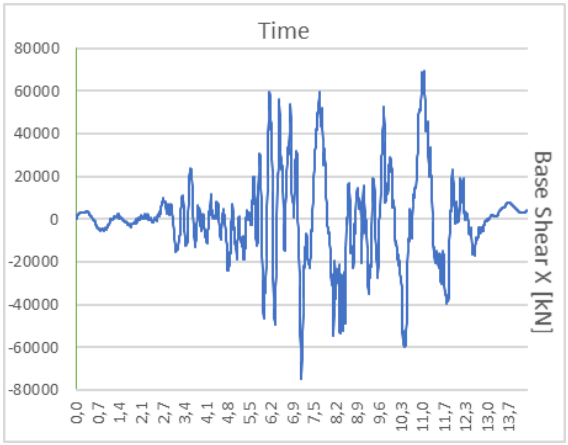

Figure 5-21 Base shear from direct integration T-H for Gazli X of shear wall

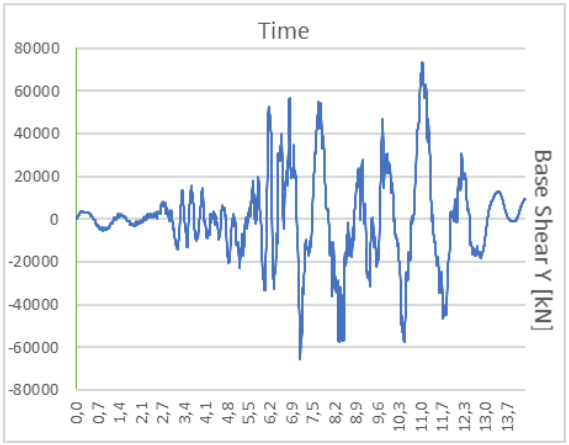

Figure 5-22 Base shear from direct integration T-H for Gazli X of shear wall

Maximum base shear for all time-history load cases are listed in Table 5.5. It is clear from the figures, as well as the table, that the Gazli earthquake leads to the largest value of base shear in both directions, which is reasonable as this earthquake is of greater magnitude than the others used for the analyses.

The results in x- and y-direction are generally similar, which is reasonable as the base shear highly depends on the mass of the building when the ground conditions are equal, and the mass is the same in both directions. For the Dursun earthquake, which is of lowest magnitude, the base shear is largest for the y-direction, while for the two larger earthquakes the largest base shear occurs in the x-direction. This may imply that the period of the Dursun earthquake is closer to the period of mode shape 1, which is in y-direction. This way, the impact will be greater for the y-direction. Oppositely, the larger earthquakes may have periods closer to the period of mode 2, which is in x-direction, further causing the largest impact in x-direction.

Table 5.5 Maximum base shear from all direct integration T-H load cases of shear wall

Direct Integration T-H Load Case	**Maximum Base Shear X/Y [kN]**
Dursun, X	17 870
Dursun, Y	23 040
Friuli, X	49 420
Friuli, Y	42 430
Gazli, X	74 800
Gazli, Y	73 770

5.3.1.2 Roof Displacement

The roof displacement in both x- and y-direction is measured from node 5660, the same node at which the target displacement was applied at in the pushover analysis.

Figure 5-23 to Figure 5-28 display the results of displacement in both x- and y-direction for the time-history load cases for Dursun, Friuli and Gazli in x- and y-direction. As can be seen, the graphs display the variation in displacement with time of each time-history load case. The graphs indicate similar response in both directions for each of the earthquakes.

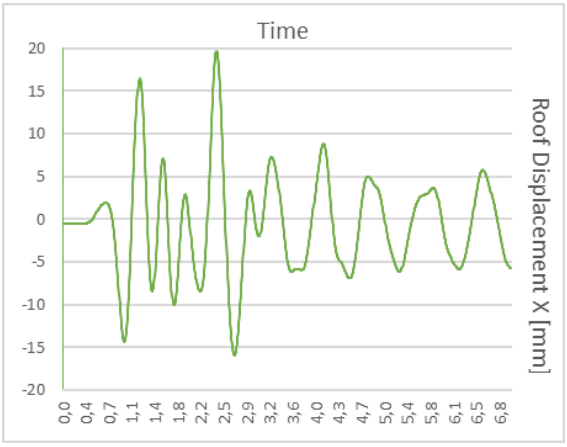

Figure 5-23 Roof displacement from direct integration T-H for Dursun X of shear wall

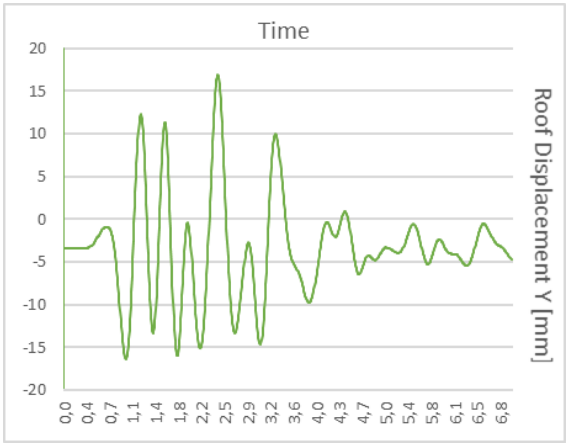

Figure 5-24 Roof displacement from direct integration T-H for Dursun Y of shear wall

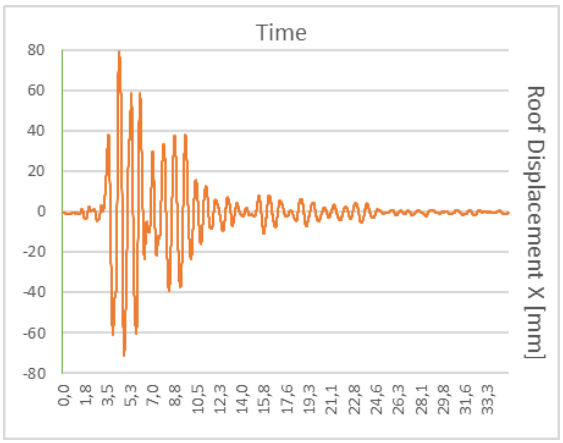

Figure 5-25 Roof displacement from direct integration T-H for Friuli X of shear wall

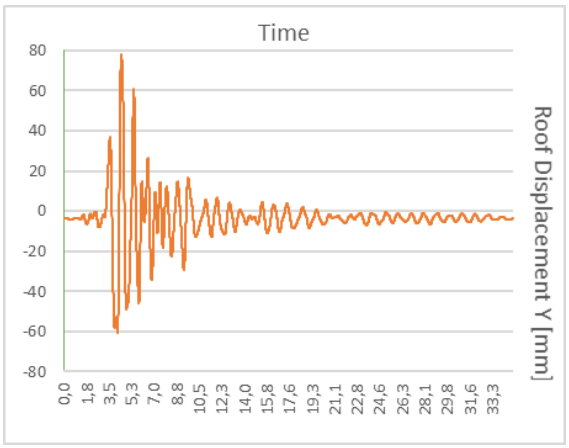

Figure 5-26 Roof displacement from direct integration T-H for Friuli Y of shear wall

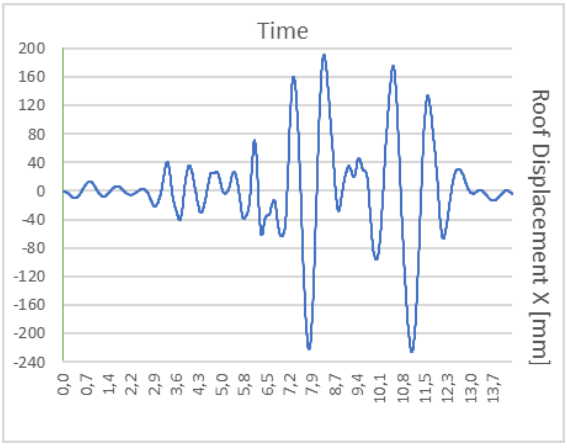

Figure 5-27 Roof displacement from direct integration T-H for Gazli X of shear wall

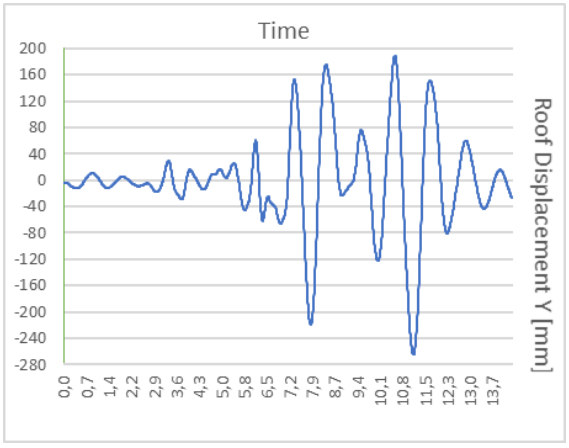

Figure 5-28 Roof displacement from direct integration T-H for Gazli Y of shear wall

Table 5.6 lists the maximum roof displacements occurring during each earthquake. The results are similar in both directions of the two smaller earthquakes, while for the Gazli earthquake the displacement in y-direction is considerably larger than in x-direction. This may be because of the difference in stiffness of the building due to the irregularity, as the building has lower stiffness in y-direction compared to x-direction. This difference is seemingly magnified as the magnitude of the earthquake increase.

Table 5.6 Maximum roof displacement from all direct integration T-H load cases of shear wall

Direct Integration T-H Load Case	**Maximum Roof Displacement X/Y [mm]**
Dursun, X	19,7
Dursun, Y	16,9
Friuli, X	79,4
Friuli, Y	78,1
Gazli, X	225,2
Gazli, Y	265,4

5.3.1.3 Drift Ratio

Figure 5-29 to Figure 5-34 illustrate the variation in roof drift for all time-history load cases as a function of time. For all three earthquakes the results are similar in both directions.

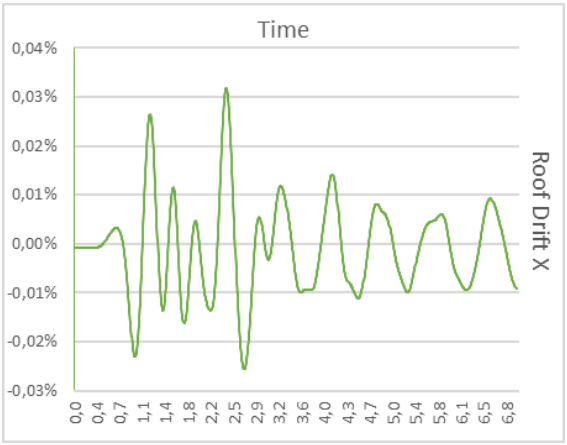

Figure 5-29 Roof drift from direct integration T-H for Dursun X of shear wall

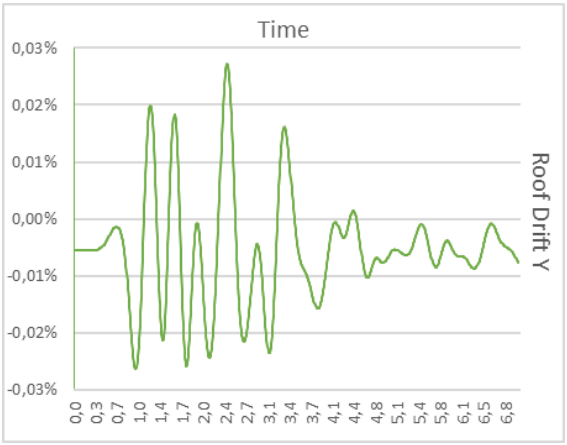

Figure 5-30 Roof drift from direct integration T-H for Dursun Y of shear wall

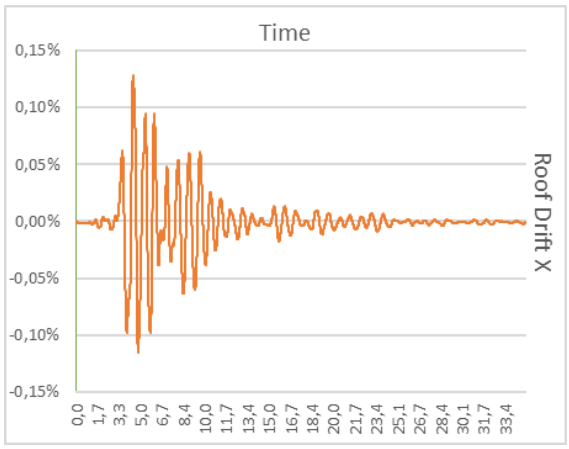

Figure 5-31 Roof drift from direct integration T-H for Friuli X of shear wall

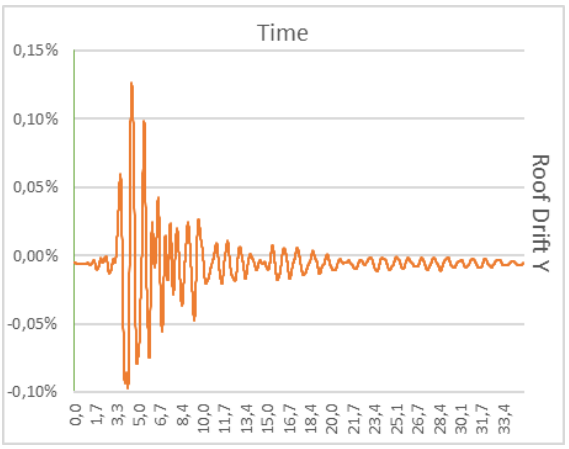

Figure 5-32 Roof drift from direct integration T-H for Friuli Y of shear wall

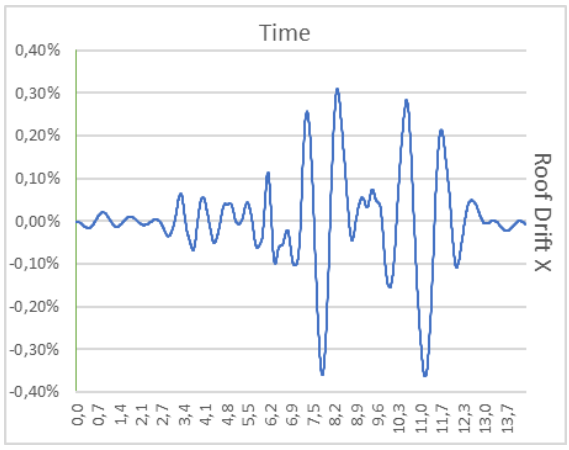

Figure 5-33 Roof drift from direct integration T-H for Gazli X of shear wall

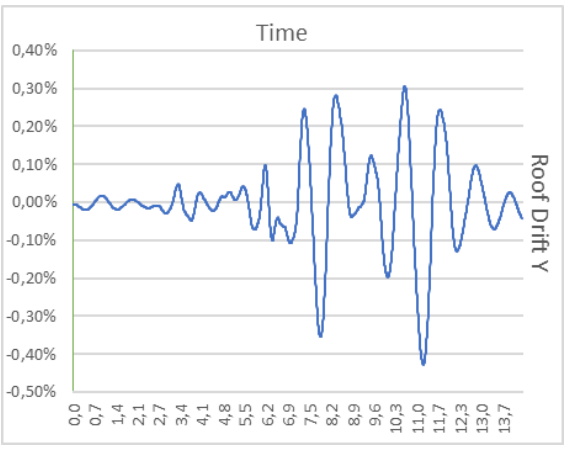

Figure 5-34 Roof drift from direct integration T-H for Gazli Y of shear wall

The peak roof drift values are listed in Table 5.7 for the different load cases. The results show that the maximum roof drift occurs during the Gazli earthquake in y-direction, which is reasonable considering previous results that also shows peak values during this earthquake. Generally, the maximum roof drift shows a larger value in y-direction, which may be due to irregularities in the geometry of the structure. Like for the roof displacements presented in Chapter 5.3.1.2, the magnitude of this irregularity is seemingly magnified as the earthquake increases and thus the difference in results of both directions is larger during the Gazli earthquake.

Table 5.7 Maximum roof drift from all direct integration T-H load cases of shear wall

Direct Integration T-H Load Case	**Maximum Roof Drift X/Y**
Dursun, X	0,031 %
Dursun, Y	0,027 %
Friuli, X	0,13 %
Friui, Y	0,13 %
Gazli, X	0,36 %
Gazli, Y	0,43 %

In addition to the automatically plotted roof drift ratios, the story drift is calculated for the time-history load cases using Eq. 6.

$$r = (U_n - U_{n-1})/h \tag{6}$$

Where *r* is the drift ratio, *U* is the displacement in the current direction, *n* is the story and *h* is the story height.

The variation in story drift over the building height for all direct integration time-history load cases is shown in Figure 5-35 to Figure 5-40. Generally, it can be seen for the smaller earthquakes that there is a sudden change in the slope in the 7^{th} to 9^{th} story, which is in the region where the lower part of the building ends. This results in a sudden change in stiffness, and thus the result is reasonable. The peak values are varying between this region and at the upper stories, which is also reasonable as the displacements are higher at the top story.

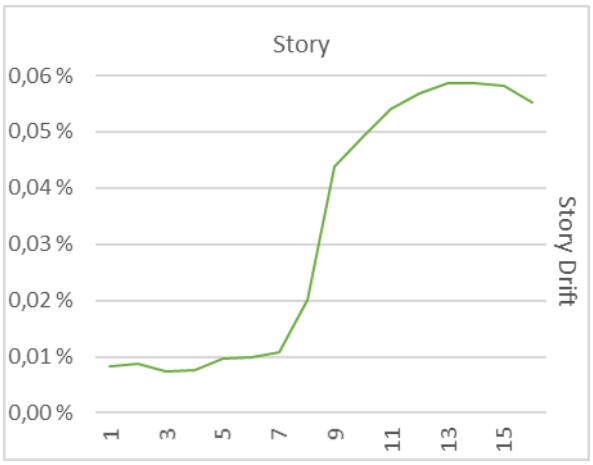

Figure 5-35 Story drift from direct integration T-H for Dursun X of shear wall

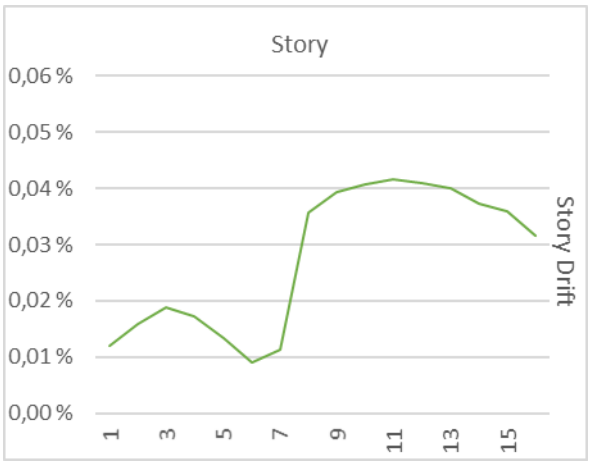

Figure 5-36 Story drift from direct integration T-H for Dursun Y of shear wall

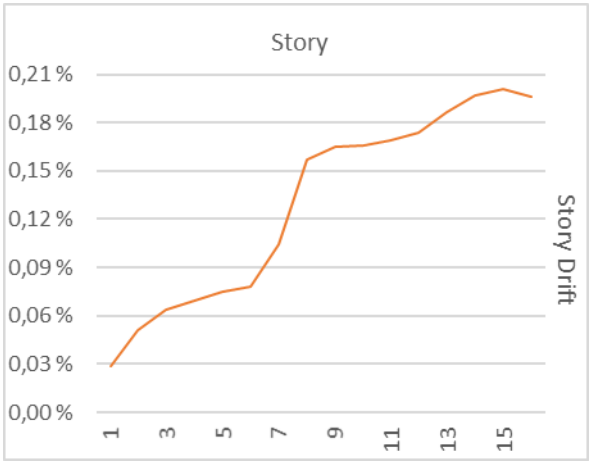

Figure 5-37 Story drift from direct integration T-H for Friuli X of shear wall

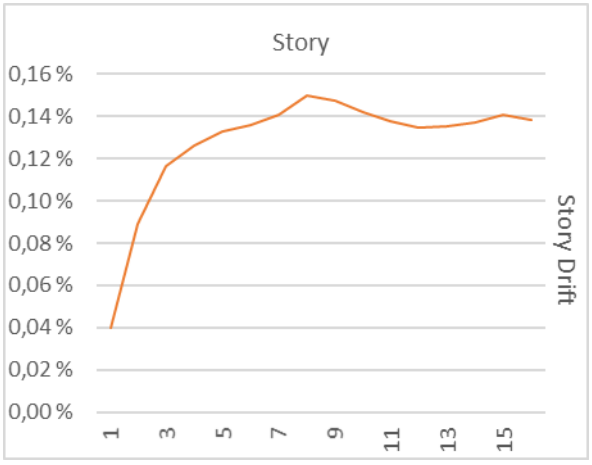

Figure 5-38 Story drift from direct integration T-H for Friuli Y of shear wall

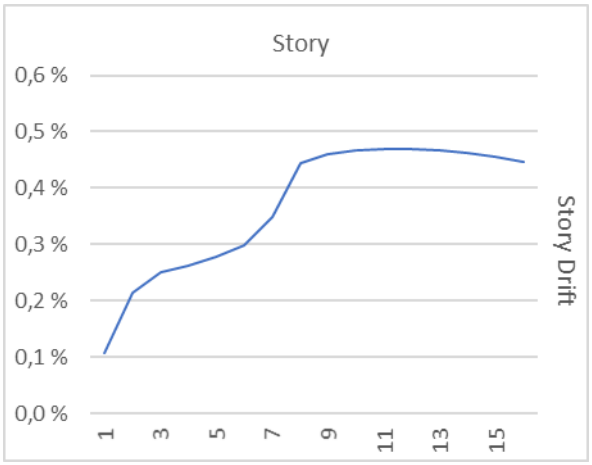

Figure 5-39 Story drift from direct integration T-H for Gazli X of shear wall

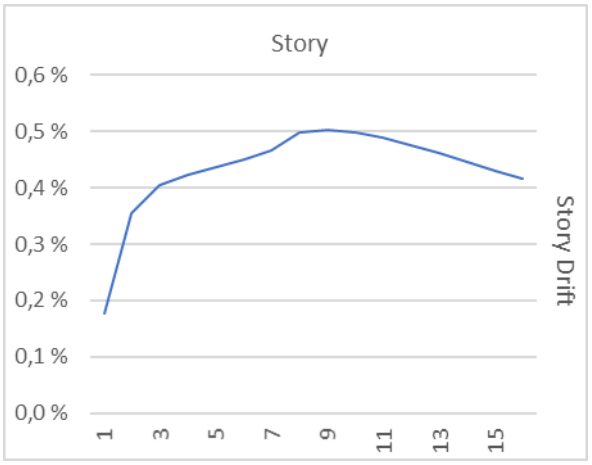

Figure 5-40 Story drift from direct integration T-H for Gazli Y of shear wall

Table 5.8 shows the maximum story drift for each direct integration time-history analysis, and the story at which the maximum drift occurs for each load case. The displacement of each story is computed at the time step at which the maximum displacement of node 5660 occurs, and the displacement is measured at the nodes directly below node 5660.

The maximum roof drifts are a bit lower than the maximum story drifts, which is as expected as the roof drift is a mean value calculated using the full structure height and not story by story. Like for the previous drift ratio results, hand calculations are performed to verify the accuracy of the calculated story drifts. The hand calculations agree with the maximum roof drift given by SAP2000 and it is therefore reasonable to assume that the story drifts are representative for the actual performance.

Table 5.8 Maximum story drift from all direct integration T-H load cases of shear wall

Direct Integration T-H Load Case	**Maximum Story Drift X/Y**	**Story**
Dursun, X	0,059 %	12-14
Dursun, Y	0,042 %	10-11
Friuli, X	0,20 %	13-16
Friuli, Y	0,15 %	7-9
Gazli, X	0,47 %	9-13
Gazli, Y	0,50 %	7-10

5.3.2 MBF

The results from the direct integration time-history analysis for the MBF system include base shear reactions, roof displacements and drift ratio for the three ground motion records: Dursun, Friuli and Gazli in both x- and y-direction. Also, the formation of plastic hinges in the MBF is presented for all the load cases. The analyses for the Gazli records stopped after approximately 9,37 seconds due to lack of convergence in the iterations, indicating global collapse of the structure. Therefore, only results up to 9,3 seconds are included for the direct integration time-history analysis even though the records for Gazli plotted in to SAP2000 were 13,5 seconds.

5.3.2.1 Base Shear Reaction

The base shear reactions for all the ground motion records in both x- and y-direction are shown as graphs in Figure 5-41 to Figure 5-46. From the graphs, it can be noticed that the base shear

is largest for Gazli and smallest for Dursun, which is as expected since the Gazli earthquake is significantly larger. Furthermore, the load cases in x-direction have in average larger amplitudes than the load cases in y-direction. The Dursun time-history records caused lowest base shear reactions on the MBF structure for the direct integration time-history analysis. The reason that the base shear is different in x- and y direction is because the geometry of the structure is irregular.

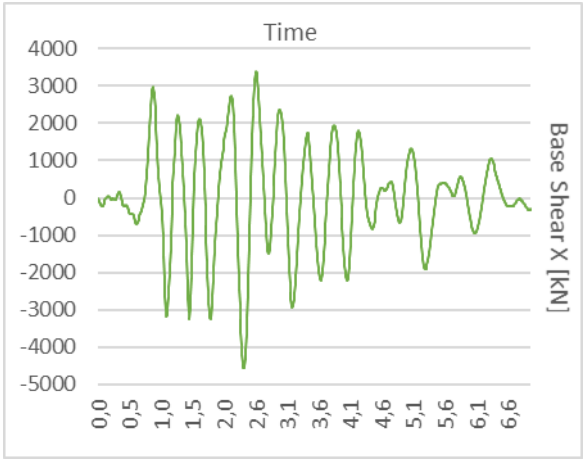

Figure 5-41 Base shear from direct integration T-H for Dursun X of MBF

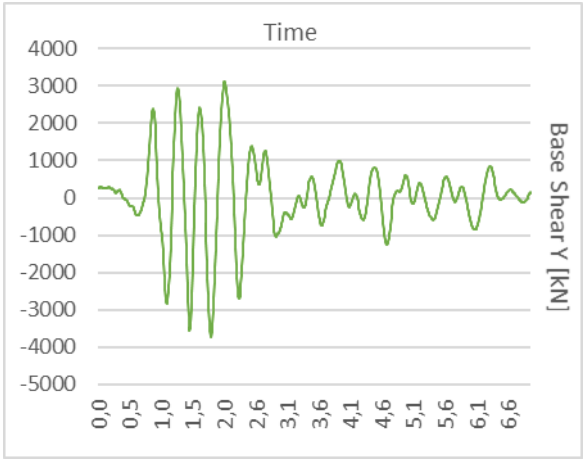

Figure 5-42 Base shear from direct integration T-H for Dursun Y of MBF

The base shear reactions for the Friuli time-history record is presented in Figure 5-43 and Figure 5-44. Friuli showed larger base shear than Dursun, but lower than Gazli. The graphs indicate that Friuli causes more seismic waves, which is due to a significantly longer time span for Friuli than the other earthquakes. If considering number of waves relative to time, Dursun and Gazli have more seismic waves.

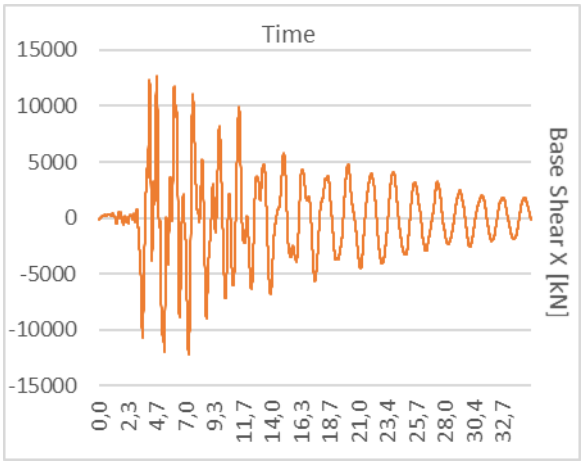

Figure 5-43 Base shear from direct integration T-H for Friuli X of MBF

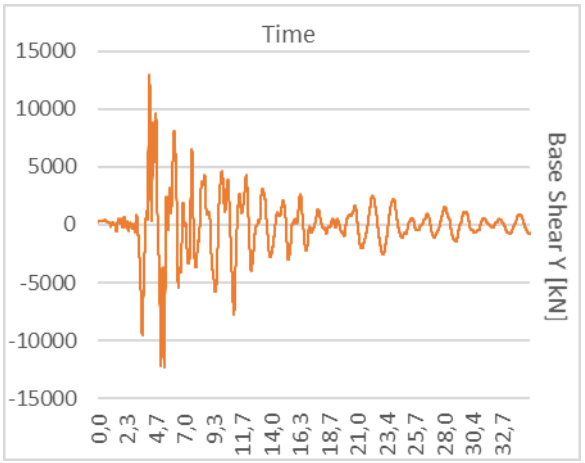

Figure 5-44 Base shear from direct integration T-H for Friuli Y of MBF

As mentioned, the direct integration time-history analysis for the Gazli record stopped due to convergence problems, which indicates global collapse. Looking at the curve in x-direction, it can be the base shear right before the structure collapse is displayed. In the graph for the x-direction, the line does not cross the "zero"-axis but turns on approximately -1000 kN and keeps decreasing. The sudden drop in the graph indicates damage of elements in the structure.

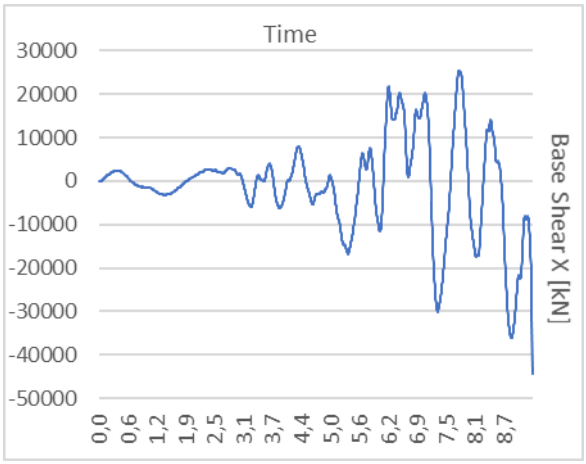

Figure 5-45 Base shear from direct integration T-H for Gazli X of MBF

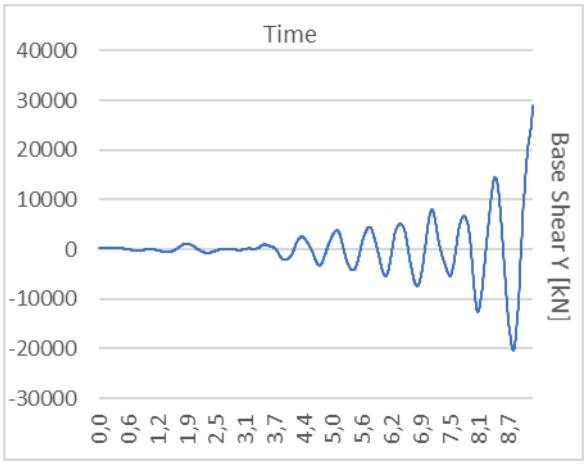

Figure 5-46 Base shear from direct integration T-H for Gazli Y of MBF

The maximum base shear is presented in Table 5.9, where the load case with the lowest base shear is Dursun in y-direction and the load case with the highest base shear is Gazli in x-direction. Which direction leads to the highest base shear varies for the different time-history records. The values are higher in x-direction for Dursun and Gazli, while for Friuli the highest value occur in y-direction. Furthermore, there is no noteworthy difference between the maximum base shear reactions for the different directions for Friuli.

Table 5.9 Maximum base shear from all direct integration T-H load cases of MBF

Direct Integration T-H Load Case	**Maximum Base Shear X/Y [kN]**
Dursun, X	4 578
Dursun, Y	3 731
Friuli, X	12 750
Friuli, Y	12 910
Gazli, X*	36 020
Gazli, Y*	20 430

**Stopped at 9,3 seconds*

5.3.2.2 Roof Displacement

The roof displacement is measured at joint 5696 for both x- and y-direction in all load cases. Figure 5-47 to Figure 5-52 show the roof displacement from the direct integration time-history analyses for all the time-history records. The maximum roof displacement for Dursun is higher in y-direction and in negative direction. This means that the monitored joint on the roof for this load case is swaying back and forth a displacement on -7,2 mm in the y-direction.

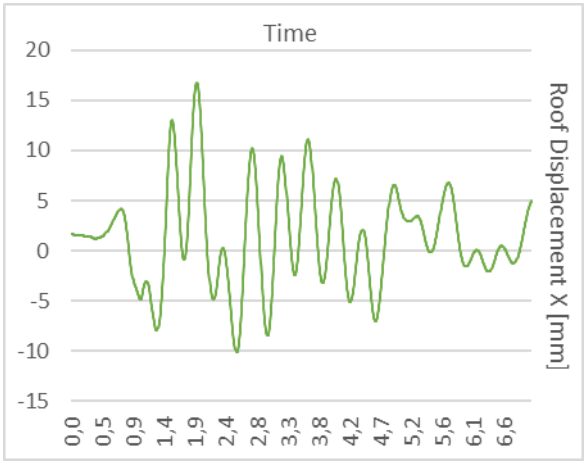

Figure 5-47 Roof displacement from direct integration T-H for Dursun X of MBF

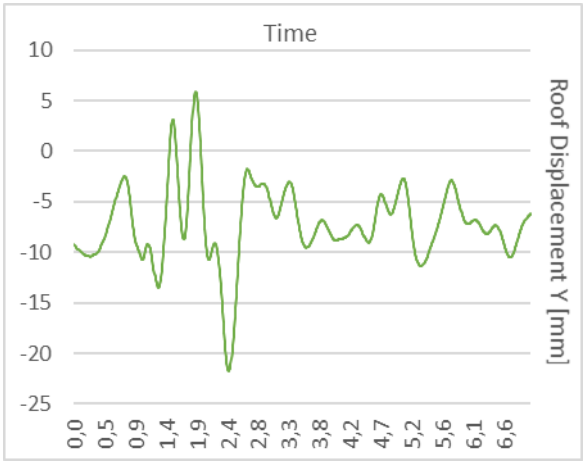

Figure 5-48 Roof displacement from direct integration T-H for Dursun Y of MBF

For Friuli, the average roof displacement of the structure is largest is x-direction, but the maximum roof displacement is in negative y-direction. Figure 5-49 and Figure 5-50 show the roof displacement over time for the Friuli time-history record.

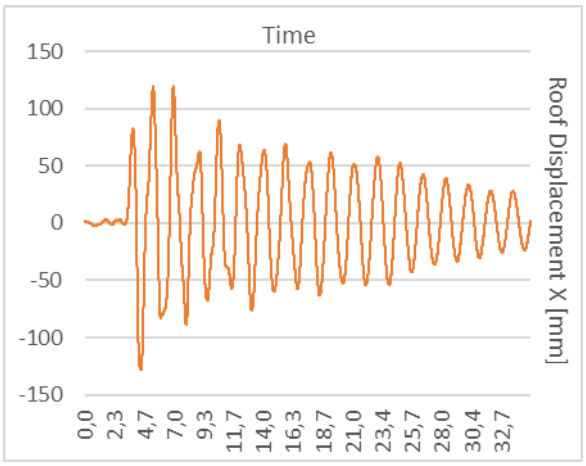

Figure 5-49 Roof displacement from direct integration T-H for Friuli X of MBF

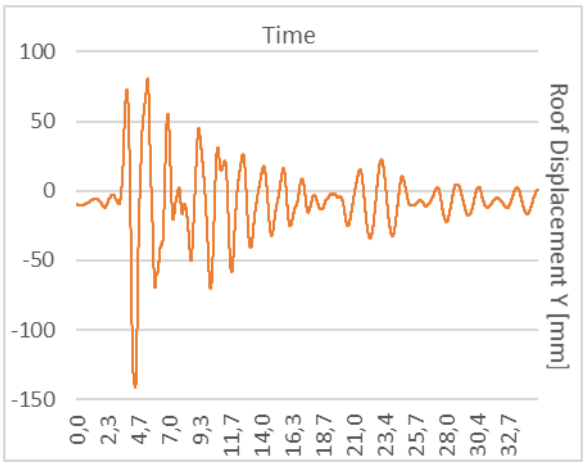

Figure 5-50 Roof displacement from direct integration T-H for Friuli Y of MBF

Both average and maximum roof displacement are highest in x-direction for the Gazli time-history record. The time where the roof displacement is highest is seemingly when the

respective elements collapse. The graphs for the roof displacements for Gazli is illustrated in Figure 5-51 and Figure 5-52.

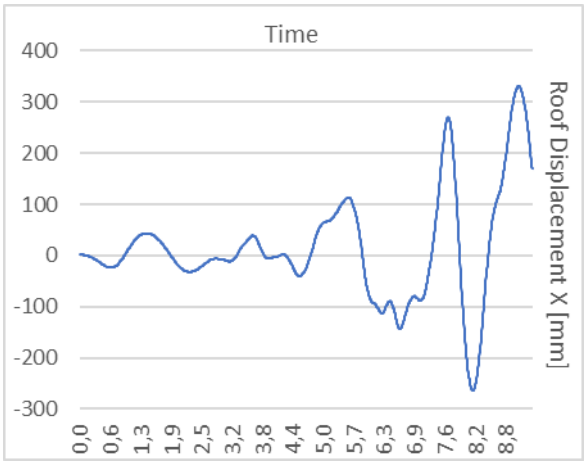

Figure 5-51 Roof displacement from direct integration T-H for Gazli X of MBF

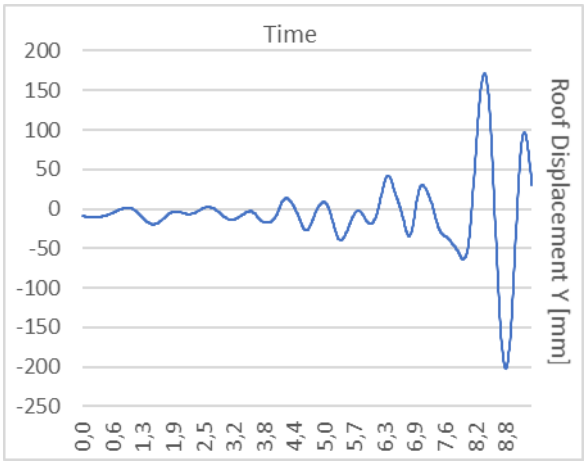

Figure 5-52 Roof displacement from direct integration T-H for Gazli Y of MBF

The maximum roof displacement for the load cases are presented in Table 5.10. It is the time-history load case for Gazli in x-direction that has the largest maximum displacement, while Dursun in x-direction has the lowest. As for the base shear, which direction that has the highest maximum roof displacement varies between the earthquakes. For Dursun and Friuli the highest maximum roof displacement in y-direction, while for Gazli it is highest in x-direction.

Table 5.10 Maximum roof displacement from all direct integration T-H load cases of MBF

Direct Integration T-H Load Case	**Maximum Roof Displacement X/Y [mm]**
Dursun, X	16,79
Dursun, Y	21,74
Friuli, X	127,90
Friuli, Y	142,00
Gazli, X*	330,80
Gazli, Y*	202,40

**Stopped at 9 seconds*

5.3.2.3 Drift Ratio

Figure 5-53 to Figure 5-58 show the roof drift for the different load cases in the x- and y-direction. The load case with the largest roof drift shown in the graphs is Gazli in x-direction.

For the Dursun time-history record, the roof drift is highest in the y-direction just like for the roof displacement, which makes sense as the roof drift is dependent on the roof displacement.

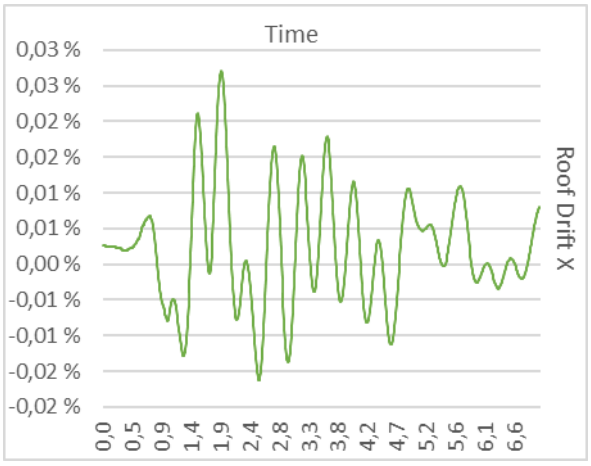

Figure 5-53 Roof drift from direct integration T-H for Dursun X of MBF

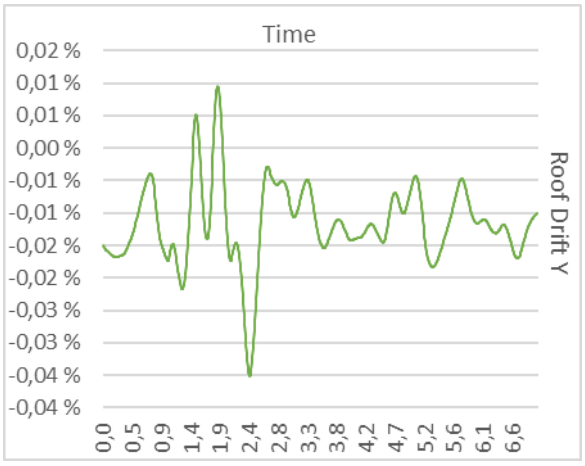

Figure 5-54 Roof drift from direct integration T-H for Dursun Y of MBF

The most critical roof drift for the Friuli time-history record is in the x-direction, as can be seen in Figure 5-55. For both directions, the roof drift is largest after around 4,7 seconds, which is displayed in Figure 5-55 and Figure 5-56.

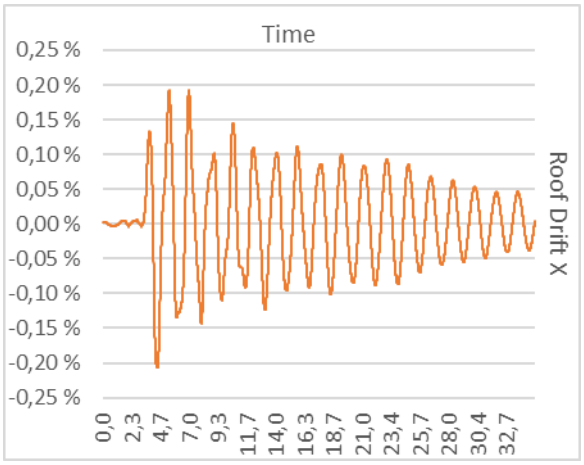

Figure 5-55 Roof drift from direct integration T-H for Friuli X of MBF

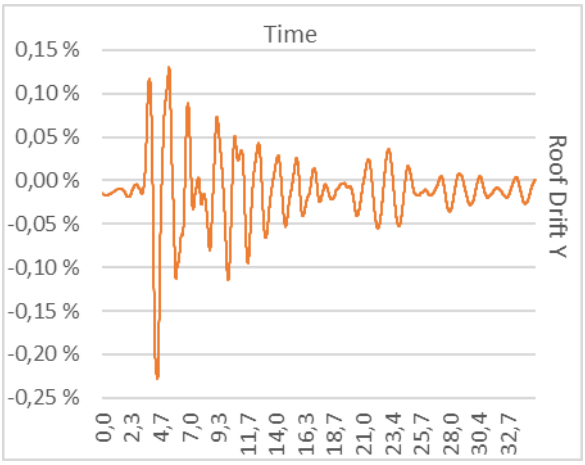

Figure 5-56 Roof drift from direct integration T-H for Friuli Y of MBF

The roof drift in both directions for the Gazli time-history record is shown in Figure 5-57 and Figure 5-58. From the graphs, it can be seen that the roof drift is significantly larger in x-direction, like the roof displacement from Chapter 5.3.2.2.

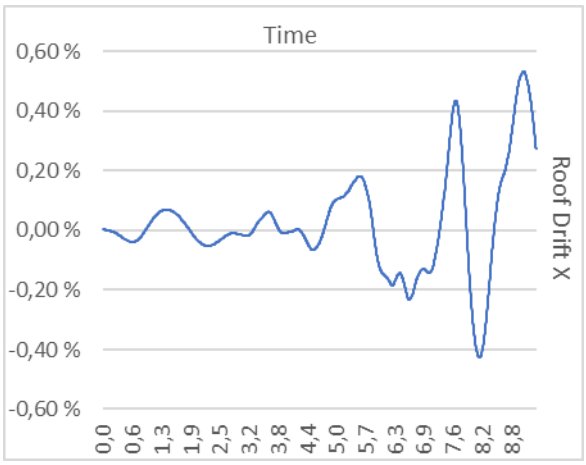

Figure 5-57 Roof drift from direct integration T-H for Gazli X of MBF

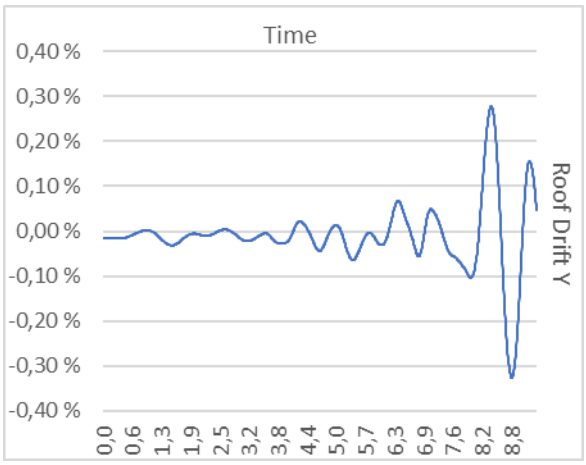

Figure 5-58 Roof drift from direct integration T-H for Gazli Y of MBF

The maximum roof drift with a generalized displacement in joint 5696 for the six load cases is presented in Table 5.11. The load case for Gazli in x-direction leads to the highest roof drift, while the load case for Dursun in x-direction results in the lowest maximum roof drift. The maximum roof drift is higher in y-direction for Dursun and Friuli while during Gazli it is higher in x-direction. This is similar to the peak values of the maximum roof displacement presented in Chapter 5.3.2.2.

Table 5.11 Maximum roof drift from all direct integration T-H load cases of MBF

Direct Integration T-H Load Case	**Maximum Roof Drift X/Y**
Dursun, X	0,027 %
Dursun, Y	0,035 %
Friuli, X	0,206 %
Friui, Y	0,229 %
Gazli, X*	0,534 %
Gazli, Y*	0,327 %

**Stopped at 9,3 seconds*

The drift from each floor is calculated and visualized as graphs in Figure 5-59 to Figure 5-64. As the braces in the MBF structure span across two floors, the story drift tends to increase every second story. Furthermore, the low part of the structure stops at the 7th floor so that makes the 8th to 16th floor more elastic, which will generally make the story drift higher. The brace in the 8th floor of the tall part of the structure is spanning from 6th to 8th, so in this case the story drifts

increases from the 9th floor. Generally, the story drift has a great amount of variations during the different earthquakes.

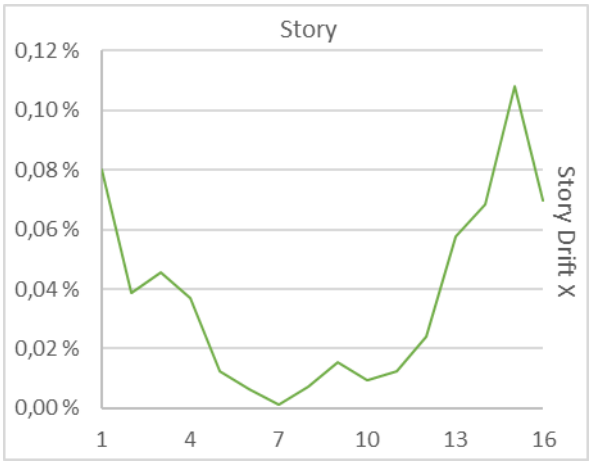

Figure 5-59 Story drift from direct integration T-H for Dursun X of MBF

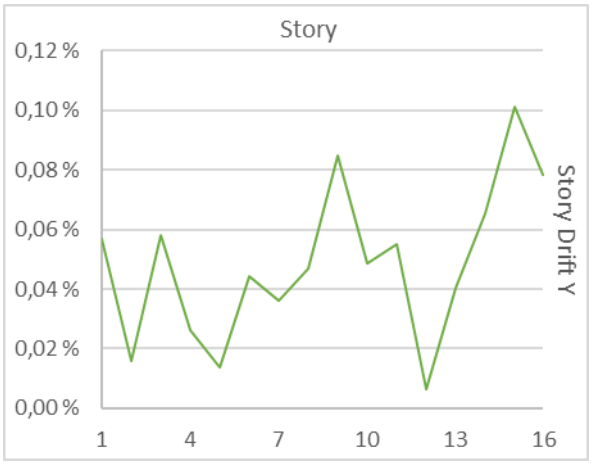

Figure 5-60 Story drift from direct integration T-H for Dursun Y of MBF

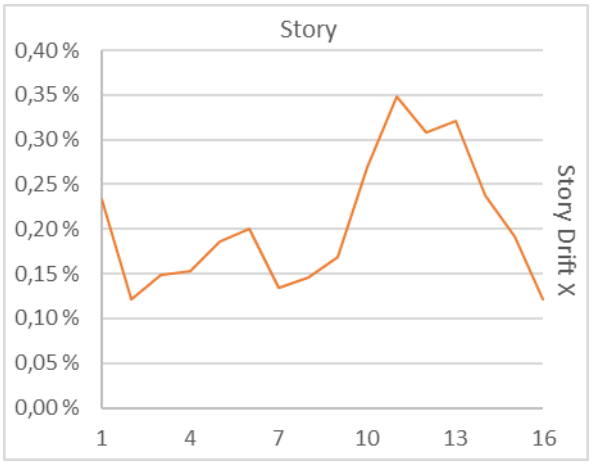

Figure 5-61 Story drift from direct integration T-H for Friuli X of MBF

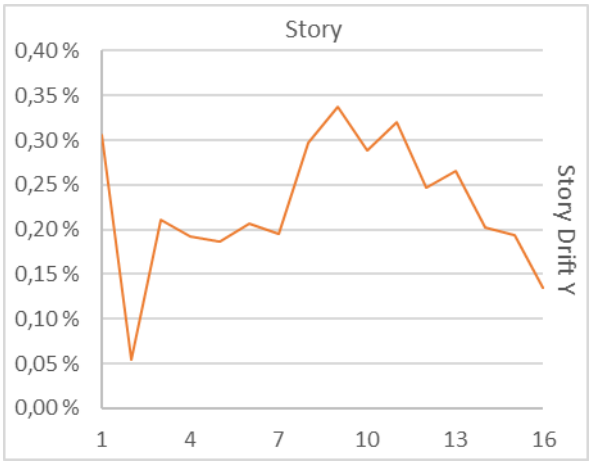

Figure 5-62 Story drift from direct integration T-H for Friuli Y of MBF

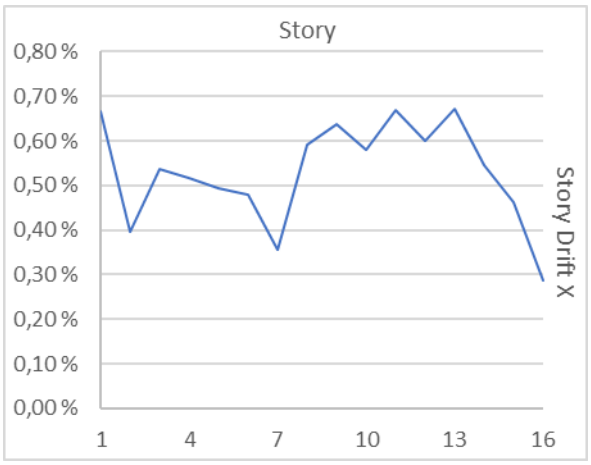

Figure 5-63 Story drift from direct integration T-H for Gazli X of MBF

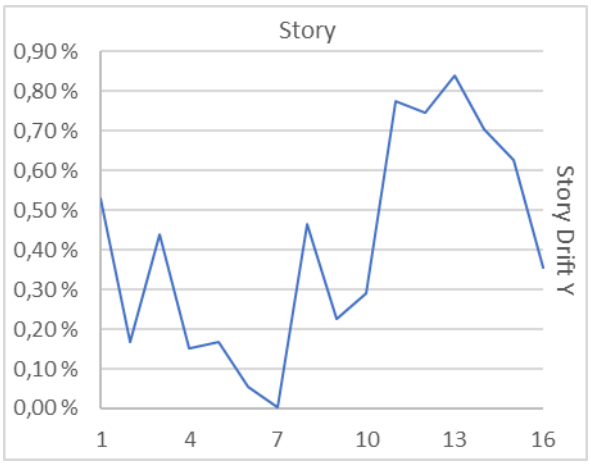

Figure 5-64 Story drift from direct integration T-H for Gazli Y of MBF

Table 5.12 shows the calculated maximum story drift and its respective story for each load case. The maximum story drift is extracted from the calculated joints in every story below the monitored joint 5696. The highest story drift from all load cases is between floor 12-13 during the Gazli earthquake in x-direction, while the lowest is between floor 14-15 for Dursun in y-direction.

Table 5.12 Maximum story drift from all direct integration T-H load cases of MBF

Direct Integration T-H Load Case	**Maximum Story Drift X/Y**	**Story**
Dursun, X	0,108 %	14-15
Dursun, Y	0,101 %	14-15
Friuli, X	0,348 %	10-11
Friui, Y	0,338 %	8-9
Gazli, X*	0,923 %	12-13
Gazli, Y*	0,839 %	12-13

**Stopped at 9,3 seconds*

5.3.2.4 Hinge Formation

Figure 5-65 to Figure 5-70 show the deformation of the lateral force resisting system in the MBF structure at the last time step for the different load cases. From the figures, the load case with the most plastic hinges is the Gazli earthquake in x-direction, while the load case for Dursun in y-direction results in no plastic hinges, meaning than none of the braces has yielded at this stage. Looking at the hinge deformation for the Gazli load cases, some of the hinges have

reached the red zone, which implies that the hinges has reached the state of total failure. The deformation of the structure is related to the story drift from the previous subchapter, varying along the building height.

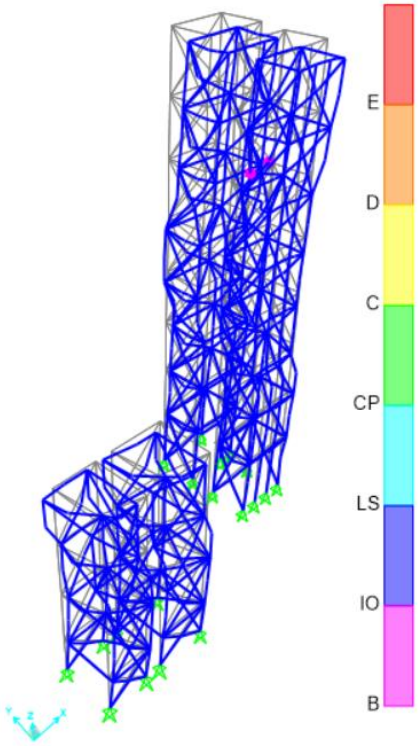

Figure 5-65 Hinge formation from direct integration T-H for Dursun X of MBF

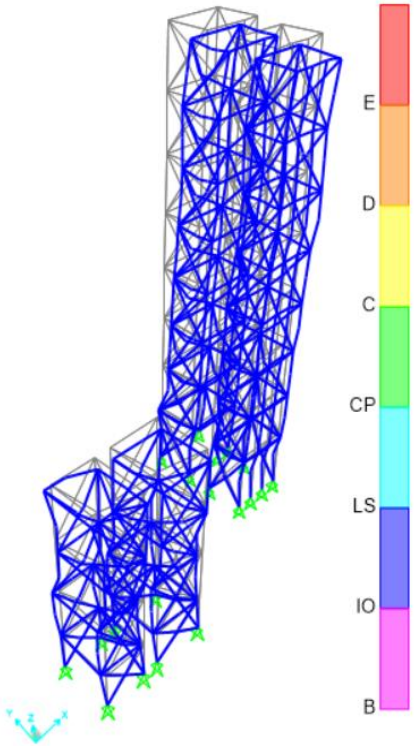

Figure 5-66 Hinge formation from direct integration T-H for Dursun Y of MBF

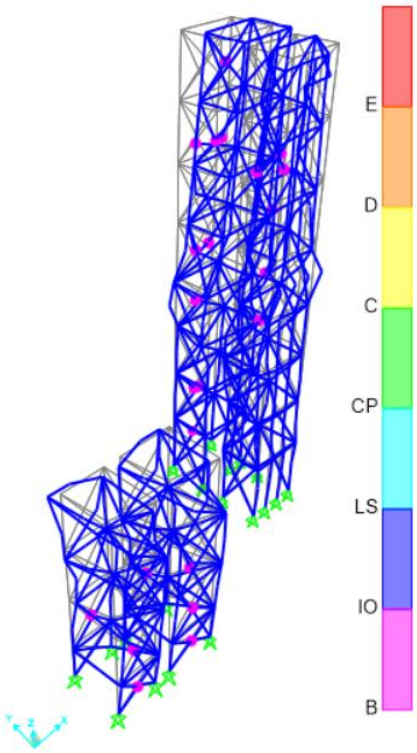

Figure 5-67 Hinge formation from direct integration T-H for Friuli X of MBF

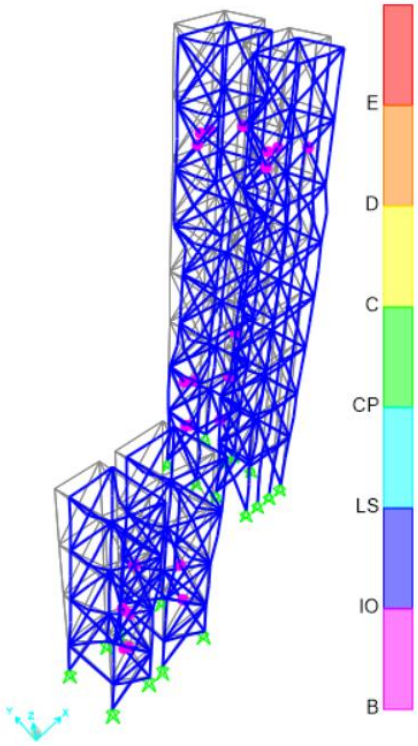

Figure 5-68 Hinge formation from direct integration T-H for Friuli Y of MBF

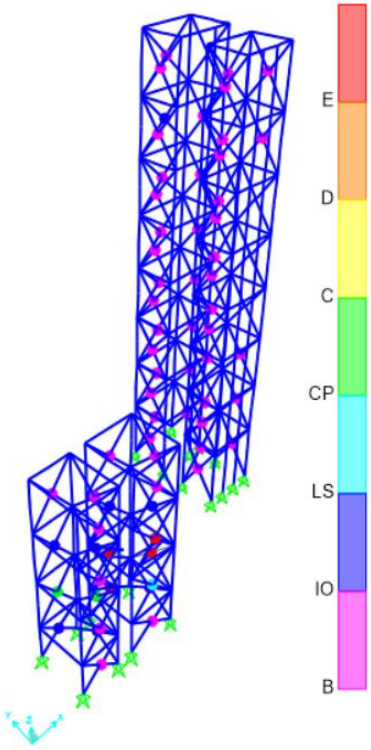

Figure 5-69 Hinge formation from direct integration T-H for Gazli X of MBF

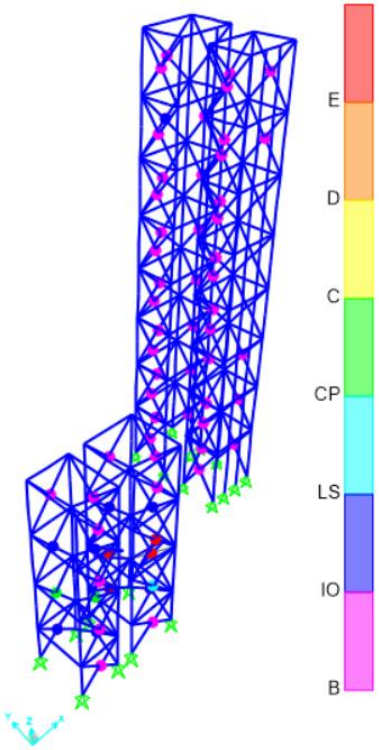

Figure 5-70 Hinge formation from direct integration T-H for Gazli Y of MBF

5.4 Modal Time-History Analysis

In the following chapter, results of the modal time-history analysis, also termed nonlinear fast analysis, of the structure with friction dampers are compared to the direct integration time-history analysis of the structure without dampers. As the dampers are placed in y-direction, only results in y-direction are obtained and presented.

5.4.1 Shear Walls

Results of the modal time-history analyses of the shear wall structure are presented in the following chapter for all modal time-history load cases.

5.4.1.1 Slip Load

Figure 5-71 shows the result of the hysteresis loop of a friction damper with initially defined slip load of 200 kN during the Dursun earthquake in y-direction. The result is plotted for element 35, which is located at the top story.

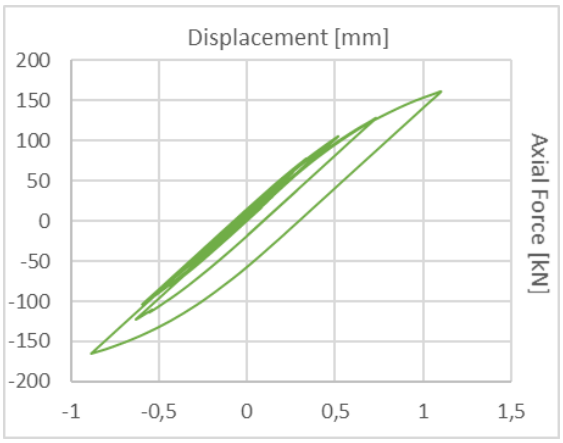

Figure 5-71 Hysteresis loop from modal T-H for Dursun Y of shear wall with 200 kN slip load of damper

As described in Chapter 2.6.3, the hysteresis loop of a Pall friction damper should look like the loop of an elastic-perfectly plastic material. The shape of the loop for the Dursun earthquake does not look like the desired shape, as the slope is too steep. By reducing the slip load of the damper to 10 kN, the hysteresis loop is starting to reach an acceptable shape, as shown in Figure 5-72. As the slip load is defined as 10 kN, which is a relatively low value, this implies that the demand of energy dissipation of the structure during this earthquake is low. The low slip load makes sense when studying the results of the time-history analyses for this earthquake, as the displacements and stresses are very low as well.

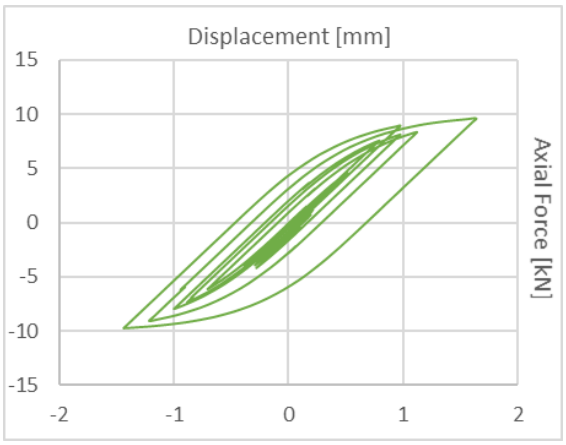

Figure 5-72 Hysteresis loop from modal T-H for Dursun Y of shear wall with 10 kN slip load of damper

A slip load of 150 kN is defined for the Friuli earthquake in y-direction. This value results in a hysteretic loop that look similar to the desired shape as shown in Figure 5-73.

It is reasonable that the optimal slip load is larger than for the Dursun earthquake, considering that the magnitude of the Friuli earthquake is larger and according to the results of the direct integration analysis Friuli affects the structure to a larger extent.

As expected, the reasonable slip load for the Gazli earthquake is larger than that of the two smaller earthquakes. According to the hysteresis loop in y-direction, shown in Figure 5-74, a slip load of 350 kN is assumed reasonable for this earthquake.

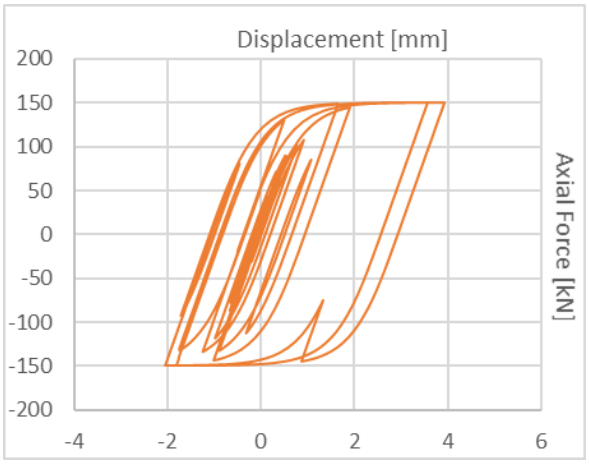

Figure 5-73 Hysteresis loop from modal T-H for Friuli Y of shear wall with 150 kN slip load of damper

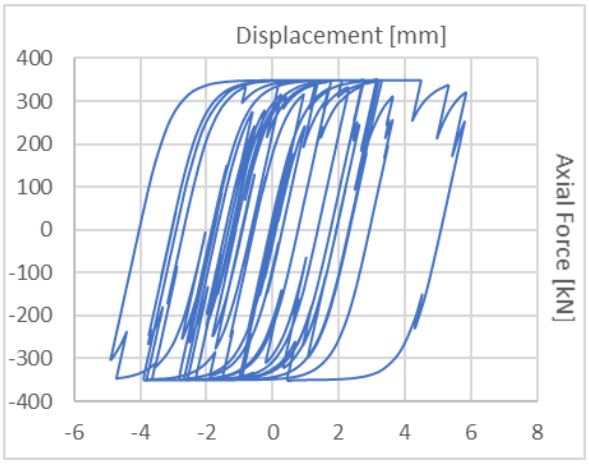

Figure 5-74 Hysteresis loop from modal T-H for Gazli Y of shear wall with 350 kN slip load of damper

The slip loads of each time-history load case that are assumed reasonable and will be used for further analysis are listed in Table 5.13.

Table 5.13 Assumed slip load for friction dampers from all modal T-H load cases of shear wall

Modal T-H Load Case	**Slip Load [kN]**
Dursun, Y	10
Friuli, Y	150
Gazli, Y	350

5.4.1.2 Base Shear Reaction

The base shear reactions are computed for all the modal time-history load cases and shown in Figure 5-75, Figure 5-76 and Figure 5-77. During the Dursun earthquake, the base shear forces are significantly lower than those of the Friuli earthquake, which again are smaller than the ones occurring during the Gazli earthquake. This is a reasonable result considering the magnitude of the earthquakes.

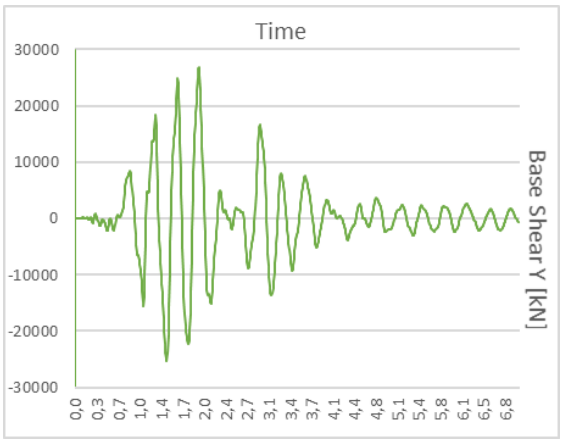

Figure 5-75 Base shear from modal T-H for Dursun Y of shear wall

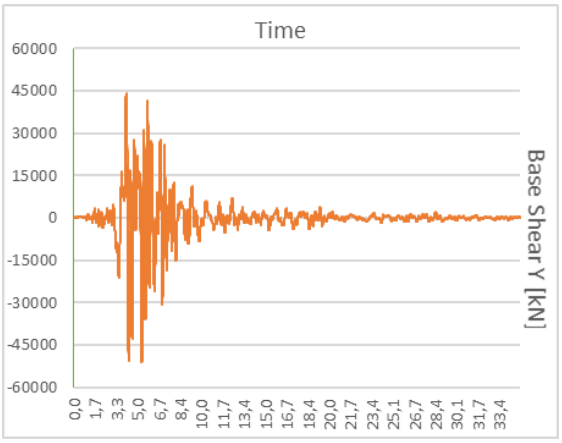

Figure 5-76 Base shear from modal T-H for Friuli Y of shear wall

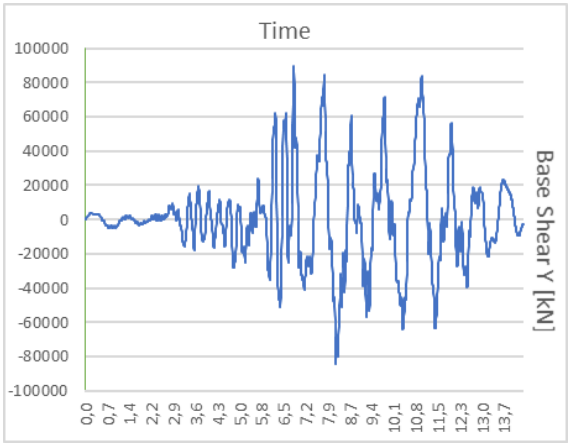

Figure 5-77 Base shear from modal T-H for Gazli of shear wall

The maximum base shear value of each case is listed in Table 5.14. For all modal time-history load cases the resulting maximum base shear is larger than for the same direction from the direct integration time-history analysis, with an increasing difference with increasing magnitude of the earthquake. Still, the results are generally similar.

Table 5.14 Maximum base shear from all modal T-H load cases of shear wall

Modal T-H Load Case	**Maximum Base Shear Y [kN]**
Dursun, Y	26 740
Friuli, Y	51 250
Gazli, Y	89 650

5.4.1.3 Roof Displacement

Figure 5-78, Figure 5-79 and Figure 5-80 present the variation in roof displacement during the three earthquakes. As for the direct integration time-history results, the Dursun earthquake leads to significantly smaller roof displacement compared to the two larger earthquakes, and the maximum roof displacement occurs during the Gazli earthquake.

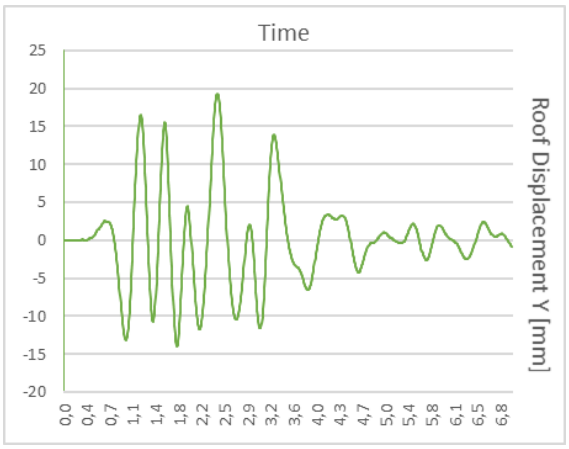

Figure 5-78 Roof displacement from modal T-H for Dursun Y of shear wall

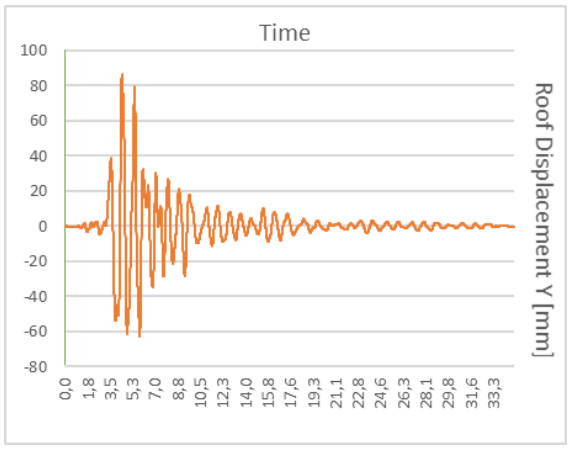

Figure 5-79 Roof displacement from modal T-H for Friuli Y of shear wall

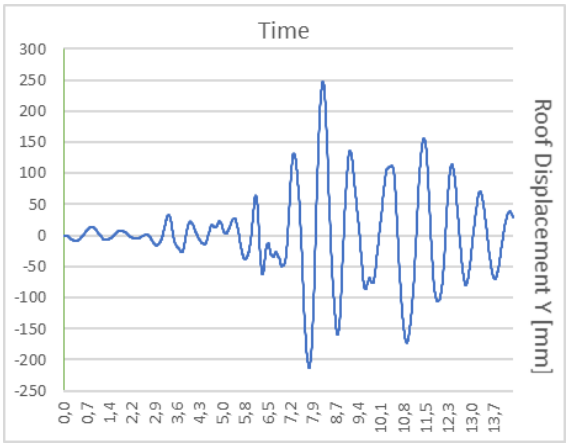

Figure 5-80 Roof displacement from modal T-H for Gazli Y of shear wall

Table 5.15 presents the peak roof displacement occurring during the different earthquakes, with the lowest roof displacement occurring during the Dursun earthquake and the largest occurring during Gazli. The values are in accordance with the maximum roof displacements obtained through the direct integration time-history analyses.

Table 5.15 Maximum roof displacement from all modal T-H load cases of shear wall

Modal T-H Load Case	**Maximum Roof Displacement Y [mm]**
Dursun, Y	19,3
Friuli, Y	86,6
Gazli, Y	247,2

5.4.1.4 Drift Ratio

The roof drift for all the pushover load cases during their respective earthquakes are plotted in Figure 5-81, Figure 5-82 and Figure 5-83. During the Gazli earthquake the drift ratio is clearly larger than the other earthquakes, both regarding peak values and variation. This is due to the roof displacement during Gazli being larger than during the two other earthquakes, as the roof drift is a function of the roof displacement.

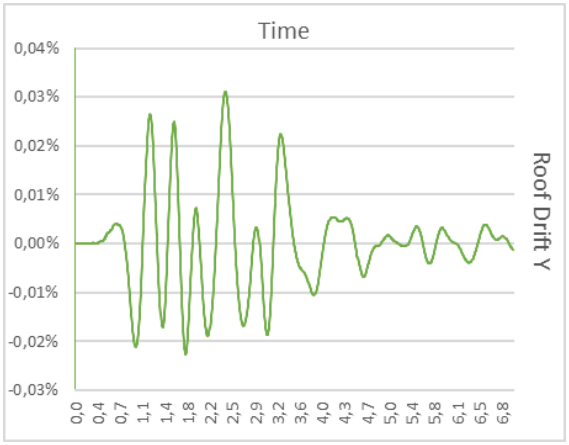

Figure 5-81 Roof drift from modal T-H for Dursun Y of shear wall

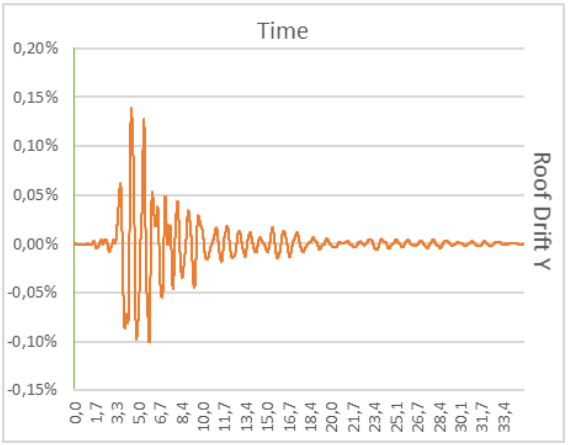

Figure 5-82 Roof drift from modal T-H for Friuli Y of shear wall

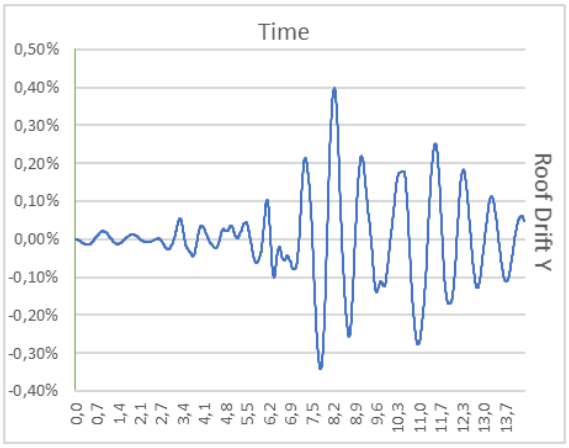

Figure 5-83 Roof drift from modal T-H for Gazli Y of shear wall

The maximum roof drift value for each modal time-history load case is listed in Table 5.16. Like for the previous results, the value increases with increasing magnitude of the earthquake, i.e. the maximum roof drift is observed during the Gazli earthquake.

Table 5.16 Maximum roof drift from all modal T-H load cases for shear wall

Modal T-H Load Case	**Maximum Roof Drift Y**
Dursun, Y	0,031 %
Friui, Y	0,14 %
Gazli, Y	0,40 %

In addition to the roof displacement, the maximum story drift is computed for each modal time-history load case. The variation in story drift over the building height during the three earthquakes are shown in Figure 5-84, Figure 5-85 and Figure 5-86.

For the two smaller earthquakes the story drift is seemingly low in the first stories, before a sudden increase in drift in stories 7-10. This is reasonable as there is an abrupt change in stiffness of the building at story 7, as only the tall part of the building continues for the above stories. Although it is not as clear from the Gazli earthquake graph, the maximum story drift is also occurring in the approximately same height. During this earthquake the story drift is generally higher, which is reasonable considering the magnitude of the earthquake compared to the two others.

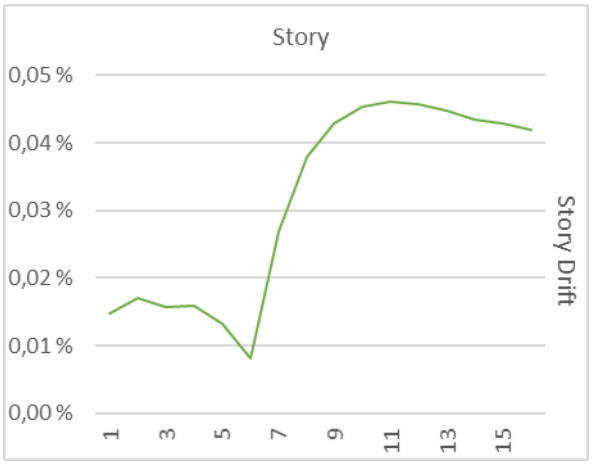

Figure 5-84 Story drift from modal T-H for Dursun Y of shear wall

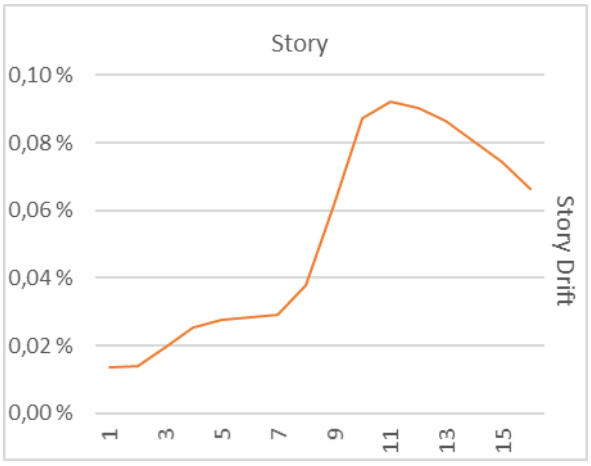

Figure 5-85 Story drift from modal T-H for Friuli Y of shear wall

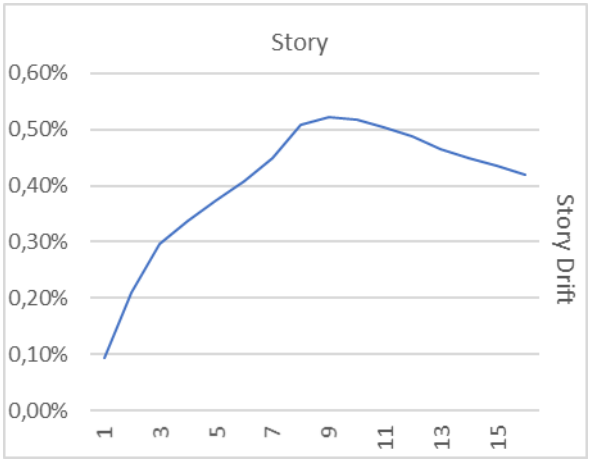

Figure 5-86 Story drift from modal T-H for Gazli Y of shear wall

The results of the calculations, presented with the maximum story drift for each case, are listed in Table 5.17. In addition, the stories at which the maximum story drift occurs in each case is given. As seen from the graphs as well, the stories where the lower part of the building "stops" are most affected and experience the largest story drifts. The difference in maximum story drift, and also the overall story drift, are significantly higher for the Gazli earthquake, which is reasonable.

Table 5.17 Maximum story drift from all modal T-H load cases of shear wall

Modal T-H Load Case	**Maximum Story Drift Y**	**Story**
Dursun, Y	0,046 %	9-12
Friuli, Y	0,09 %	9-13
Gazli, Y	0,52 %	7-11

5.4.2 MBF Structure

For the MBF structure the defined slip load of the friction dampers varies from the different load cases. This chapter presents the results from the modal time-history analyses for all the time-history records in the y-direction, as the friction dampers are only placed in this direction.

5.4.2.1 Slip Load

The slip load for the dampers in the different load cases of the MBF structure has been found the same way as for the slip loads for the dampers in the shear wall structure, where different slip loads have been defined until the hysteresis loop looks like an elastic-perfectly plastic

material. Figure 5-87 to Figure 5-89 show the results of the hysteresis loops presented by deformation and axial force from a damping element in the top story for the different load cases.

The hysteresis loop for the Dursun load case indicates that the slip load is too high as the energy dissipating demand is low, which is due to the low magnitude of the earthquake. For the Gazli load case, on the other hand, the hysteresis loop indicates that the energy dissipating demand and slip load is larger, which makes sense as the earthquake is significantly larger.

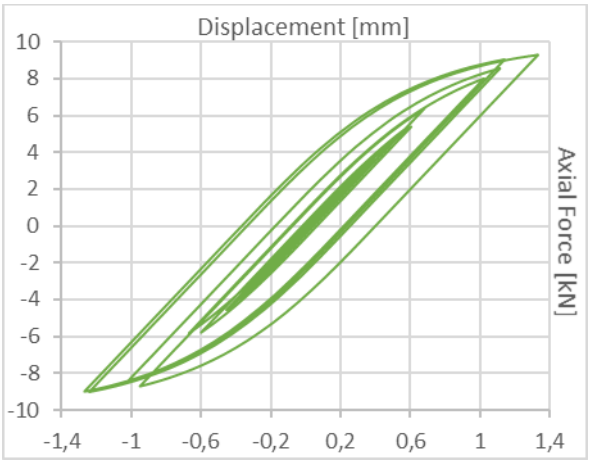

Figure 5-87 Hysteresis loop from modal T-H for Dursun Y of MBF with 10 kN slip load of damper

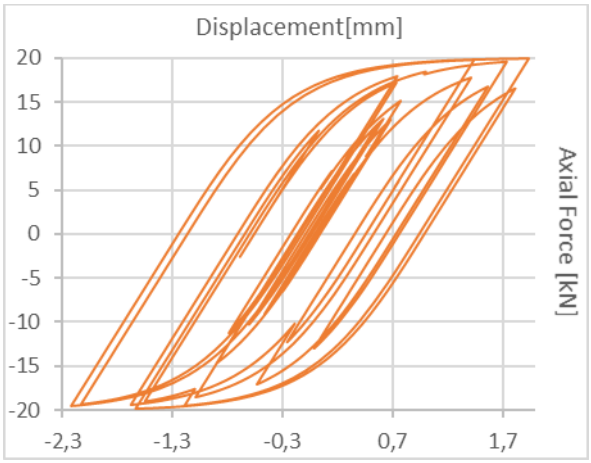

Figure 5-88 Hysteresis loop from modal T-H for Friuli Y of MBF with 20 kN slip load of damper

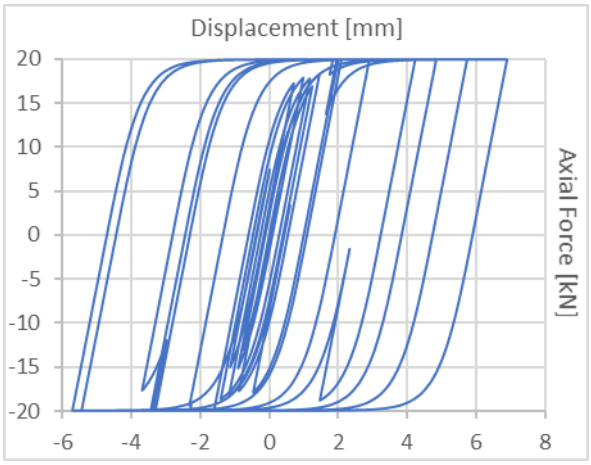

Figure 5-89 Hysteresis loop from modal T-H for Gazli Y of MBF with 20 kN slip load of damper

The results of the assumed slip loads for the friction dampers for each load case are presented in Table 5.18. The Dursun earthquake is significantly smaller than the other analyzed earthquakes, and for that reason the slip load for the Dursun time-history record is smaller than the slip load for the Friuli and Gazli records.

Table 5.18 Assumed slip load for friction dampers from all modal T-H load cases of MBF

Modal T-H Load Case	**Slip Load [kN]**
Dursun, Y	10
Friuli, Y	20
Gazli, Y	20

5.4.2.2 Base Shear Reaction

Figure 5-90 to Figure 5-92 illustrate the base shear reactions for all the load cases with relevant slip load of the friction damper. In comparison to the direct integration time-history analysis for Gazli, the modal time-history analysis manages to complete the analysis for the whole time-history record. The resulting base shear is largest for Gazli and smallest for Dursun, due to the difference in magnitude.

For the Dursun time-history record, the base shear reaction is highest at 1,75 s. The maximum base shear reaction is highest at approximately 4 and 5 s for the Friuli time-history record, which can be seen in Figure 5-91. For the Gazli time-history record, the maximum base shear reaction is at approximately 11 s, as seen in Figure 5-92.

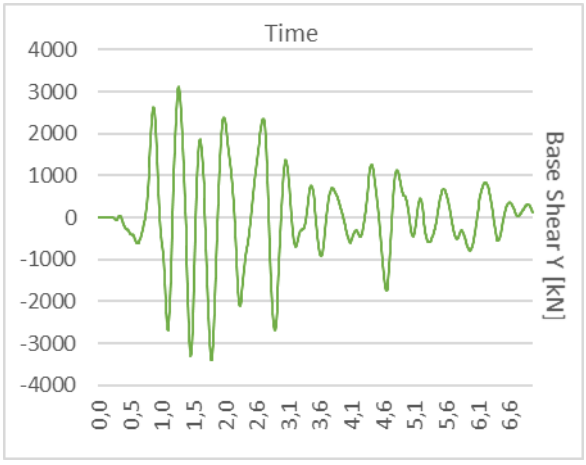

Figure 5-90 Base shear from modal T-H for Dursun Y of MBF

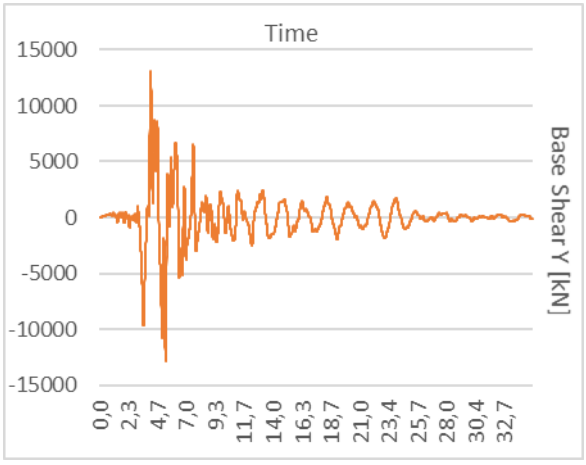

Figure 5-91 Base shear from modal T-H for Friuli Y of MBF

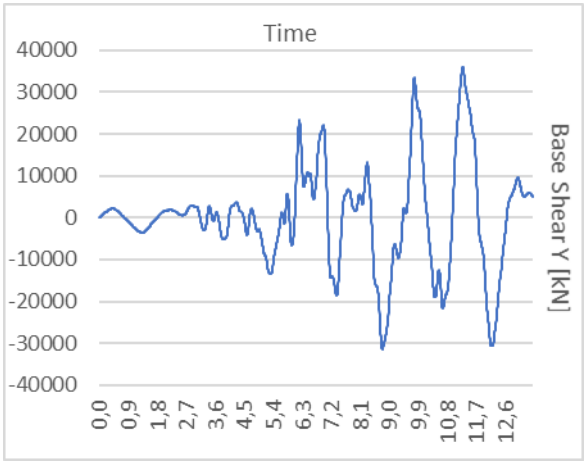

Figure 5-92 Base shear from modal T-H for Gazli Y of MBF

The maximum base shear for the modal time-history load cases with friction dampers is displayed in Table 5.19. The maximum base shear obtained from the load case for Gazli is essentially larger than the maximum base shear for Dursun and Friuli, which is due to the magnitude of the earthquake, which is significantly larger.

Table 5.19 Maximum base shear from all modal T-H load cases of shear wall

Modal T-H Load Case	**Maximum Base Shear Y [kN]**
Dursun, Y	3 471
Friuli, Y	13 050
Gazli, Y	36 020

5.4.2.3 Roof Displacement

The roof displacement for all the modal time-history is shown in Figure 5-93 to Figure 5-95. The Gazli time-history record shows the largest maximum roof displacement and the lowest maximum roof displacement occurs during the Dursun time-history record. This seems reasonable, as Dursun is the smallest earthquake and Gazli is the largest. Further, it can be seen that the maximum roof displacement occurs at approximately 1,9 and 2,4 seconds for Dursun, 4,7 seconds for Friuli and 11 seconds for Gazli.

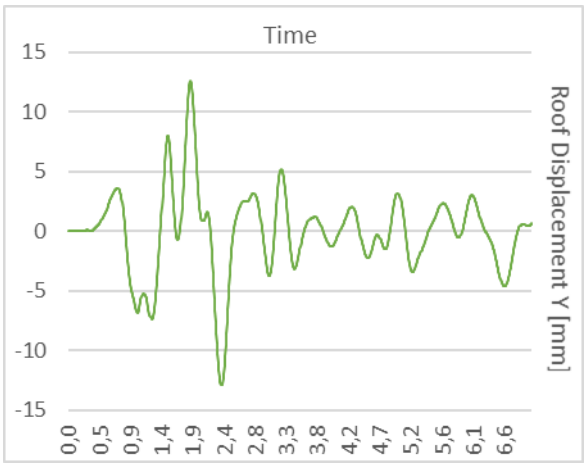

Figure 5-93 Roof displacement from modal T-H for Dursun Y of MBF

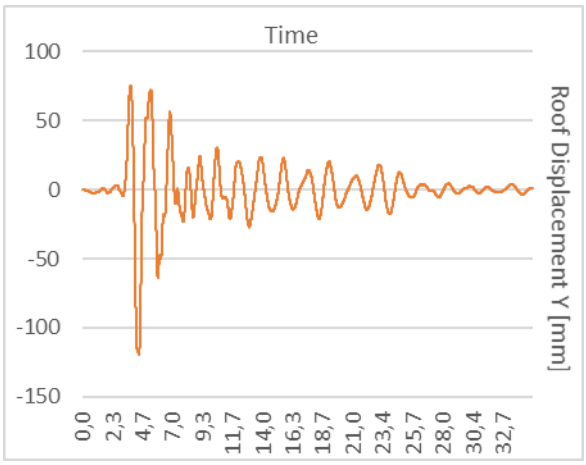

Figure 5-94 Roof displacement from modal T-H for Friuli Y of MBF

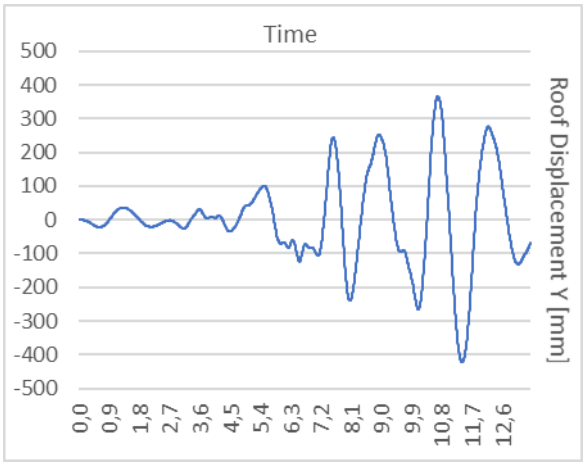

Figure 5-95 Roof displacement from modal T-H for Gazli Y of MBF

Table 5.20 shows the maximum displacement of the monitored joint on the roof of the MBF structure for each modal time-history load case. As stated earlier in the thesis, the Gazli earthquake is significantly larger than the Dursun and Friuli earthquakes and it is therefore rational that the Gazli load cases result in larger maximum displacement than the Dursun and Friuli load cases. Additionally, the Dursun earthquake is a lot smaller and leads to a considerably lower maximum roof displacement.

Table 5.20 Maximum roof displacement from all modal T-H load cases of MBF

Modal T-H Load Case	**Maximum Roof Displacement Y [mm]**
Dursun, Y	12,97
Friuli, Y	119,4
Gazli, Y	422,6

5.4.2.4 Drift Ratio

The roof drift at the monitored joint for all the load cases is illustrated in Figure 5-96 to Figure 5-98. Maximum roof drift is highest for the Gazli load case and lowest for the Dursun load case, which is as expected based on the previous results from the different earthquakes also showing peak values during Gazli. All the graphs for the roof drift for the load cases seem reasonable considering the results from the previous analyses of the MBF structure.

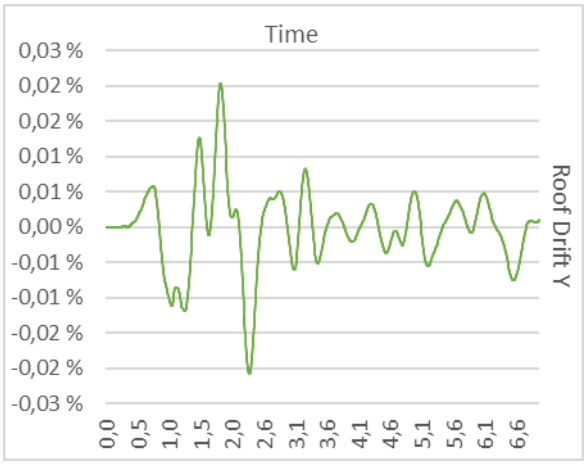

Figure 5-96 Roof drift from modal T-H for Dursun Y of MBF

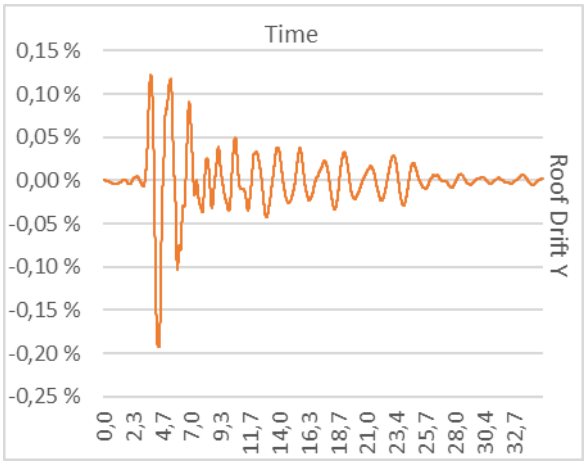

Figure 5-97 Roof drift from modal T-H for Friuli Y of MBF

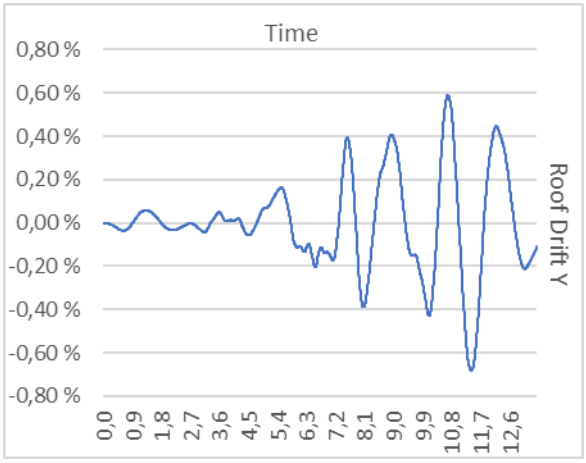

Figure 5-98 Roof drift from modal T-H for Gazli Y of MBF

The maximum roof drift at the generalized joint 5696 for all the modal time-history load cases is collected from SAP2000 and are displayed in Table 5.21.

Table 5.21 Maximum roof drift from all modal T-H load cases for MBF

Modal T-H Load Case	**Maximum Roof Drift Y**
Dursun, Y	0,0209 %
Friuli, Y	0,1926 %
Gazli, Y	0,6817 %

The graphs in Figure 5-99 to Figure 5-101 display the story drift from each modal time-history analysis of the MBF structure. The drift varies a lot for each story in all the load cases, which may be due to irregularities in the geometry of the structure. Also, as the braces are spanning across two stories, the drift increases or decreases every second story. This was also seen from the direct integration time-history analysis and presented in Chapter 5.3.2.3.

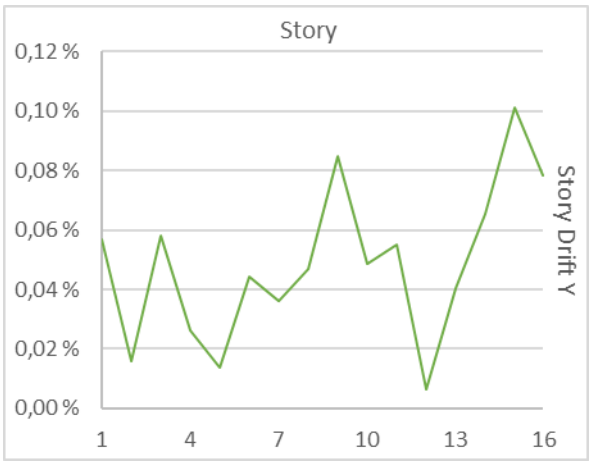

Figure 5-99 Story drift from modal T-H for Dursun Y of MBF

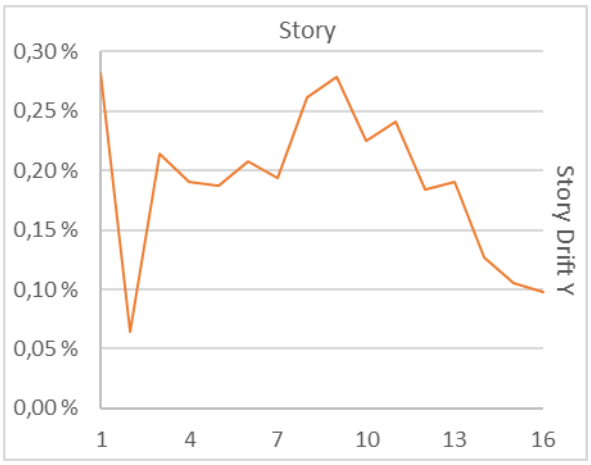

Figure 5-100 Story drift from modal T-H for Friuli Y of MBF

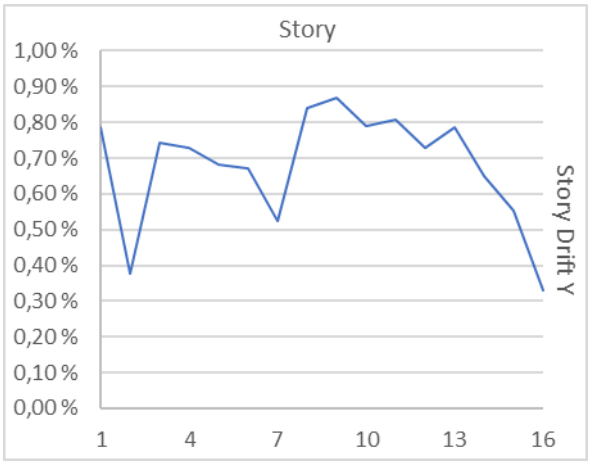

Figure 5-101 Story drift from modal T-H for Gazli Y of MBF

Table 5.22 presents the maximum story drift and the respective story. The story with the maximum story drift for the Dursun load cases is almost on the top of the building, while for Friuli it is in the first floor. Further, for the Gazli load case it is in the 9th floor, which is right above where the low part stops and only the tall part continues.

Table 5.22 Maximum story drift from all modal T-H load cases of MBF

Modal T-H Load Case	**Maximum Story Drift Y**	**Story**
Dursun, Y	0,076 %	14-15
Friuli, Y	0,283 %	0-1
Gazli, Y	0,869 %	8-9

5.5 Comparison of Shear Walls and MBF

The calculated target displacement for the MBF structure is significantly higher than the calculated target displacement for the shear wall structure. The different values when calculating the target displacements is damping ratio, natural fundamental period and as the period for the MBF is higher the resulting response spectrum is different, leading to a higher target displacement.

For all the load cases, the maximum base shear for the shear wall structure are higher than the maximum base shear for the MBF structure, even though the displacement for the shear wall is lower. This means that the pushover curve for the shear wall has a much steeper slope than the pushover curve for the MBF structure. The reason that the base shear reactions are higher for the shear wall structure is because of the mass, which is considerably higher of the shear wall structure.

From the pushover analysis, the roof drift ratio for the MBF structure is much larger compared to the shear wall structure, as the displacement is larger and as the roof drift is a function of roof displacement this is reasonable. Further, the MBF structure is more elastic which also can increase the displacement.

For the MBF structure, the direct integration time-history load case for Gazli was not completed due to convergence errors at 9,3 seconds, likely due to collapse initiation. For the shear wall structure, the analysis of the Gazli earthquake was completed and results were obtained for the whole duration.

Considering the direct integration time-history analysis, the MBF structure experiences larger maximum roof displacement and maximum roof drift than the shear wall structure, during all load cases except the Dursun load case in x-direction and the Gazli load case in y-direction. For the modal time-history analysis, the roof displacement and the maximum roof drift obtained from the Dursun load case in both directions are bigger for the shear wall structure. That implies that the period of the ground motion for these two load cases are closer to the natural fundamental period in x-direction for the shear wall structure.

The maximum story drift is higher for the MBF structure in all load cases for both direct integration and modal time-history analysis. Further, the assumed slip loads in the modal analysis are higher for the shear wall structure than the MBF structure.

5.6 Comparison of Nonlinear Analysis Methods

Regarding the resulting reaction base shear forces, the pushover analyses lead to large values compared to the direct integration time-history analyses. The exception is the Gazli earthquake, which leads to larger values from both time-history analyses of the shear walls, compared to the pushover results. As seen in the results, the Dursun and Friuli earthquake generally affects the structure less than the Gazli earthquake, so it is reasonable that these two smaller earthquakes are smaller than the values from the pushover analysis.

The maximum obtained deviation is for the Dursun earthquake acting on the MBF structure in y-direction, which is, according to the direct integration time-history analysis, only 9,6 % of the obtained base shear from the pushover analysis. The minimum deviation is found for the MBF structure during the Friuli earthquake in y-direction. The deviation is only 1,1 % between the direct integration and modal time-history analysis. Generally, there is a good agreement between the base shear result of the direct integration and modal time-history analyses for the two smaller earthquakes. The difference increases with increasing magnitude of the earthquake, and the modal results mostly lead to larger values compared to those obtained by the direct integration method. This is illustrated for the Friuli earthquake subjected to the shear wall structure in Figure 5-102.

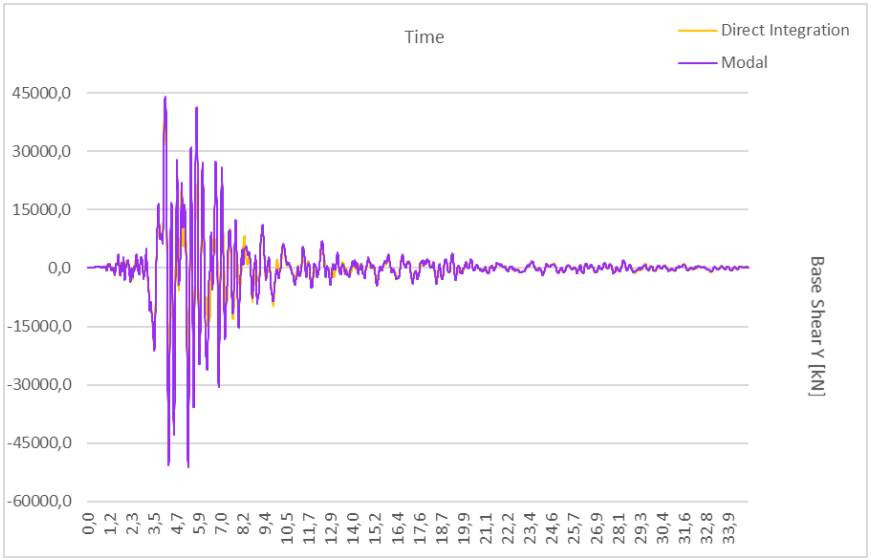

Figure 5-102 Base shear from direct integration and modal T-H for Friuli Y of shear wall

Further, the pushover base shear results clearly show larger values than the ones obtained for the two smaller earthquakes. The exception is during the Gazli earthquake, where both time-history methods showed larger values compared to the pushover load case. Figure 5-103 shows

the variation in base shear during the Friuli earthquake in y-direction, showing relatively small deviations between the results of the two methods.

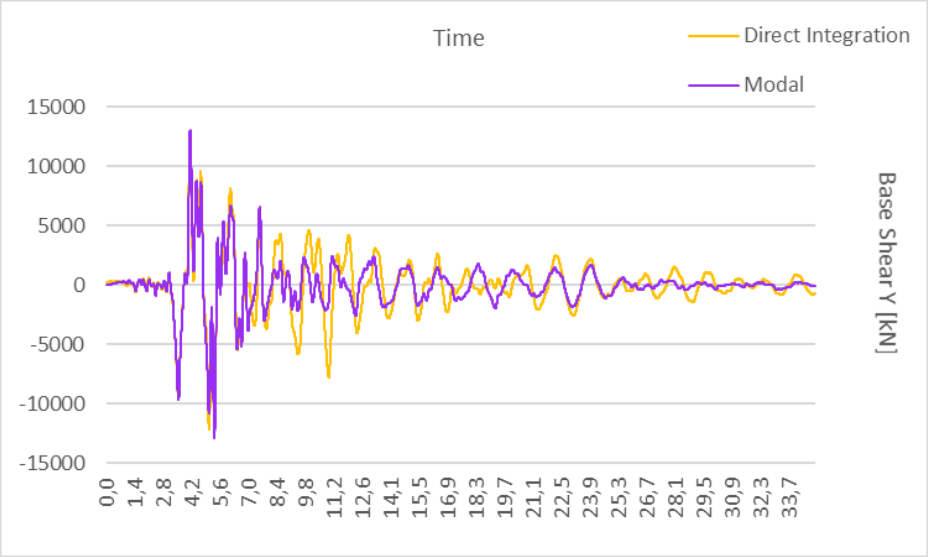

Figure 5-103 Base shear from direct integration and modal T-H for Friuli Y of MBF

For the MBF structure, the base shear values from the modal time-history analysis were in accordance with the ones obtained from the pushover analysis during the Gazli earthquake, apart from the direct integration analysis in y-direction. As mentioned earlier this analysis is incomplete and it is reasonable to believe that the base shear value would be similar to the values of the other methods.

The calculation of the target displacement is significantly larger than the obtained roof displacement of both structures in all methods. The target displacement is 422 mm and 786 mm for the shear wall and MBF structure, respectively. Compared to the roof displacement occurring during the earthquakes analyzed through nonlinear dynamic analyses, both the direct integration and the modal method, these values are significantly larger. When considering the results of the two time-history methods alone, the results are generally similar, but are significantly deviating from the calculated target displacement. The maximum deviation, if not considering the Gazli earthquake of the MBF structure, is observed for the MBF structure during the Friuli earthquake. The maximum deviation is 40,1 % between the two time-history methods. During the Gazli earthquake the lowest deviation is seen between direct integration and modal time-history analysis, with an overestimation of 7,4 % from the direct integration compared to the modal method.

In Figure 5-104, the variation in roof displacement is plotted for the Friuli earthquake in Y-direction according to both time-history methods of the shear wall structure. The graph shows a general compliance between the results of the two methods.

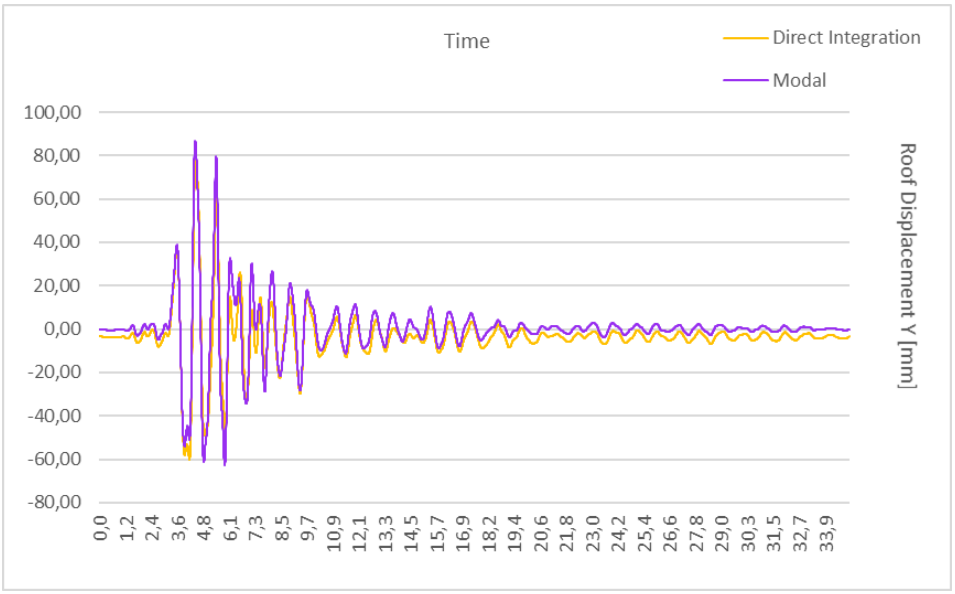

Figure 5-104 Roof displacement from direct integration and modal T-H for Friuli Y of shear wall

The same graph is plotted for the MBF structure during the Friuli earthquake in Y-direction, shown in Figure 5-105. The results show that the modal analysis leads to lower values of the roof displacement during the earthquake, but that there are generally small deviations in the result.

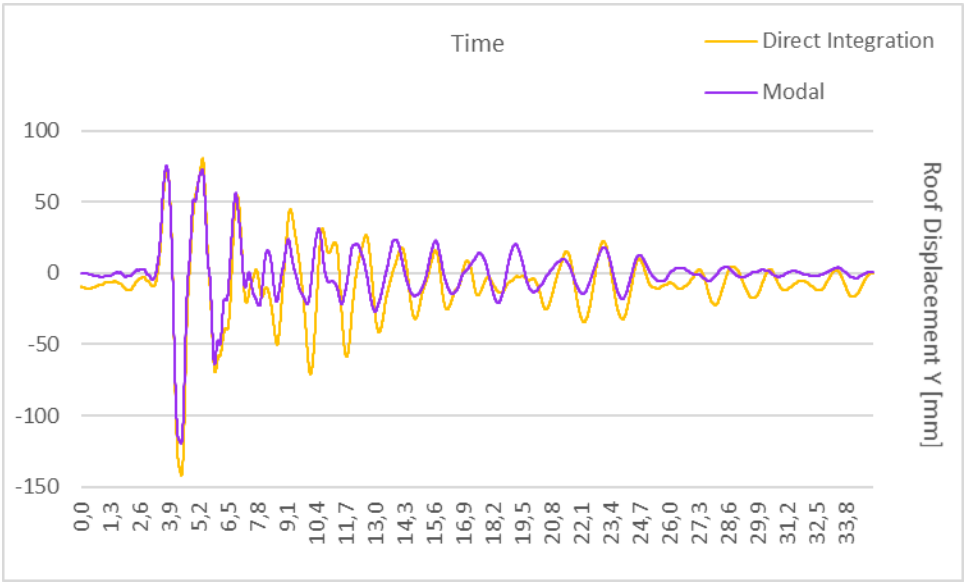

Figure 5-105 Roof displacement from direct integration and modal T-H for Friuli Y of MBF

The drift ratios were generally larger for the pushover analysis when considering roof drift. This applies for both structures and for both time-history analysis methods. Compared to the calculated maximum story drifts of each load case in each building, these values were more in correspondence with the roof drifts from the pushover analysis. Again, the values closest to the ones obtained through the pushover analyses were obtained during the Gazli earthquake.

Plastic hinge formation was investigated for the braces of the MBF structure only. During the pushover analysis, several plastic hinges occurred. The most critical hinge was, according to the result, within point C, indicating that the maximum capacity is not exceeded. During the Gazli earthquake analyzed through direct integration time-history analysis, the most critical hinges reached point E, which corresponds to total failure of the hinge, and is probably the reason that the analysis was terminated. During the other two earthquakes, almost no hinges were formed. The modal time-history analysis showed no hinge formation for all load cases, which is reasonable as the structure is equipped with dampers.

6 DISCUSSION

6.1 Lateral Force Resisting Systems

In this thesis, a relatively brittle structure, the shear wall structure, and a ductile structure, MBF system, are compared based on base shear reactions, displacements and drift ratio through different analysis methods. To determine which structure is most suitable regarding seismic performance, the seismic behavior for different levels of seismic action must be assessed and discussed.

Base shear forces are related to soil, records and mass, and since the soil and records are equal for the two models, the mass of the shear wall structure then has a significant effect on the base shear reactions compared to those of the MBF structure. Thus, as the mass of the shear wall structure is larger it is reasonable the shear force is larger.

The MBF structure has overall larger displacement than the shear wall structure, as the MBF structure is significantly more elastic. However, larger displacements occur in the shear wall structure when considering the displacement in proportion to the target displacements. This indicates that the target displacement is more accurate for the shear wall structure than the MBF structure, as the target displacement is a calculated predicted displacement.

The earthquake record of Gazli analyzed with direct integration time-history analysis could not be completed for the MBF structure, as the analysis was terminated at 9,3 seconds due to convergence error. This implies that global collapse of the structure is initiated. Oppositely, the shear wall structure does not experience collapse according to the results. This may imply that the shear wall structure is able to withstand earthquakes of greater magnitude than the MBF structure, when considering the height of the case study building and the seismic events analyzed in this study.

For the height of this structure, the shear wall shows better results for seismic performance, but if the structure were to be higher, the MBF structure might be more a more suitable LFRS as ductile structures are often considered more beneficial for taller structures. This is also a reasonable assumption based on the prohibition stated in ASCE7-10 [18], which was mentioned in Chapter 2.6.1. The prohibition does not allow concrete shear walls as the only LFRS in structures taller than 50-75 m, if they are located in high seismicity regions, implying that more ductile LFRS are preferable for taller structures.

In the modal time-history analysis, the results imply that the slip load of the dampers in the shear wall structure should be higher than the slip load for the dampers in the MBF structure. This further indicates that the energy dissipation demand during the seismic loading imparted from the analyzed earthquakes is higher for the shear wall structure than for the MBF structure. The reason for that may be because the shear wall structure is stiffer and more brittle.

6.2 Nonlinear Analysis Methods

The large variation in calculated target displacement and resulting roof displacement may imply that the two smaller earthquakes are not suitable as design earthquakes in this particular region. As mentioned, it is decided to locate the structure in the most high-seismicity region in Norway, which increases the target displacement calculated for the pushover analysis. Oppositely, as the earthquake records chosen for analysis are not affected by parameters related to ground characteristics, the location of the building is irrelevant as long as the same earthquakes are considered. This implies that if the same earthquakes were used for the time-history analyses, but the location of the building was set to a region with lower seismicity, the target displacement would be lower and closer to the roof displacements obtained through time-history analyses.

Although, based on the points made in the above section, it can be argued that the target displacement gives a better indication of the actual displacement, a monotonic, gradually applied force cannot represent the actual application pattern of loads during a seismic event. In reality, the ground motion affects the building in seismic waves with changes in acceleration causing the building to vibrate. As described in Chapter 2.1 , continuous vibration may cause damage to the structure, as well as the phenomena of resonance can occur during the vibration. This is not considered through a pushover analysis and may be crucial for the behavior of the structure.

As the calculated target displacements were significantly higher than the roof displacements obtained from the various analyses for both structures, it is reasonable that the peak roof drift value is larger. What was also observed was that the maximum story drifts were generally in more accordance with the roof drift from the pushover analysis, as the time-history analyses have a varying load pattern that may cause larger drifts in lower stories than the roof.

There is seemingly good agreement with the results obtained from the direct integration and modal time-history analyses, implying that the assumed slip loads are reasonable regarding the energy dissipating demand during the various earthquakes.

Even though the results obtained from the pushover analysis generally deviated from the results of the two time-history methods, it should be taken into consideration that the pushover is considered not accurate for irregular and tall buildings, as mentioned in Chapter 3.1. As the case study structure is both irregular and tall, this indicates that the results from the pushover analyses may not be accurate, and that the time-history analyses are more likely to provide accurate results for a structure of this kind.

Although nonlinear time-history analysis is often considered to provide the "exact" seismic behavior of a structure, this can be discussed as the chosen time-history functions are of great influence on the results. As earthquakes are random in nature, they are impossible to predict, and even though ground motion accelerations can be considered through a time-history analysis, it is not guaranteed that the design earthquakes are representative for the potential earthquakes that will occur in the life time of the structure. Still, the possibility of analyzing different ground motions affecting the structure increases the probability of achieving a safe seismic design of the building.

Further, the variation in computational demand and time investment are worth considering. Direct integration time-history analysis is significantly more time consuming than the pushover analysis and especially the modal time-history analysis. Compared to the other analyses the modal time-history analysis is undoubtedly faster. Further, the computational demand is much larger when performing a direct integration time-history analysis. Especially when abrupt changes occur, software and computers may have a hard time dealing with the progress. This was seen for the MBF structure exposed to the Gazli earthquake, resulting in termination of the analysis as the hinges failed. Additionally, the amount of results and data to process after the analysis is performed is noteworthy larger than for the pushover analysis, as more steps are usually required for more complex analyses. As results usually are collected at each step, the output data may be comprehensive.

7 CONCLUDING REMARKS

- The MBF structure generally experienced larger deformations and story drifts during the earthquakes, while the shear wall structure was exposed to larger base shear forces due to the high mass.
- Based on results and discussion of this study, the shear wall structure is considered to provide more beneficial seismic behavior compared to the MBF structure. This is based on the deformation, story drift and base shear reactions from the performed analyses. The obtained results are only valid for this specific structure and the specific analyses conducted in this thesis. The main argument for this conclusion is the collapse of the MBF structure in the direct integration time-history analyses during the Gazli earthquake in x- and y-direction. As this time-history record lead to a maximum roof displacement closest to the calculated target displacement, this load case should be considered.
- The pushover analysis generally showed larger peak values of the roof displacement and roof drift than the other analyses.
- Although the target displacement of the pushover analysis is calculated with consideration of ground type and location, the monotonic applied forces don't consider the effect of varying seismic waves causing vibration of the structure, which itself can be damaging to the structure if acting for a long period of time.
- In general, the results obtained from the direct integration and modal time-history analyses were in agreement and mostly indicated similar responses, both regarding peak values and variation with the time. As pushover analysis is not considered applicable for irregular and tall structures, it is assumed that the time-history analyses provided the most accurate results.
- Choosing reasonable time-history functions is of great importance of the results, as different magnitudes and shapes of the seismic waves affect the building differently. The results show significant variation in the seismic behavior when comparing the three analyzed earthquakes. According to the results, the Dursun earthquake does not have a significant impact on the structure. On the other end, the Gazli earthquake leads to large deformations and even failure of several hinges in the MBF structure. Thus, it is crucial to choose time-history functions that are representative for the current location. According to the results, it is reasonable to believe that the Dursun earthquake is not a suitable choice for design earthquake of this structure at the chosen location.

- Time investment and computational demand is significantly reduced for the pushover analysis and the modal time-history analysis compared to the direct integration time-history analysis. Additionally, the amount of data to process after the time-history analyses are much larger than that of the pushover analysis.

RECOMMENDATIONS FOR FURTHER WORK

The research on the accuracy of fast nonlinear analysis as an alternative to direct integration analysis should be further studied. In the results of this thesis it was found that nonlinear analyses in general are time consuming and computationally demanding, but that the fast nonlinear analysis significantly reduces the demands. Whether or not this method is more beneficial or more accurate than the direct integration time-history analysis could not be concluded during this thesis, as more research is necessary.

As the modal time-history analysis is especially suitable for structures equipped with energy dissipating devices, this was also performed in this study with friction dampers as a third LFRS. Thus, it would be interesting to investigate the direct integration method on damped structures to see whether similar results can be obtained. According to the results the direct integration method without friction dampers generally provide similar results as those obtained by the modal time-history analysis of a damper-equipped structure. If further research can validate the method and the accuracy of the results, seismic analyses can be accurately computed with significant reduction in time investment and complexity.

When comparing the shear walls and MBF as LFRS in high-rise buildings, it would be interesting to not only consider the structural and seismic behavior, but also the environmental and economic differences. Factors that are worth considering is the initial greenhouse gas (GHG) emission and costs, as well as the maintenance need. Further, based on damage from seismic analyses in the structure the environmental and economic consequences of potential repairs or replacements can be studied, of both structural and non-structural elements.

Additionally, as the two LFRS have relatively varying properties, the possibility of a hybrid solution utilizing the strengths from the two systems could be investigated.

REFERENCES

[1] A. S. Pall and R. Pall, "Friction-dampers for seismic control of buildings–a Canadian experience," in *Eleventh World Conference on Earthquake Engineering, Acapulco, Mexico*, 1996.

[2] *Eurocode 8: Design of structures for earthquake resistance - Part 1: General rules, seismic actions and rules for buildings*, NS-EN 1998-1:2004+A1:2013+NA:2014, 2014.

[3] W. M. Hassan and J. C. Reyes, "Assessment of modal pushover analysis for mid-rise concrete buildings with and without viscous dampers," *Journal of Building Engineering,* vol. 29, p. 101103, 2020.

[4] C. Arnold, "Earthquake effects on buildings 4," *Risk management series designing for earthquakes a manual for architects providing protection to people and buildings. FEMA, Oakland, California,* 2006.

[5] K. Y. Billah and R. H. Scanlan, "Resonance, Tacoma Narrows bridge failure, and undergraduate physics textbooks," *American Journal of Physics,* vol. 59, no. 2, pp. 118-124, 1991.

[6] *Minimum Design Loads and Associated Criteria for Buildings and Other Structures*, ASCE 7-16, 2017.

[7] *Prestandard and Commentary for the Seismic Rehabilitation of Buildings*, FEMA 356, 2000.

[8] *Seismic Evaluation and Retrofit of Existing Buildings*, ASCE/SEI 41-13, 2014.

[9] *Seismic Evaluation and Retrofit of Concrete Buildings Volume 1*, ATC-40, 1996.

[10] *Seismic Provisions for Structural Steel Buildings*, ANSI/AISC 341-16 (ASCE341), 2016.

[11] A. Urbanski, E. Spacone, M. Belgasmia, J. Sarf, and T. Zimmermann, "Static Pushover Analysis," ed: Z_Soil. PC.

[12] C. Oliveira, A. Campos-Costa, and M. Sousa, "Definition of seismic action in the context of EC-8: topics for discussion," in *Proceedings of the Twelfth World Conference on Earthquake Engineering, Auckland*, 2000.

[13] A. Patil and P. Kumbhar, "Time history analysis of multistoried RCC buildings for different seismic intensities," *International Journal of Structural and Civil Engineering Research,* vol. 2, no. 3, pp. 194-201, 2013.

[14] S. W. Martin, "Structural analysis," in *Seismic Design of Buildings to Eurocode 8*: CRC Press, 2016, ch. Structural analysis.

[15] A. Kasimzade, E. Şafak, C. Ventura, F. Naeim, and Y. Mukai, *Seismic Isolation, Structural Health Monitoring, and Performance Based Seismic Design in Earthquake Engineering Recent Developments: Recent Developments*. 2019.

[16] I. F. Kara and C. Dundar, "Prediction of deflection of reinforced concrete shear walls," *Advances in Engineering Software,* vol. 40, no. 9, pp. 777-785, 2009/09/01/ 2009, doi: https://doi.org/10.1016/j.advengsoft.2009.02.002.

[17] M. AlHamaydeh, K. Galal, and S. Yehia, "Impact of lateral force-resisting system and design/construction practices on seismic performance and cost of tall buildings in Dubai, UAE," *Earthquake Engineering and Engineering Vibration,* vol. 12, no. 3, pp. 385-397, 2013/09/01 2013, doi: 10.1007/s11803-013-0180-2.

[18] *Minimum Design Loads for Buildings and Other Structures*, ASCE/SEI 7-10, 2013.

[19] FEMA, "NEHRP guidelines for the seismic rehabilitation of buildings (FEMA 273)," ed: Federal Emergency Management Agency Washnigton, DC, 1997.

[20] R. Sabelli, S. Mahin, and C. Chang, "Seismic demands on steel braced frame buildings with buckling-restrained braces," *Engineering Structures,* vol. 25, no. 5, pp. 655-666, 2003/04/01/ 2003, doi: https://doi.org/10.1016/S0141-0296(02)00175-X.

[21] S. Kazemzadeh Azad, C. Topkaya, and A. Astaneh-Asl, "Seismic behavior of concentrically braced frames designed to AISC341 and EC8 provisions," *Journal of Constructional Steel Research,* vol. 133, pp. 383-404, 2017/06/01/ 2017, doi: https://doi.org/10.1016/j.jcsr.2017.02.026.

[22] A. Pall and R. T. Pall, "Performance-based design using pall friction dampers-an economical design solution," in *13th World Conference on Earthquake Engineering, Vancouver, BC, Canada*, 2004, vol. 70, no. 7, pp. 576-571.

[23] I. F. Khatib, S. A. Mahin, and K. S. Pister, *Seismic behavior of concentrically braced steel frames*. Earthquake Engineering Research Center, University of California Berkeley, 1988.

[24] D. M. Patil and K. K. Sangle, "Seismic Behaviour of Different Bracing Systems in High Rise 2-D Steel Buildings," *Structures,* vol. 3, pp. 282-305, 2015/08/01/ 2015, doi: https://doi.org/10.1016/j.istruc.2015.06.004.

[25] O. Alshamrani, G. Schierle, K. Galal, and D. Vergun, *Optimal bracing type and position to minimize lateral drift in high-rise buildings*. 2009, pp. 155-166.

[26] B. Kioumarsi, A. Kheyroddin, M. Gholhaki, M. Kioumarsi, and S. Hooshmandi, "Effect of Span Length on Behavior of MRF Accompanied with CBF and MBF Systems," *Procedia Engineering,* vol. 171, pp. 1332-1340, 2017/01/01/ 2017, doi: https://doi.org/10.1016/j.proeng.2017.01.431.

[27] L. Di Sarno and A. S. Elnashai, "Bracing systems for seismic retrofitting of steel frames," *Journal of Constructional Steel Research,* vol. 65, no. 2, pp. 452-465, 2009/02/01/ 2009, doi: https://doi.org/10.1016/j.jcsr.2008.02.013.

[28] L. Tirca, "Friction dampers for seismic protections of steel buildings subjected to earthquakes: Emphasis on structural design," *Encyclopedia of Earthquake Engineering, Springer, Berlin,* vol. 1058, p. 1070, 2015.

[29] R. Chandra, M. Masand, S. Nandi, C. Tripathi, R. Pall, and A. Pall, "Friction-dampers for seismic control of La Gardenia towers south city, Gurgaon, India," in *12 th World Conference on Earthquake Engineering, Auckland, New Zealand*, 2000.

[30] Pall Dynamics Limited. "Design With Friction Dampers." http://www.palldynamics.com/DesignWithFrictionDampers.htm (accessed April 24, 2020).

[31] H. Krawinkler and G. D. P. K. Seneviratna, "Pros and cons of a pushover analysis of seismic performance evaluation," *Engineering Structures,* vol. 20, no. 4, pp. 452-464, 1998/04/01/ 1998, doi: https://doi.org/10.1016/S0141-0296(97)00092-8.

[32] M. A. Khan, "Chapter Ten - Seismic Design for Buildings," in *Earthquake-Resistant Structures*, M. A. Khan Ed. Boston: Butterworth-Heinemann, 2013, pp. 283-315.

[33] R. Leslie and A. Naveen, "A Study on Pushover Analysis using Capacity Spectrum Method based on Eurocode 8," in *16th World Conference on Earthquake Engineering, Reg Code: S-P148645023, Santiago, Chile*, 2017.

[34] R. K. Goel, "Variability and accuracy of target displacement from nonlinear static procedures," *ISRN Civil Engineering,* vol. 2011, 2011.

[35] FEMA, "Improvement of nonlinear static seismic analysis procedures (FEMA440)," *FEMA-440, Redwood City,* vol. 7, no. 9, p. 11, 2005.

[36] A. K. Chopra and R. K. Goel, "A modal pushover analysis procedure for estimating seismic demands for buildings," *Earthquake engineering & structural dynamics,* vol. 31, no. 3, pp. 561-582, 2002.

[37] S. ANTONIOU and R. PINHO, "Advantages and limitations of adaptive and non-adaptive force-based pushover procedures," *Journal of Earthquake Engineering,* vol. 8, no. 04, pp. 497-522, 2004.

[38] V. Boonyapinyo, N. Choopool, and P. Warnitchai, "Seismic Performance Evaluation of Reinforced-Concrete Buildings by Static Pushover and Nonlinear Dynamic Analyses," in *14th World Conference on Earthquake Engineering*, 2008.

[39] S. Oğuz, "Evaluation of pushover analysis procedures for frame structures," *Master of Science Thesis, METU,* 2005.

[40] R. Taghinezhad, A. Taghinezhad, V. Mahdavifar, and V. Soltangharaei, "Evaluation of story drift under pushover analysis in reinforced concrete moment frames," *Int. J. Res. Eng,* vol. 5, no. 1, pp. 296-302, 2018.

[41] Y. Endo, L. Pelà, and P. Roca, "Review of Different Pushover Analysis Methods Applied to Masonry Buildings and Comparison with Nonlinear Dynamic Analysis," *Journal of Earthquake Engineering,* vol. 21, no. 8, pp. 1234-1255, 2017/11/17 2017, doi: 10.1080/13632469.2016.1210055.

[42] Computers & Structures Inc., "CSI Analysis Reference Manual For SAP2000®, ETABS®, SAFE® and CSiBridge®," *Computers and Structures, Inc., Berkeley, California, USA,* 2017.

[43] Ö. Akar and K. Willner, "Application of the fast nonlinear analysis method on a clamped beam with a cubic spring," *PAMM,* vol. 19, no. 1, p. e201900022, 2019.

[44] C. S. Inc. "Comparison between FNA and direct-integration time-history analyses." (accessed May 22nd, 2020).

[45] H. Krawinkler, D. G. Lignos, and C. Putman, "Prediction of nonlinear response—Pushover analysis versus simplified nonlinear response history analysis," in *Structures Congress 2011*, 2011, pp. 2228-2239.

[46] R. Mohan and C. Prabha, "Dynamic analysis of RCC buildings with shear wall," *International Journal of Earth Sciences and Engineering,* vol. 4, no. 6, pp. 659-662, 2011.

[47] *Specification for structures to be built in disaster areas*, Turkish Earthquake Code 1975 (TEC1975), 1975.

[48] *Specification for structures to be built in disaster areas*, Turkish Earthquake Code 2007 (TEC2007), 2007.

[49] Ö. Çavdar and A. Bayraktar, "Pushover and nonlinear time history analysis evaluation of a RC building collapsed during the Van (Turkey) earthquake on October 23, 2011," *Natural hazards,* vol. 70, no. 1, pp. 657-673, 2014.

[50] J. Goggins and S. Salawdeh, "Validation of nonlinear time history analysis models for single-storey concentrically braced frames using full-scale shake table tests," *Earthquake engineering & Structural dynamics,* vol. 42, no. 8, pp. 1151-1170, 2013.

[51] *Eurocode 1: Actions on structures - Part 1-3: General actions - Snow loads*, NS-EN 1991-1-3:2003+A1:2015+NA:2018, 2018.

[52] *Eurocode 1: Actions on structures - Part 1-4: General actions - Wind actions*, NS-EN 1991-1-4:2005+NA:2009, 2009.

[53] *Eurocode 3: Design of steel structures - Part 1-1: General rules and rules for buildings*, NS-EN 1993-1-1:2005+A1:2014+NA:2015, 2015.

[54] P. E. E. R. Center. "PEER Ground Motion Database." https://ngawest2.berkeley.edu/site (accessed May 13, 2020).

[55] M. Surana, "Non-linear static analysis using SAP 2000," *Non-Linear Analysis, Department of Earthquake Engineering, IIT Roorkee,* 2000.

[56] C. Murty, R. Goswami, A. Vijayanarayanan, and V. Mehta, "Earthquake behaviour of buildings," *Gujarat State Disaster Management Authority, Gandhinagar,* pp. 53-79, 2012.

APPENDIX A

Snow Loads and Wind Loads
According to EC1-3 [51] and EC1-4 [52]

A.1 Snow Load for building in Bremanger, Sogn og Fjordane				**EC1-3 [51]**				
Table NA.4.1 (901)	Sk,0	2,5	kN/m2					
Table NA.4.1 (901)	Hg	150	m					
Table NA.4.1 (901)	Delta_Sk	1	kN/m2					
Table NA.4.1 (901)	Sk_maks	-	kN/m2					
(5.1)	S	2	kN/m2					
Table 5.1	C_e	1		*Exposure factor. Assumes normal topography*				
5.2 (8)	C_t	1		*Thermal coefficient*				
Table 5.2	μ(α)	0,8		*Flat roof*				
Lower part of building (next to a taller building) 5.3.6								
(5.6)	μ_1	0,8		*Lower roof is flat. --> s=2*				
(5.7)	μ_s	0		*Flat roof*				
(5.8)	μ_w	0,87		*Shape factor from wind*	μ_w_max	171	> μ_w -->	ok
	b_1	15,6	m	*Width tall part of building*				
	b_2	43,8	m	*Width low part of building*				
	h	34,2	m	*Height difference*				
(5.8)	ϒ	2	kN/m2	*Gravity of snow*				
(5.7)	μ_2	0,87	kN/m2	*Negligible*				
(5.9)	l_s	68,4		*Recommended restriction 5-15m. Uses 15m*				
	s_2	2,17	kN/m2					

A.2 Wind Load	**EC1-4 [52]**									
Tab. NA.4(901.1)	vb0	29	m/s	*Bremanger*						
	cdir	1								
	cseason	1								
(4.1) $v_b = c_{dir} \cdot c_{season} \cdot v_{b,0}$	vb	29	m/s							
Fig 7.5+7.6	**X+/X- direction**			**Shape factors**						
	Shape factors									
	h/d	**A**	**B**	**C**	**D**	**E**	**F**	**G**	**H**	**I**
Tab. 7.1+7.2	2,7	-1,2	-0,8	-0,5	0,8	-0,6	-1,8	-1,2	-0,7	0,2
	5	-1,2	-0,8	-0,5	0,8	-0,7				
	1	-1,2	-0,8	-0,5	0,8	-0,5				
	0,25	-1,2	-0,8	-0,5	0,7	-0,3				

		d	66,6	m			d	22,8	m	e>d	
	Low part	b	36,6	m		**Tall part**	b	36,6	m		
	cpe10 for design of structure					**cpe10 for design of structure**					
	e		36,6	m	*b*	e		36,6	m		
	A		7,3	m	*e/5*	A		7,3	m		
	B		29,3	m	*4/5*e*	B		15,5	m		
	F_1		9,15	m	*e/4*	F_1		9,15	m		
	F+G		3,66	m	*e/10*	F+G		3,66	m		
	G		18,3	m	*b-2*e/4*	G		18,3	m		
	H		14,64	m	*e/2-e/10*	H		14,64	m		
	I		48,3	m	*d-e/2*	I		4,5	m		
Fig 7.5+7.6	**Y+/Y- direction**				**Shape factors**						
	Shape factors										
	h/d		**A**		**B**	**C**	**D**	**E**	**F**	**G**	**H**	**I**
Tab 7.1+7.2	1,7		-1,2		-0,8	-0,5	0,8	-0,5	-1,8	-1,2	-0,7	0,2
	5		-1,2		-0,8	-0,5	0,8	-0,7				
	1		-1,2		-0,8	-0,5	0,8	-0,5				

		d	36,6	m		d	36,6	m	e<d
	Low part	b	66,6	m	**Tall part**	b	22,8	m	
	cpe10 for design of structure				**cpe10 for design of structure**				
	e	66,6	m	*b*	e	22,8	m	*b*	
	A	13,3	m	*e/5*	A	4,6	m	*e/5*	
	B	23,3	m	*4/5*e*	B	18,2	m	*4/5*e*	
					C	13,8	m	*d-e*	
	F_1	16,65	m	*e/4*	F_1	5,7	m		
	F+G	6,66	m	*e/10*	F+G	2,28	m		
	G	33,3	m	*b-2*e/4*	G	11,4	m		
	H	26,64	m	*e/2-e/10*	H	9,12	m		
	I	3,3	m	*d-e/2*	I	25,2	m		

APPENDIX B

Target Displacement

According to FEMA273 [19] and EC8 [2]

Target displacement			**FEMA273 [19]**					
			Concrete Shear Wall					
			T_1	0,96163	s			
Concrete shear wall					S_a from EC8 [2]:			
δ	0,422	m	*(3-11)*					
C_0	1,5		*Table 3-2*	*Tab. NA.3.3*	S	1,4		*Assumed ground type C*
S_a	12,00	g	*From EC8*	*Tab. NA.3.4*	T_B	0,1	s	
C_1	1		*T_e>T_0*	*Tab. NA.3.5*	T_C	0,3	s	
C_2	1		*Table 3-1*	*Tab. NA.3.6*	T_D	1,5	s	
C_3	1		*Positive post-yield stiffness*	*(3.6)*	η	1		
T_e=T_1	0,96163		*(3-10) Assumed K_i=K_e*		ξ	5	%	*Damping*
g	9,81	m/s^2		Fig. NA.3(901)	a_g40Hz	1		
				4.2.5(3)	a_gR	0,8		
				Tab. NA.4(901)	ϒ_1	1,4		*Importance class III*
					a_g	1,12	g	
				(3.4)	S_a	12,00		$T_c \leq T_e \leq T_D$
			Steel MBF					
			T_1	1,8905	s			
Steel MBF								
δ	0,786	m	*(3-11)*		ξ	2		
C_0	1,5		*Table 3-2*		η	1,20	%	*Damping*
S_a	5,79	g	*From EC8*	(3.5)	S_a	5,79		$T_D \leq T_e \leq 4s$
C_1	1		*T_e>T_0*					
C_2	1		*Table 3-1*					
C_3	1		*Positive post-yield stiffness*					
T_e=T_1	1,8905		*(3-10) Assumed K_i=K_e*					
g	9,81	m/s^2						